

# Dynamics of Circumstellar Disks III: The case of GG Tau A

Andrew F. Nelson

*XCP-2, Mailstop T082, Los Alamos National Laboratory, Los Alamos NM, USA, 87545*

andy.nelson@lanl.gov

F. Marzari

*Università di Padova, Dipartimento di Fisica, via Marzolo 8, 35131 Padova, Italia*

francesco.marzari@pd.infn.it

## ABSTRACT

We present 2-dimensional hydrodynamic simulations using the Smoothed Particle Hydrodynamic (SPH) code, VINE, to model a self-gravitating binary system. We model configurations in which a circumbinary torus+disk surrounds a pair of stars in orbit around each other and a circumstellar disk surrounds each star, similar to that observed for the GG Tau A system. We assume that the disks cool as blackbodies, using rates determined independently at each location in the disk by the time dependent temperature of the photosphere there. We assume heating due to hydrodynamical processes and due to radiation from the two stars, using rates approximated from a measure of the radiation intercepted by the disk at its photosphere. We simulate a suite of systems configured with semi-major axes of either  $a = 62$  AU ('wide') or  $a = 32$  AU ('close'), and with assumed orbital eccentricity of either  $e = 0$  or  $e = 0.3$ . Each simulation follows the evolution for  $\sim 6500$ - $7500$  yr, corresponding to about three orbits of the torus around the center of mass. Our simulations show that strong, sharply defined spiral structures are generated from the stirring action of the binary and that, in some cases, these structures fragment into 1-2 massive clumps. The torus quickly fragments into several dozen such fragments in configurations in which either the binary is replaced by a single star of equal mass, or radiative heating is neglected. The spiral structures extend inwards to the circumstellar environment as large scale material streams for which most material is found on trajectories which return it to the torus on time scale of 1-200 yr, with only a small fraction accreting into the circumstellar environment. The spiral structures also propagate outwards through the torus, generating net outwards mass flow and eventually losing coherence at large distances from the stars. The torus becomes significantly eccentric in shape over most of its evolution. In all configurations, accretion onto the stars occurs at a steady rate of a few  $\times 10^{-8} M_{\odot}/\text{yr}$ , with the net result that, without replenishment, the disk lifetimes would be shorter than  $\sim 10^4$  yr. Our simulations show that only wide orbit configurations are able to retain circumstellar disks, by virtue of accretion driven from the robust material streams generated in wide configurations, which are very weak in close configurations. In wide, eccentric orbit configurations, accretion is episodic and occurs preferentially onto the secondary, with rates strongly peaked near binary periape. Based on our results, we conclude that the GG Tau A torus is strongly self gravitating and that a major contribution to its thermal energy input is the shock dissipation associated with spiral structures generated both by self gravitating disturbances and by the stirring action of the binary. We interpret the sharply defined features observed in the torus as manifestations of such spiral structures. We interpret the low density disk surrounding it as an excretion disk created by the outward mass flux generated by the spiral arms as they propagate outwards. Typical eccentricities calculated for the shape of the tori modeled in our simulations are large enough to account for the supposed  $\sim 20^{\circ}$  mutual inclination between the stellar orbit plane of GG Tau A and its surrounding torus,

through a degeneracy between the interpretation of inclination of the torus and its eccentricity. We therefore interpret the observations in favor of a coplanar system with an eccentric torus. Because accretion onto the disks occurs at rates sufficient to sustain them only in wide orbit configurations, we conclude that the gas currently resident in the circumstellar disks of the GG Tau A system has been accreted from the torus within the past few thousand years. Although circumstellar disks will persist over time spans long enough to permit planet formation, the overall environment remains unfavorable due to high temperatures and other conditions. Given, the presence of circumstellar disks, robust accretion streams, and our interpretation of the GG Tau A stellar orbit plane as coplanar with the torus surrounding it, we conclude that the GG Tau A system is in an eccentric,  $a \sim 62$  AU orbit, resolving questions in the literature regarding its orbit parameters.

*Subject headings:* Stars:Formation, Stars:Binary, Accretion Disks, Numerical Simulations, Hydrodynamics

## 1. Introduction

In the early stages of the formation of a star (see, e.g., the review paper of Shu *et al.* 1987), a cloud of gas and dust collapses and forms a protostar with a disk surrounding it. Later on, while the accretion from the cloud continues, the star/disk system also begins to eject matter into outflows whose strength varies in time. Finally, accretion and outflow cease and over the next few million years the star loses its disk and evolves onto the main sequence. A major refinement of this paradigm has been an exploration of the parameter space for which multiple objects form from a single collapse (see e.g. Bodenheimer *et al.* 2000; Monin *et al.* 2007). The dynamical evolution of multiple systems, once they are formed, remains insufficiently well understood however.

Observations (Mathieu *et al.* 2000) have shown that in fact more stars in low mass star forming regions (e.g. the Taurus star forming region) are found in binary or higher order multiple systems than is the case for older systems like the field stars in the solar neighborhood. Further, nearly all of these stars show evidence for circumstellar disks. The existence of such multiple stars in forming systems suggests that the evolution of circumstellar material in orbit around or infalling onto those stars will be significantly altered from the evolution in a single star+disk system.

Several observed binary star+disk systems do in fact show evidence of mutual interactions of various strengths (e.g. Close *et al.* 1998; Rodriquez *et al.* 1998). In the L1551 IRS 5 system for example, in which the observed angular separation on the sky corresponds to a  $\sim 50$  AU physical separation, disks around each component of the binary are truncated at about 10 AU, a size which is far smaller than is typically observed in single systems or in binaries with larger orbital separations (e.g. that observed in the HK Tau system; Stapelfeldt *et al.* (1998)). In addition to disk truncation, tidal interactions due to the companion star can significantly alter the evolution of the circumstellar disks by generating large scale shocks and other internal heating. These factors act to accelerate mass transport through the disk, significantly reducing its lifetime unless that mass is replenished from a circumbinary disk on a similar timescale. Such heating and transport may negatively influence the formation of planets in binary systems, as described in Nelson (2000).

The situation becomes significantly more complex when the binary system is also surrounded by a circumbinary torus and/or disk. This additional player may exchange mass and angular momentum with each star and its disk, affecting both the binary orbit and the mass evolution of the circumstellar disks. For example, their dispersal due to accretion onto the star, enhanced by the binary perturbations, may be slowed by continued replenishment from circumbinary material. If this reservoir is massive enough, the feeding mechanism may extend the lifetime of the inner disks so that their dissipation timescale is not significantly different from to single stars (Prato & Simon (1997), see

also Monin *et al.* (2007) for a review). Evidence for such replenishment has recently been observed with using high resolution interferometry on ALMA (Dutrey *et al.* 2014).

### 1.1. The GG Tau system

The total number of observed circumbinary disks is not large. Of those, most are found in binaries with a small separations, such as GW Ori, DQ Tau, AK Sco, V4046 Sgr (Monin *et al.* 2007). Circumbinary disks in wider binaries have been imaged in only a few cases, such as L1551 IRS 5, Sr 24 N, UY Aur and GG Tau. GG Tau is particularly interesting because of the wealth of observational data available for it, which can be compared to theoretical models.

GG Tau was first determined to be a multiple system in the early study of Cohen & Kuhl (1979). Later observations of Leinert *et al.* (1991), using speckle interferometry, confirmed this observation and set the projected separation between the components to be  $\sim 10''$ . The same observations also resolved both the primary and secondary components into a binaries. Imaging by White *et al.* (1999), refined the distance measurements, setting projected separations of  $0.25''$  and  $1.48''$  between the components of the A and B binaries respectively, and  $10.1''$  between the hierarchical binary pairs. At an assumed 140 pc distance of Taurus, these separations correspond to distances of  $\sim 35$  AU and  $\sim 207$  AU, for the binaries, and a distance of  $\sim 1400$  AU, for the hierarchical pairs.

The much more massive ‘primary’ component of the system, GG Tau A, has received extensive attention since its discovery, and a progressively more detailed picture of the system has emerged. Measurements have been made of the stellar masses, luminosities and spectral types, their age, accretion rates, their relative motions and orbit characteristics, the mass and mass distribution of the circumbinary ring and disk and its rotation curve, and estimates of the circumstellar disk configurations and substructure (an incomplete list of references includes Simon & Guilloteau 1992; Dutrey, Guilloteau & Simon 1994; Roddier *et al.* 1996; Guilloteau, Dutrey & Simon 1999; White *et al.* 1999; Silber *et al.* 2000; Itoh *et al.* 2002; Krist, Stapelfeldt & Watson 2002; Tamazian *et al.* 2002; Duchêne *et al.* 2004; Krist *et al.* 2005; Piétu *et al.* 2011; Beck *et al.* 2012; Dutrey *et al.* 2014; di Folco *et al.* 2014).

Among the most detailed models of the various components of the GG Tau A system is that described in Guilloteau, Dutrey & Simon (1999, hereafter GDS99), which we summarize here. In their model, the circumbinary material is composed of two components, consisting of a ring or torus and a disk with a combined mass of  $\sim 0.12M_{\odot}$ , of which some 70% of the total is contained in the torus. Both the torus’ inner and outer edges are quite sharp, with edges  $\leq 10$  AU in width, and are located at distances of 180 and 260 AU from the apparent system center, respectively. Assuming that the torus is circular, its inclination is determined from the observed projected image to be 37 degrees. The disk component is fit to a rather steep power law in density with exponent  $s = 2.75$ , and a similarly steep power law in temperature with exponent  $q = 0.9$ .

The disk’s outer edge is not as well resolved, but appears to extend to approximately 800 AU, a distance consistent with tidal truncation due to the B components of the combined quadruple system. Kinematic measurements of the circumbinary material constrain the total mass of the A components to be  $1.28 \pm 0.07M_{\odot}$ . Unresolved emission originating from the circumstellar environment sets a lower limit on the mass of such material to be  $\sim 0.8 \times 10^{-4}M_{\odot}$ .

The wealth of observations of GG Tau is not without inconsistencies, based both in the data themselves, and in attempts to fit theoretical models to it. For example, while the combined mass of the ‘A’ components has been determined (as noted above) to be  $\sim 1.28 M_{\odot}$ , the masses of the two stars have been estimated from their spectral signatures to be  $\sim 0.78M_{\odot}$  and  $\sim 0.68M_{\odot}$  for the primary and secondary, respectively, based on spectroscopic measurements and fits to evolutionary tracks (White *et al.* 1999). Much of the question regarding the system masses may be resolved with the recent discovery of di Folco *et al.* (2014), that the secondary, GG Tau Ab, is itself a close binary with separation

of  $\sim 4.5$  AU and masses estimated to be  $0.38 M_{\odot}$  and  $0.25\text{--}0.35 M_{\odot}$ , respectively.

Similarly, the orbital parameters of the stars have been established from fits to their relative motions, and are estimated to define an orbit with semi-major axis  $a \sim 32.4$  AU and eccentricity  $e = 0.34$  (Beust & Dutrey 2006). These parameters appear to be inconsistent with the expectations of theoretical models which predict a semi-major axis  $> 50$  AU (Artymowicz & Lubow 1994) based on the positions of various orbital resonances and the  $\sim 180$  AU inner diameter of the circumbinary disk. Beust & Dutrey (2006) explored this discrepancy in an analysis of their results, noting that with a slightly increased error bar on the system’s observed inclination, an alternate fit to the data yield a semimajor axis of 62 AU and an eccentricity of 0.35. This orbit is consistent with the dynamical constraints implied by the inner disk edge location and with the observed projected separation of  $\sim 36$  AU (see, e.g. di Folco *et al.* 2014).

## 1.2. Goals of this work

Our goals in this work are to understand the dynamical influences that the disks and stars in a forming multiple star system have on each other, what their observational consequences are and to make inferences regarding the physical characteristics and behavior of the system based on the outcomes of numerical simulations. To those ends, we will present a series of two dimensional numerical simulations configured to model systems like GG Tau A, using the numerical code VINE. The GG Tau A system is interesting because of the depth and quality of the observations made of it, which permit it to serve as representative of a larger class of objects in which there are significant dynamical interactions between the various components. Our strategy will be largely qualitative in nature and will focus on comparisons between the observations and simulations modeling a range of plausible physical conditions for the system. Comparisons of features seen in the simulations with those in the observations will then permit us to rule out or confirm various physical properties of the system, by virtue of being consistent (or not) with those observations, and to assign their origin to specific physical phenomena active in the system.

The presence and characteristics of the binary will have influences on the circumstellar and circumbinary materials at all scales. As noted above however, the orbital parameters of the GG Tau A binary are not yet uniquely defined by observations, so the characteristics of the influence are likewise not uniquely determined. Therefore, a logical starting point for our explorations will be to study the spectrum of outcomes that different orbital parameters may produce in the behavior of the gaseous material in the system. With this in mind, our strategy will be to run a suite of simulations in which each member consists of the same circumbinary initial condition and physical model, but stars with different orbit parameters. Each member of the suite will then define a unique numerical experiment to display the consequences that a particular set of binary orbit parameters have for the system behavior, and which characteristics are common to all members of the suite. Given the simulation results, we can make assessments in terms of comparisons of the appearance of the various gaseous components to the observations. In particular, we will address three broad categories of questions appropriate for the evolution at different spatial scales. First, what are the influences of the binary on the large scale structure of the circumbinary material and what structures develop from independently of the binary? Second, what are the influences of the binary on the circumstellar material and the material ‘in transition’ between the circumbinary and circumstellar regions? Third, what are the likely orbit parameters of the binary?

We begin in section 2 with specifications of the initial conditions, the physical models and the numerical methods used to simulate their evolution. Then, in section 3, we introduce the suite of models that form the basis of our study and describe the evolution of each of the systems at large scales. In section 4, we revisit many of these same simulations, but turn our focus towards the smaller scale characteristics of the circumstellar environment. We will find

that many of the results described in these two sections are relevant to more than one of the questions just noted. We therefore limit our initial discussion to the various characteristics of the simulations themselves, with limited reference to particular observations. Then, in section 5, we compare our results to the observed GG Tau A system. There, we focus first on assessing their consistency with the observations in order to rule out less likely configurations, and then on assessing the results for their physical significance, i.e., what the models may reveal about the physical state and the evolution of the system. Finally, in 6, we summarize our results, comparing them to previous work and discussing a number of questions which may be of interest to address in the future.

### 1.3. An overview of our numerical experiments

As a guide to the reader, we briefly introduce the various numerical experiments and the goals we set for them. We introduce the main suite of simulations and begin our characterization of the evolution at large spatial scales in sections 3.1 and 3.2. A similar introduction to many of the same simulations appears in section 4.1, where we concentrate on the smaller scale, circumstellar evolution. These sections will focus on exploring the morphology of large and small scale structures developing under the tidal force of the central stellar system.

At large scales, the presence of a binary affects the evolution of the torus by continuously stirring the material, generating morphological features in response, and by heating it. Also, in the specific example of the GG Tau A torus, where the observed temperature and mass imply that it is susceptible to gravitational instabilities, we expect that features due to such instabilities to develop as well. As noted above, GG Tau A is known to harbor asymmetries and other features within its torus. Given these features, our first analyses will be qualitative: are any similar features identifiable in our simulations? We address this question in section 5.1.

After finding qualitative correspondence between features in the observed and simulated systems, we turn to investigations to couple the physical processes that are active in the system with the features they are responsible for producing. The most striking feature of the GG Tau A circumbinary material is that it is composed of two very distinct components: a torus and a disk, with a sharp boundary distinguishing them from each other. In section 3.3, we test the possibility that these two components actually have a common origin as a single primordial torus, out of which the disk forms as an ‘excretion’ feature generated by the outward mass transport driven by the propagation of spiral arms. We run simulations initially configured to include only a torus, in order to compare the behavior of such systems to the torus+disk systems already studied, focusing specifically on the relative efficiency of outward mass transport and the resulting circumbinary mass distribution.

We continue with a study to determine the relative importance of various sources of heating in the torus. This question is important because of its bearing on the susceptibility of the torus to fragment. Depending on its characteristics, if indeed any fragmentation occurs, such fragmentation may lead to the formation of additional planetary, brown dwarf or stellar components of the system. In section 3.4, we describe the behavior of two simulations in which we suppress, respectively, the radiative heating from the stars and the internal heating due to the dissipation of shocks generated both by the tidal action of the binary and self gravitating instabilities. We will expect changes in the behavior of the evolution if in fact either of these heating sources are important.

The physical significance of our results depends critically on having both an accurate inventory of the important physical processes and an accurate numerical realization of the evolution. When fragmentation driven by gravitational instabilities plays a role, accurate numerical simulations require that certain minimum resolution conditions be observed over the lifetime of the simulation. We assess the physical and numerical significance of the fragmentation behavior seen in our simulations in 5.2. Other properties of our simulations may also be affected by numerical issues, with one notable case being that they provide only very coarse resolution of the circumstellar disks. An important

consequence may be that numerical dissipation there is unphysically high, leading to unphysically high accretion rates onto the stars. As a component of our investigation of the accretion in section 4.2, we describe simulations run with two very different particle counts, thereby resolving the circumstellar accretion disks to different extents, in order to test whether or not this numerical issue affects our results.

Our suite of simulations cover a parameter space within which we expect the actual GG Tau A system to reside, though its exact state is currently uncertain. In order to set more stringent constraints, in section 3.5 we will make a number of quantitative comparisons between our simulations and the observations. In particular, we fit ellipses to the torus to determine its size and shape over time and thereby infer other properties of the system, such as the binary orbit parameters and the system’s inclination.

Other system constraints can be derived by considering the influence that the binary orbit has on the characteristics of both the circumstellar disks and material in the gap between the circumstellar disks and the torus. In section 4.2, we calculate the amount of mass transferred from the circumbinary torus onto the circumstellar disks in our simulations, to test how much this mass flux depends on the orbit parameters of the binary. We also evaluate the rates at which mass accretes from the circumstellar disks onto the stars in different system configurations. The net rate of accretion into and out of the circumstellar disks determines their lifetimes. Given long enough lifetimes, planet formation may be enhanced. We discuss this possibility in section 5.5.

## 2. Physical Assumptions and Numerical Model

The initial conditions for the simulations performed in this work are based on the observed configuration of the GG Tau A system, as discussed above, except that we have not incorporated the newly discovered binary nature of GG Tau Ab into our models. In order to investigate various aspects of the evolution, we vary the initial conditions over the plausible parameter space outlined by both observational data and theoretical analyses, exploring uncertainties in that data. The details of the physical models and the methods used to set up the initial configurations are similar to those used in Nelson *et al.* (1998, 2000, hereafter DynI and DynII, respectively) and we refer the reader to those works for a more complete exposition. In this section, we shall summarize the models described previously, and describe the details of the set up specific to the present study here.

### 2.1. The Numerical Method

We use the Smoothed Particle Hydrodynamics (SPH) code ‘VINE’ (Wetzstein *et al.* 2009; Nelson, Wetzstein & Naab 2009), to evolve our simulations forward in time. SPH is a particle based, Lagrangian method for solving the hydrodynamic equations, and so is very well suited to the complex geometry present in the multi-component systems we study. Particles naturally follow the flow, concentrating resolution specifically in regions where mass itself concentrates, and removing it and the accompanying computational cost, from uninteresting regions where little material exists. This property permits the evolution of both the circumbinary torus/disk and the circumstellar disks to be modeling at the same time in the same simulation, despite their very large difference in spatial scales. It also permits detailed studies of the the mass and momentum exchange among the different components of the system, such as between the circumbinary material and the circumstellar disks.

## 2.2. Initial Conditions

We consider a simplified model of the GG Tau system in which the ‘B’ component of the system is not included. This approximation will be reasonably accurate unless the orbit of GG Tau B has a pericenter smaller than  $\sim 800$  AU. Even when such conditions exist, we expect it to affect only the outer portions of the circumbinary disk (Beust & Dutrey 2006), at distances well beyond the regions of interest for our investigations. We further simplify our simulations by neglecting the recent observation of di Folco *et al.* (2014) that the GG Tau Ab component is also a multiple. Instead, we model the GG Tau A system as two stars, each harboring a circumstellar disk, and a distribution of circumbinary material, as described by GDS99 as a combined torus/disk configuration in orbit around the binary. Following this description, we configure the initial conditions for each of the three components of the system independently, then combine them together to create a synthesized, complete initial condition for each simulation. We discuss the set up of each component in turn.

### 2.2.1. Circumbinary Material

We model the mass distribution of the circumbinary material as a torus+disk combination. We set the dimensions of the combination such that its inner and outer edges each define a circle 180 AU and 800 AU in diameter, respectively. The outer boundary of the torus is set to 260 AU. The center of mass of the circumbinary material is set to coincide with the system barycenter. The initial conditions of the circumbinary material are summarized graphically in figure 1.

SPH particles are initially laid out on a series of concentric rings centered on the origin and extending from the inner torus/disk edge at a radius of 180 AU outwards to a radius of 800 AU. The particle distribution follows a surface density power law:

$$\Sigma(r) = S_T \Sigma_T + S_D \Sigma_0 \left[ 1 + \left( \frac{r}{r_c} \right)^2 \right]^{-\frac{p}{2}}, \quad (1)$$

where the values of  $\Sigma_T$  and  $\Sigma_D$  are adjusted to give the desired mass ratio between the torus and disk masses. GDS99 fit a power law to the volume density in the disk with a proportionality  $r^{-2.75}$ . Assuming a constant ratio of scale height to radius ( $H/r$ ), this translates to a surface density power law with exponent  $p = 1.75$ . This exponent is broadly consistent with that expected for most circumstellar disk configurations and, for the sake of simplicity, we choose the exponent  $p = 3/2$ , used in our previous work for both the circumbinary disk and for the circumstellar disks, discussed below.

The core radius  $r_c$  for the power laws is set to  $r_c=1$  AU, a value insignificant for the circumbinary material, but important for the circumstellar disks described below. In the suite of simulations described in this work, we explore both torus+disk configurations and torus-only configurations. For the torus+disk models, we define the torus mass such that it contains 70% of the total, consistent with GDS99. The two factors,  $S_T$  and  $S_D$ , are linearly decreasing functions near the torus or disk boundary, respectively. They are each defined by:

$$S = \begin{cases} 1 & \text{for } r < R - \delta; \\ 1 - \frac{(r-(R-\delta))}{2\delta} & \text{for } R - \delta < r < R + \delta; \\ 0 & \text{for } r > R + \delta; \end{cases} \quad (2)$$

where  $R$  plays the role of the defined torus or disk edge, for  $S_T$  and  $S_D$ , respectively. With this definition, the outer torus and disk edges are smoothed in the region within a distance  $\delta$  inward and outward of their nominally defined radii.

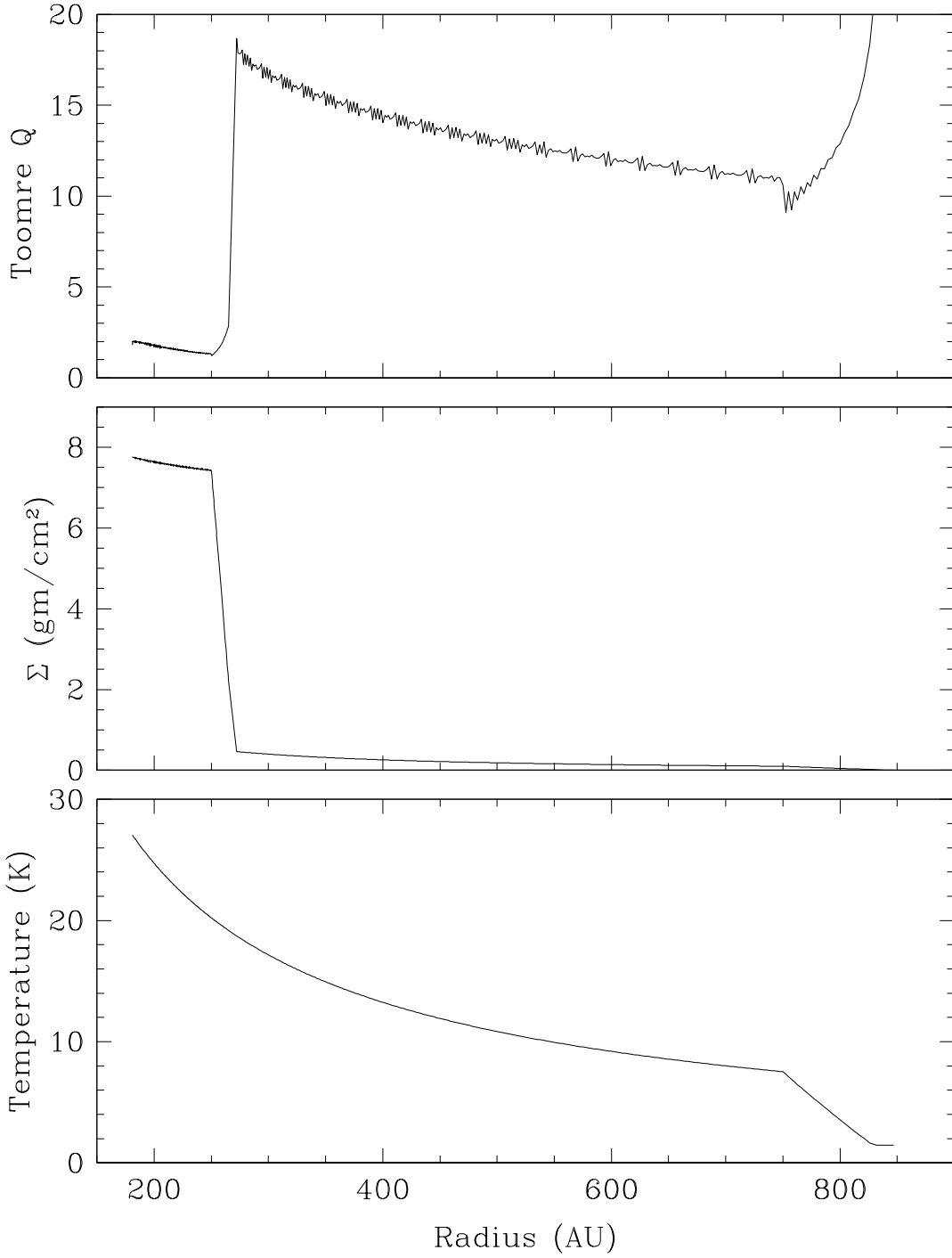


Fig. 1.— The initial condition profile in the circumbinary torus. The top panel shows the local value of the Toomre  $Q$  parameter. The middle panel shows the surface density and the bottom panel shows the temperature.



We smooth both the outer edge of the disk and the torus/disk interface. This smoothing both improves consistency with the observed width of the interface, where data are available, and side-steps the unphysically large pressure gradients that would otherwise perturb the initial condition if the interface were perfectly sharp. Consistent with the observed width as discussed in GDS99, we have chosen the width of the smoothed torus/disk interface to be  $\delta = 10$  AU. No observational constraints are readily available for the disk’s outer edge, and we choose a wider smoothing parameter of  $\delta = 50$  AU for the outer edge of the disk. As a practical matter, the inner edge of the circumbinary material is unsmoothed in order to permit a more evenly distributed initial particle configuration throughout the torus. In consequence, some small shear instabilities develop over the course of the first few hundred years of the simulations. These features are quickly overwhelmed by the larger scale evolution of the system, and so are not significant on any longer time scale.

We specify the initial thermodynamic state of the disk assuming that the specific internal energy, or equivalently, temperature, in the torus and disk follows a single power law profile, given according to:

$$u(r) = u_D \left[ 1 + \left( \frac{r}{r_c} \right)^2 \right]^{-\frac{q}{2}}. \quad (3)$$

The exponent, is set to  $q = 0.9$ , a value chosen to reproduce the fitted value obtained by GDS99 and the value  $u_D$  is chosen to reproduce, in combination with the equation of state, the observed temperature of  $T \approx 20$  K at a distance of 300 AU from the origin. As for the surface density law, the core radius,  $r_c$ , is set to  $r_c=1$ AU, which will not significantly alter the profile for the circumbinary material, but will influence the inner edge of the circumstellar disks defined below. At the outer edge of the disk, we modify the temperature profile following the same smoothing procedure as used for the surface density, such that it falls to a minimum of 3 K at the outermost extent.

Matter is set up on initially circular orbits around the origin assuming rotational equilibrium. Radial velocities are set to zero. For purposes of generating an initial state only, we replace the two binary components with a single point mass at the origin. It’s mass, of  $1.3M_\odot$ , is the sum of that assumed for the two stars used in the actual simulations. Gravitational and pressure forces are balanced by centrifugal forces by setting

$$\Omega^2(r) = \frac{GM_*}{r^3} + \frac{1}{r} \frac{\partial \Psi_D}{\partial r} + \frac{1}{r} \frac{\nabla P}{\Sigma}, \quad (4)$$

where  $\Psi_D$  is the gravitational potential of the disk and the other symbols have their usual meanings. The magnitudes of the pressure and gravitational forces are small compared to the stellar term, therefore the disk is nearly Keplerian in character.

The circumbinary material, at a mass of one tenth the combined stellar masses, contains sufficient mass to be marginally self-gravitating. The extent to which this is true is quantified by the well known, Toomre  $Q$  parameter defined as:

$$Q = \frac{\kappa c_s}{\pi G \Sigma}, \quad (5)$$

where  $\kappa$  is the local epicyclic frequency and  $c_s$  is the sound speed. Together, the conditions specified above combine to determine the radial profile for  $Q$  shown in figure 1. Within the torus values range from  $\sim 1.5 - 2$ , and we may therefore expect significant signatures of self gravitating flows. Further out, in the disk, values increase to  $Q \sim 12 - 18$ , and we expect this region will be largely insensitive to self gravitating disturbances. Note that the  $Q$  profile shown includes small amplitude ‘ringing’ oscillations, particularly in the disk, which are artifacts of the numerical derivatives (of  $\Omega$  with respect to radius) that are used to determine the epicyclic frequency. They are of little significance and may be disregarded.

### 2.2.2. *The stars and circumstellar material*

The two stellar components are each independently defined as point masses, and each is orbited by a circumstellar disk. The stars have masses of  $M_* = 0.7$  or  $M_* = 0.6M_\odot$  for the primary and secondary, respectively. These values are consistent with the total system mass determined from the rotation curve of the circumbinary material (GDS99) and from orbital motions (Tamazian *et al.* 2002). It lies slightly below the ‘best’ values derived from their luminosities and fits to evolutionary tracks (see, e.g., White *et al.* 1999, where values of  $0.78M_\odot$  and  $0.68M_\odot$  are fit for the primary and secondary, respectively), but remain within the error bars imposed by those models. As discussed in section 2.3.3, below, we incorporate a simple model of the radiative heating on the disks, supplied by the stars. Following (Roddier *et al.* 1996), we specify their luminosities to be  $L_p = 1.0L_\odot$  and  $L_s = 0.76L_\odot$ , for primary and secondary, respectively. Gravitational forces due to the stars are softened, with a softening radius of  $r_s = 0.3$  AU and, as the systems evolve, mass may be accreted onto the star if its trajectory takes it inside this radius. The mass and momenta of accreted particles are added to that of the star.

We assume that the mass of the disk around each star is  $M_D = 10^{-3}M_*$ , consistent with the observed lower limit on the mass of  $\gtrsim 10^{-4}M_\odot$  imposed by millimeter observations of the circumstellar emission (GDS99). This assumption is also consistent with the masses inferred from the more recent observations of Piétu *et al.* (2011), of  $\sim 1.5 \times 10^{-3}M_\odot$ . As for the circumbinary material, we assume the mass distribution follows a surface density power law using equation 1, with an exponent of  $p = 3/2$ . For the circumstellar disks, we omit the contribution in equation 1 due to the torus. We set the spatial dimensions of the disks to be approximately consistent with the maximum radius dynamically permitted by the orbital parameters we assume for a given simulation. Specifically, for simulations with  $a = 62$  AU, we assume the initial outer radius of each disk to be 10 AU, and for simulations with  $a = 32$  AU, we set the outer radius to be 4 AU. In each case, we smooth the outer edge, over a range  $\pm 1$  AU of the nominal edge location, following the same prescription used above for the circumbinary material.

No observations of sufficient detail exist, which may be used to determine an initial thermal state for the circumstellar disks with any precision. We are therefore free to choose conditions that provide a simple and convenient starting point, from which the disks may evolve as the various components of the system interact. Therefore, as for the circumbinary disk, we set the initial specific internal energy distribution to be a power law, identical in form to equation 3. Here again, we choose an exponent of  $q = 0.9$  for the power law, and a radial scale of  $r_c = 1$  AU. We set the initial scale of the power law,  $u_D$ , to be such that the disks are assumed to have initial minimum Toomre stability  $Q_{\min} = 1.5$ .

In practice, and as one of us found in previous work on binary systems (Nelson 2000), we will find that the initial thermodynamic properties of the disks matters very little, since they readjust both their mass and temperature distributions within a few orbits around their primary, as the system evolves. Similarly, the mass distribution also changes in response to the evolution, though on a slower ( $\sim 1000$  yr) timescale.

### 2.2.3. *Combining the Components*

Once specified as isolated systems, the two star/disk systems defined in the last section are combined to form a binary system, assuming a Keplerian orbit around the system barycenter, defined to be at the origin. For systems with an initial eccentricity, the initial positions of the stars are such that the system is at apoapse, so that the interactions between the components are at their weakest levels. We then embed this combined system into the circumbinary environment defined in section 2.2.1, replacing the single point mass originally used to as a place-holder to configure the circumbinary system in isolation. Once configured, the combined system, including the orbital elements of the

binary, is free to evolve in response to gravitational forces between all of the components.

### 2.3. Thermal Energy in the System

The thermodynamic properties of the system are very similar to those presented in DynII, and interested readers should consult that work for a detailed description. Briefly summarized, we assume that the disk matter can be approximated by an ideal gas and that radiative cooling from the disk surfaces is the only thermal energy sink. Thermal energy is generated by internal sources (shocks and viscous turbulence), implemented by means of an artificial viscosity term in the numerical method. In addition, for this work, we also employ a radiative heating model, with the two stars as the sources of radiant heating, as described below.

#### 2.3.1. The Equation of State

The hydrodynamic equations are solved assuming a vertically integrated gas pressure and a single component, ideal gas equation of state given by:

$$P = (\gamma - 1)\Sigma u \quad (6)$$

where  $\gamma$  is the ratio of specific heats,  $P$  is the vertically integrated pressure and  $u$  is the specific internal energy of the gas. The value of  $\gamma$  assumed for these calculations is the same as that in DynII, of  $\gamma = 1.53$ , for the hydrodynamical evolution and  $\gamma = 1.42$ , for the three dimensional calculation of the disk vertical structure.

#### 2.3.2. Thermal Energy Dissipation

As in DynII, thermal energy in the disks is permitted to escape from the system using a simple model of the disk’s vertical structure to determine a ‘photosphere temperature’ based on local conditions at each time step. The temperature is then used as an input into a blackbody cooling rate. The blackbody temperature is derived for each particle and at each time, using the surface density, specific internal energy and a distance as input parameters for a calculation of the temperature and density structure as a function of altitude,  $z$ , above the midplane. This calculation assumes the disk is instantaneously vertically adiabatic, plane parallel and self gravitating. From the newly derived  $(\rho(z), T(z))$  structure, we derive the photosphere temperature by integrating the optical depth,  $\tau$ , downwards from  $z = \infty$  to the altitude at which

$$\tau = 2/3 = \int_{\infty}^{z_{phot}} \rho(z)\kappa(\rho, T)dz. \quad (7)$$

In our previous work, the opacities were derived from a combination of the tabulations of Pollack, McKay & Christofferson (1985) and Alexander & Ferguson (1994). For this work, we have updated our model to use the Rosseland mean opacities from the work of Semenov *et al.* (2003). In optically thin regions, for which  $\tau < 2/3$  at the midplane, we assume the photosphere temperature is that of the midplane. As in DynII, we multiply the opacity by a factor  $R = 0.005$  in regions where the midplane temperature is above that of the grain destruction temperature, in order to crudely model the effect of grain destruction and reformation on the opacity.

The present configuration is considerably more complex than that described originally in DynII, where the disk’s vertical structure was defined assuming only the gravitational influence of a single star contributed to the vertical structure. In this work, of course, two stars contribute, each with a different relative magnitude depending on the distance of a given location from those stars. To simplify the specification of the vertical structure, we define three

distinct regions, in which one or another limiting case holds and only one point mass can be assumed to contribute the only significant external contribution to the disk’s vertical structure. For each of these limiting cases, we create separate tabulations of the vertical structure. The regions are, respectively, locations where we may assume that the gravitational forces of either the primary or secondary alone dominate the vertical structure, and locations where the combined effect of both stars contribute to the vertical structure. We assume arbitrarily that all material at distances greater than 150 AU from the system center of mass falls into the latter case. For purposes of defining the disk’s vertical structure in this region, the mass used to define the gravitational influence of the two stars is set to the sum of the masses of both stars, and its location is set artificially to the system center of mass. For material inside this 150 AU limit, we determine the distance to each star and define the material as ‘belonging’ to the closer of the two.

Given the blackbody temperature, each SPH particle loses thermal energy at a rate defined by

$$\frac{du_i}{dt} = \frac{-2\sigma_R T_{eff}^4}{\Sigma_i} \quad (8)$$

where  $\sigma_R$  is the Stefan-Boltzmann constant,  $u_i$  and  $\Sigma_i$  are the specific internal energy and surface density of particle  $i$  and  $T_{eff}$  is its photosphere temperature. The surface density  $\Sigma_i$  serves the dual purposes of first, relating the blackbody flux (quantified as an energy flux ‘per unit area’) to the specific internal energy (quantified as an energy ‘per unit mass’) used in our simulations and, second, of disambiguating the ‘surface area’ of a single SPH particle, which would otherwise suffer from confusion because of the overlap of SPH particles with each other. The factor of two accounts for the two surfaces of the disk. In regions where  $\tau < 1$  we multiply the derived flux by the optical depth,  $\tau$ , in order to more correctly model the cooling of optically thin regions.

### 2.3.3. Thermal Energy Generation

Thermal energy in the disk is generated from bulk mechanical energy via both reversible and irreversible processes during the course of the system’s evolution. Thermal energy is generated reversibly as spiral arms and similar dynamical structures become compressed and  $PdV$  work is done on the gas. Thermal energy is generated irreversibly in viscous processes and shocks. Both of the latter processes are modeled through the use of an artificial viscosity, as is common in many implementations of hydrodynamic codes. Two time and space dependent artificial viscosity terms are included. As discussed in DynII, the first is proportional to  $\nabla \cdot \mathbf{v}$  (the ‘bulk viscosity’) and corresponds to unresolved viscous turbulence in the system. The second is proportional to  $|\nabla \cdot \mathbf{v}|^2$  (the ‘von Neumann-Richtmyer’ viscosity) and corresponds to shock dissipation.

Because of the time and space dependence, an exact equivalence between the artificial viscosity and Shakura & Sunyaev (1973) ‘ $\alpha$ ’ models does not exist. However, a correspondence can be drawn between the bulk viscous term in the code and the local value of the Shakura & Sunyaev 1973  $\alpha$  (Murray 1996), which we can use to calibrate the magnitude of internal dissipation in our simulations in comparison to the model. In 2D, the correspondence can be expressed for particle  $j$  as

$$\alpha_{SS}^j = \frac{f_j \bar{\alpha}_j h_j \Omega_j}{8c_j}, \quad (9)$$

where  $f_j$  is the coefficient to reduce numerical shear viscosity for SPH simulations defined by Balsara (1995),  $\bar{\alpha}$  is the artificial bulk viscosity coefficient,  $\Omega_j$  is the orbit frequency,  $c_j$  the sound speed and  $h_j$  the smoothing length of particle  $j$ . Averaged over many particles in some suitable radial range, equation 9 provides a useful estimate of the magnitude of the artificial viscosity.

The calculations of DynII showed that the artificial viscosity produced a dissipation comparable in magnitude to an  $\alpha$  equal to a few  $\times 10^{-3}$ , but that the dissipation was resolution dependent so that the physical dissipation of the

real system was probably lower than this value. The circumbinary torus/disk configuration used in this work is both different than the circumstellar disks in DynII and is resolved with far more particles, so we do not expect dissipation at comparable levels to that work. Indeed, using the relationship quoted in Murray (1996), we find energy dissipation rates in typical regions of the torus to be an order of magnitude or more smaller, comparable to models with  $\alpha \sim 10^{-4}$  or less. In the case of the circumstellar disks, which are configured similarly to Nelson (2000), we estimate the energy generation rates to correspond to those in  $\alpha$  models where  $\alpha \sim 10^{-2}$ .

It is important to note in these estimates that while the magnitude of the dissipation in our simulations does correspond to that in a Shakura & Sunyaev (1973) model with a given parameter, the physics as realized in the simulation does not correspond directly to the physics underlying such models. Specifically, the turbulent eddies out of which the dissipation is assumed to arise are absent in our simulations, because we model only two dimensions. Rather, the presence of such dissipation is effectively an assumption that such turbulent eddies are present and are the only source of internal energy generation in the fluid. As discussed in DynII, this includes the assumption that the flow is reasonably smooth, and that strong shocks are not present.

We shall find this assumption is violated in the work presented here, as it was in our earlier work on binary systems (Nelson 2000). Strong interactions between the binary components produce large amplitude spiral structures in the circumstellar disks, including strong shocks that inevitably accompany such structures. The circumbinary material also produces large amplitude spiral structures and shocks generated by the stirring motion of the binary itself. In both cases, additional heating of the disk matter occurs. In comparison to the bulk viscosity, these heating events generate internal energy at several times the smooth ‘background’ rate in the torus, though only in a much smaller fraction of the total volume, where the spiral structures themselves are present.

In early simulations, performed only with internal heating sources, we found that temperatures in the circumbinary torus and disk fell to values well below those observed for the GG Tau A system and, in the outer regions of the disk, even to the lower limit of 3 K we have implemented in the code itself. The rate of thermal energy generation due to internal processes is less than is required to balance the radiative cooling in the circumbinary material. We conclude that a correct model of the system requires that additional, external heating sources be included in the inventory of physical processes describing the system.

Although insufficient by themselves to heat the disk and balance radiative cooling losses, we will show below (e.g. section 3.4) that heating from dynamical processes does still provide a significant source of energy input to the system. Therefore a passive radiative heating model, such as described by Chiang & Goldreich (1997), will also not be an appropriate ingredient to an accurate physical model of the system. We have therefore developed a simple model for the radiative heating of the disks by the stars, using a prescription which is similar in spirit to the radiative cooling model described above. Specifically, we assume that each star radiates isotropically at a constant luminosity, and that all of the stellar radiation impinging on the two disk surfaces (i.e. both above and below the disk midplane) is absorbed. We estimate that energy absorption rate as follows. By definition, a star’s luminosity is the energy flux that it emits per unit time, with its value per unit area of any spherical volume centered on that star being  $L_*/4\pi r^2$ . This flux falls on the two surfaces of the disk, each oriented at an angle to the radially outward directed stellar flux. The flux absorbed per unit area by the disk’s surface will be diluted from the stellar flux due to the mismatch between the normal directions of the stellar flux and the disk surface. In order to quantify the energy absorbed correctly, we must determine the size relationship between a surface element oriented radially and one oriented normal to the disk surface.

Following GDS99, we assume that stellar flux impinges on the disk horizontally and that the disk surface’s normal vector is tilted at an angle  $\gamma$ , as measured downwards from a vector pointed towards the disk’s north or south ‘pole’. Then, simple geometric arguments provide the relationship we require: the flux per unit area of disk surface will

be diluted from the flux per unit area of stellar flux by the dot product of the unit vectors defining their respective orientations. That dot product reduces to the cosine of the angle between them and, if we assume that the disk is not significantly flared, it's value will be defined at every location by it's radial distance from the star and the altitude of surface at which the disk material becomes optically thick to stellar radiation:

$$\cos(\gamma) = \frac{H_0}{r}. \quad (10)$$

Then, the rate of energy absorption of the stellar flux at any given location of the disk's surface will be given by the relation

$$\frac{du_i}{dt} = \frac{2 \cos(\gamma)L_*}{4\pi r^2 \Sigma_i}. \quad (11)$$

The factor of two accounts for the fact that both the upper and lower disk surfaces will be heated by the stellar flux. The surface density term plays the same role in this equation that it does in equation 8 above. Namely, to recast the energy flux per unit area in terms of the specific internal energy (i.e. as a change to the energy per unit mass), which is the conserved quantity employed in VINE.

The remaining unknown in equation 11 is the value of  $H_0$ , through its presence in the cosine term in equation 10. In general, the value of  $H_0$  will be different than the altitude of the disk's photosphere however, because the latter characterizes an optical thickness to its own internal radiation, rather than to stellar photons. We therefore utilize a measure of the disk's scale height, derived from the same vertical structure calculation used to determine the cooling rates described in in section 2.3.2.

As for the cooling calculations, and to simplify the model, we employ the same three limiting regions as were used in the radiative cooling model. At distances more than 150 AU from the system center of mass, we calculate vertical structure assuming a single star at the origin whose mass is the sum of the two binary components. At closer distances, the scale height is determined assuming that each SPH particle belongs to the nearer of the two stars in the binary.

#### 2.4. Limitations of the radiative heating and cooling models relevant for our simulations

The radiative heating and cooling models used in this work are deliberately simplified from the actual radiative transfer processes present in the real systems. Here we explore the implications that these simplifications make on our simulations, in order to provide insights into the conclusions we may draw from them.

As noted above, we multiply the derived flux by the optical depth,  $\tau$ , in regions where  $\tau < 1$ , in order to more correctly model the cooling of optically thin regions. The circumstellar disks and the torus region of the circumbinary material are optically thick to their own radiation throughout the calculation, so that in practice, this modification has little effect. In the circumbinary disk region however, the optical depth falls to near unity, making the disk only marginally optically thick and endangering the assumptions made in deriving the cooling rates there. Because the focus of our work is mainly on the interactions between the stars, their circumstellar material, and the torus, errors in the cooling rates at large distances, and their consequences for the dynamical behavior, will be comparatively small.

For other regions, such as the gap between the circumstellar and circumbinary material, material densities become even more tenuous, with correspondingly smaller optical depths as well. In these regions, the coupling of the material to the radiation becomes increasingly tenuous as well, and the radiative heating and cooling treatments used in our work fail to provide accurate treatments of the energy flow. Since we expect that the radiative energy fluxes into and out of the material will be substantially diminished by the reduced coupling efficiency, we simply disable both the radiative heating and cooling entirely when such conditions are found in our simulations. Specifically, when the surface density

of any given SPH particle falls to a value less than  $.05 \text{ gm/cm}^2$ , we assume that no radiative heating or cooling occurs for that particle.

As for radiative cooling, the accuracy of the radiative heating suffers in the outer regions of the circumbinary disk. Because our model assumes that thermal energy is deposited in an entire vertical column of material, rather than only in a surface layer, we overestimate the actual amount of heating there, since in fact most of the column is shielded by material closer to the stars. Because we are interested primarily in the dynamical behavior of the torus and circumstellar disks where the effect is smaller, the over estimates at larger radii will be of limited concern for interpreting our results.

## 2.5. Relevant Physical Scales

The dimensions of the GG Tau A system are typical of a number of similar systems, as noted in section 1.1, so that our models serve as prototypes for the behavior of that class. Of course, the exact dimensions of each system vary and, with them, so do the time scales important for their evolution. In order to provide a calibration for our readers, we define here several relevant time and distance scales for the initial conditions used in our simulations.

Together with the masses of the binary components, the semi-major axis assumed for the binary orbit defines its orbital period. The initial conditions defined for our simulations include setups with semi-major axes of  $a = 32 \text{ AU}$  and  $a = 62 \text{ AU}$ , which correspond to orbital periods of 158 yr and 426 yr, respectively. The orbital period of material in the torus provides another interesting timescale. Given its initial inner boundary at 180 AU and the initial condition specification above, we can estimate its orbit period to be  $\sim 2100 \text{ yr}$ . These orbit radii, together with the inner torus edge, define dimensionless ratios of  $R_T/a \sim 5.6$  for the 32 AU semi-major axis, and  $R_T/a \sim 2.9$  for the 62 AU semi-major axis, where  $R_T$  is the torus' inner radius.

We defined the initial configuration of the circumstellar disks to have outer radii that are each a large fraction of the orbital separation between the components making up the binary, consistent with our expectation that such a configuration will be nearer to the 'asymptotic' long term configuration. As the simulations proceed, they will grow or shrink according to the amount of accretion into the circumstellar environment from the torus and the amount of accretion out of the disks onto the star around which they orbit. In this context, another relevant dimension for the system is the limiting distance for stable orbits around the star to exist. Holman & Wiegert (1999) have calculated such criteria for a variety of system configurations and, for the systems studied here, derive outermost stable radii of  $\sim 10.5$  and  $\sim 15.5 \text{ AU}$  for the  $a=62 \text{ AU}$  systems with eccentricity of  $e = 0.3$  or  $e = 0$ , respectively, and  $\sim 5.4 \text{ AU}$  and  $\sim 8 \text{ AU}$  for the  $a=32 \text{ AU}$  systems with  $e = 0.3$  and  $e = 0$ , respectively. These radii are slightly larger than the initial sizes of the disks in our study. The difference does not imply any inconsistency in the model because we anticipate (and as we shall observe below, correctly so) that the disks will quickly reconfigure themselves according to the dynamical evolution of the system, and because the present calculations include hydrodynamical effects not addressed in Holman & Wiegert (1999).

## 3. Evolution of the Circumbinary Environment

Using the initial conditions and physical models described above we have performed a number of simulations modeling systems similar to GG Tau A. The simulations typically follow the evolution for 6500 yr, corresponding to approximately three orbits of the inner edge of the circumbinary disk. These times also correspond to  $\sim 16$  binary orbits for the 62 AU series, and to  $\sim 41$  orbits for the 32 AU series. Complete specification of the initial parameters

of the simulations are listed in table 1. In the discussion below, we will often refer to the two classes of simulations as the ‘wide’ (62 AU) binary simulations and ‘close’ binary (32 AU) simulations. We examine the qualitative nature of our simulations first, then examine in detail the structures which form and their physical origin.

### 3.1. Systems with Eccentric Orbits

The analyses of the proper motion data lead to two alternatives for the orbital motion of the stars in GG Tau A, with  $a = 32$  AU and  $a = 62$  AU. In both cases, the orbital eccentricity is calculated to be  $e \approx 0.3$ . In this section, we examine the results of two simulations, each with eccentricity  $e = 0.3$ , but with differing semi-major axis, referenced in Table 1 as simulation *Wide3ehi* ( $a = 62$  AU) and *Clos3ehi* ( $a = 32$  AU).

#### 3.1.1. Wide Separation

In figure 2 we show twelve images<sup>1</sup> of the same simulation, *Wide3ehi*, at the same orbital phase, spread over 16 orbits of a binary orbiting with semi-major axis  $a = 62$  AU. The mass distribution in the initial condition, seen in the first frame, is completely axisymmetric and clearly shows the various components in the idealized initial configuration we employ in all of our simulations. As the simulation time increases and the system begins to evolve (frames 1-3), the mass density begins first to exhibit many small scale disturbances at the interface between the torus and disk near  $\sim 250 - 300$  AU, which penetrate into the low density disk surrounding it. Larger scale disturbances are present in the mass distribution at the torus’s inner boundary as well. We attach little physical significance to these early time features and instead attribute them merely to the growth and relaxation of ‘start up transients’ related to our idealized initial condition for the actual complex system.

After the first several orbits of the binary, such small scale instabilities have been largely overwhelmed by the growth of features driven by the strong stirring action of the stars on the circumbinary material. Initially, the torus condenses into a narrowly peaked structure some 10-20 AU in radial extent, with several higher density lumps approximately equally spaced in azimuth. Later, after 6-8 binary orbits and as the results of interactions between the torus and binary begin to accumulate, the density inhomogeneities become more and more widespread. At this time, the lumps have largely dissipated, and the ring itself has broken up into several filamentary spiral arms, each of which contain still finer scale substructure.

Over time, the original sharp inner edge of the torus becomes progressively more ragged and diffuse as the binary interactions perturb it. As it evolves, it both moves inwards towards the stars and its shape changes, becoming significantly non-circular and producing spiral streams that extend inwards towards the binary. As pictured, the inner edge of the torus appears similar to an ellipse whose semi-major axis is approximately perpendicular to the axis joining the two stars. Because each of the images in the mosaic is generated at the same orbital phase, the relative phase of the binary orbit and the elliptical torus edge appears nearly constant. We will explore the extent to which this is always true in section 3.5, below.

At larger radii, and as they begin to overwhelm the start-up transients, spiral structures become ubiquitous features

---

<sup>1</sup>Note that for ease of comparison, we will use identical color maps, with identical scales and limits in this and all other similar figures throughout the paper, although in a few images the limits will be exceeded in small regions. Also, note that each of our figures show the system as represented by the positions of each SPH particle directly, rather than as interpolated onto a grid based graphical representation. We believe that although the images may appear somewhat granular using this manner of presentation, the viewer will be left with a better sense of both the physical system state and its numerical realization.



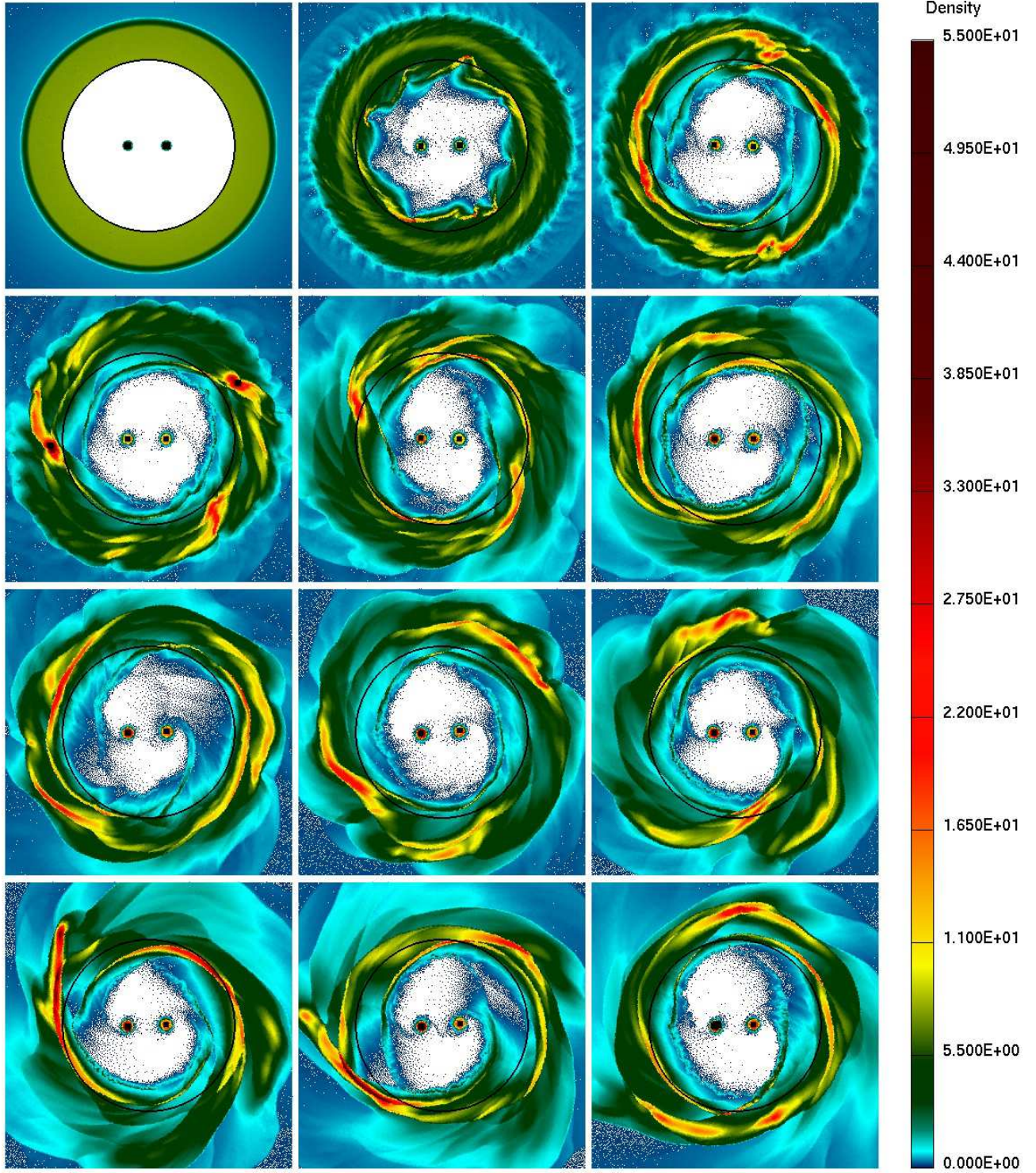


Fig. 2.— The morphology of the circumbinary material at successive apoapse passages of the binary, for simulation *Wide3ehi*. Each frame defines a  $600 \times 600$  AU region centered on the system center of mass. Ordered from top left, the first five frames are shown at time intervals of two complete binary orbits, while the next seven frames are separated intervals of one orbit.

throughout the torus at all times in the simulation. The spiral structures are generated by a combination of self gravitating instabilities and the stirring action of the stars in their orbit. The finer scale substructures in the torus are largely the remnants of streams of material which propagate through the gap region and return to the torus. The details of the size and shape of these streams vary from one orbit to the next. For some orbits, long streamers of material are visible extending inwards towards one or the other star, while in others they are nearly absent. We will discuss the behavior of these streams over the course of one binary orbit in detail in section 4.1. Of importance for our discussion here however is the fact that comparatively little material is actually accreted into the circumstellar environment compared to the fraction that returns to the torus. Instead, most material falls through the gap, interacting with one or both stars only through a relatively distant encounter during which only its trajectory is changed. Then, as it continues on its new trajectory, material begins to propagate outward again, returning to the torus from which it originated.

### 3.1.2. Close Separation

In figure 3, we show twelve images of the *Close3ehi* simulation, each at the same orbital phase, spread over 47 orbits of a binary orbiting with semi-major axis  $a = 32$  AU. As in the prototype wide orbit configuration in the last section, the mass distribution in the circumbinary disk first begins to exhibit small scale inhomogeneities which we attribute to start up transients as the simulation begins to evolve away from its idealized initial configuration. After  $\sim 1500$  yr of evolution (frame 3), larger scale structures develop in the torus, which extend throughout its radial extent. Unlike the wide orbit case however, the structures are more filamentary in character, with no features comparable to the radially narrow, peaked structure noted in panel of figure 2 developing, even at later times. Instead, smaller amplitude spiral structures develop which, after  $\sim 5000$  yr (panel 7-9), begin to organize into larger scale condensations. These condensations continue to grow and coalesce over the next  $\sim 2000$  yr and, in the final configuration of the simulation, only one remains. We expect that if the simulation were to continue, this fragment would continue to grow, perhaps to a size at which it would begin to disrupt the disk itself. We will discuss what interpretation should be given to such fragments in section 5.2.

Over the lifetime of the simulation, the inner portion of torus material migrates inwards towards the stars, with its inner edge eventually reaching distances from the system center of mass of only about half of its original distance. Unlike the wide orbit case, large streamers of material do not appear in the gap region and, to the extent that they are present at all, they do not change their character from one orbit to the next. This behavior is consistent with the increased distance from the stars to the inner edge of the torus and the correspondingly smaller perturbing influence that they exert on it. Even at late times, when the streamers appear most distinct, they do not extend inwards to the positions of the stars or their disks as much as is seen in the wide orbit case above. Instead, they appear as extensions of the spiral structures further out, and we associate their presence to the fact that precursors of the fragments noted above have begun to influence the torus morphology.

## 3.2. Systems with Circular Orbits

The behavior of the circumbinary environment surrounding a system with an eccentric orbit will of course differ from that of a circular orbit, due to the presence or absence of time variations in the strength of the gravitational forces exerted by the stars. We have investigated these differences with a set of simulations whose conditions are identical to those in sections 3.1.1 and 3.1.2, except that we assume that the orbit of the binary is defined by an eccentricity of  $e = 0$ . We show the system configurations at the end of each simulation in figure 4, for the same two semi-major axes

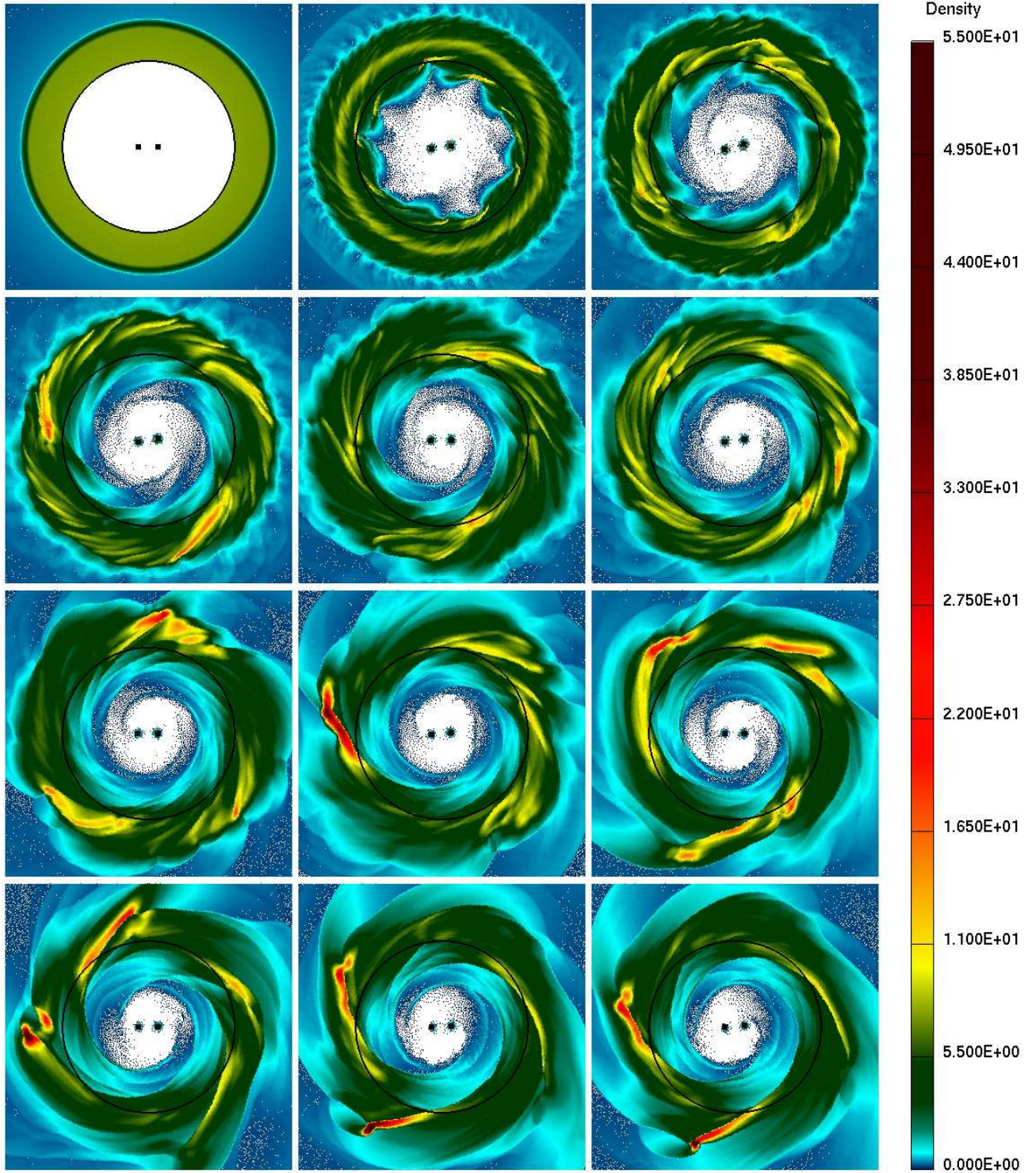


Fig. 3.— The morphology of the circumbinary material at successive apoapse passages of the binary for simulation *Clos3ehi*. Each frame defines a  $600 \times 600$  AU region centered on the system center of mass. Ordered from the top left, the first nine frames are shown at time intervals of five binary orbits, while the last three frames show intervals of three, three and one binary orbits each.

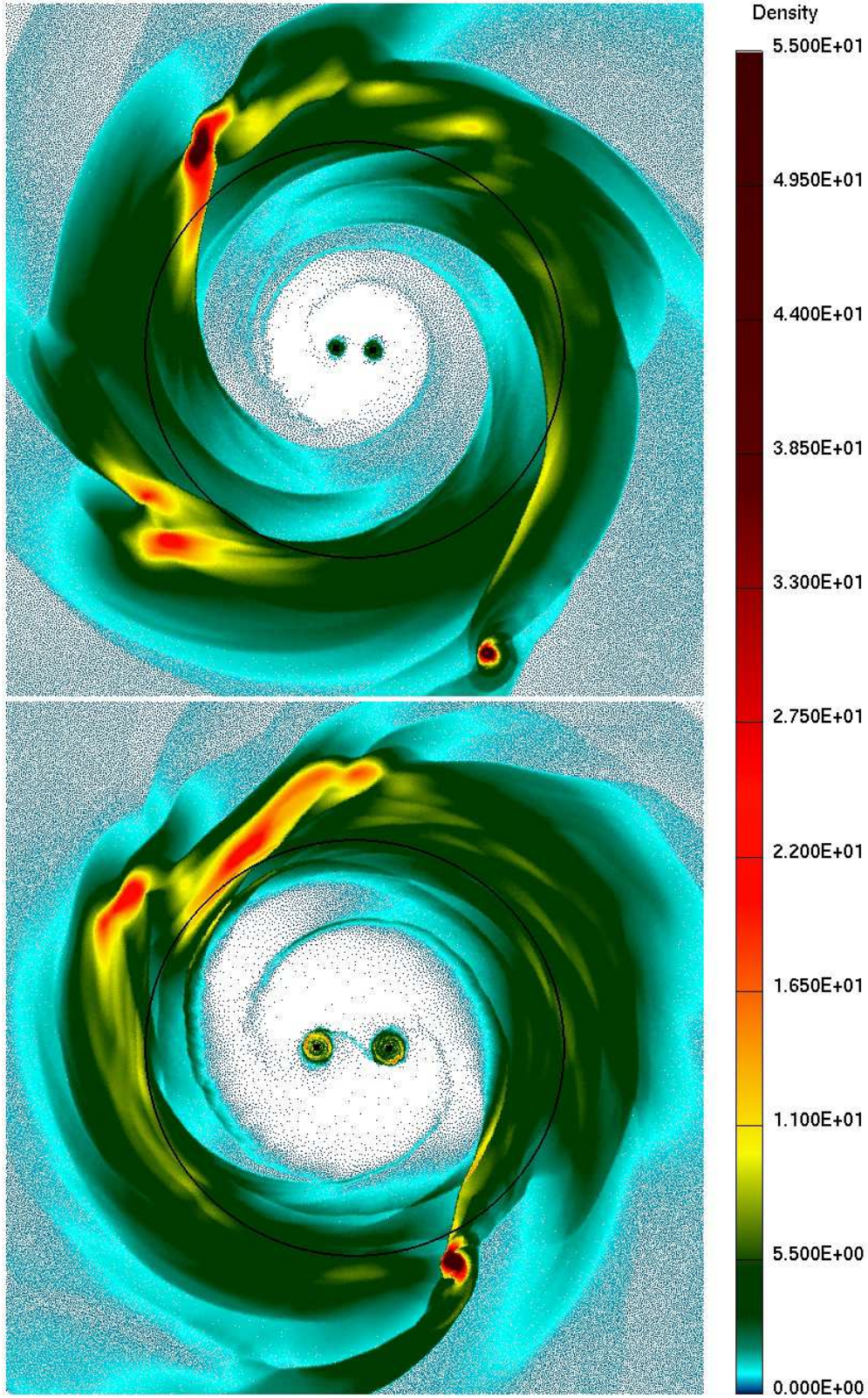


Fig. 4.— The morphology of the circumbinary material at the end of each of the two  $e = 0$  configurations in our study. In the top panel we show the variant with the ‘close’ binary orbit separation ( $a = 32$  AU, *Clos0ehi*), while in the bottom panel, matching ‘wide’ binary orbit separation ( $a = 62$  AU, *Wide0ehi*) simulation. Each frame defines a  $600 \times 600$  AU region centered on the system center of mass, shown after evolving for a time of  $t \sim 3.3$  (top) and  $t \sim 3.1$  (bottom) orbits of the torus’ inner edge, as noted in table 1.

( $a = 62$  AU and  $a = 32$  AU) described in sections 3.1.1 and 3.1.2 above.

In both the wide and close cases, the inner edges of the tori have moved inwards over the time scale of the simulation to radii of 120-140 AU from the system barycenter or less. Both models show evidence of streams of material present in the gap region. Although less pronounced than in the  $e = 0.3$  cases, they extend further inwards towards the stars, likely because they are not disrupted to as great an extent by close encounters with the stars. Relative to each other the wide binary configuration shows more massive streams than the close binary configuration, as was the case in the  $e = 0.3$  models. In addition, the wide configuration also exhibits a small band of material joining the two components, which appear to originate from material pulled from the outermost extents of the circumstellar disks. Closer to the stars, the circumstellar disks exhibit only minimal spiral structure, with the highest densities found in the outer extents of the disks rather than close to the stars.

The spiral structures that develop in each torus are much more diffuse in character than in the corresponding  $e = 0.3$  simulations, and exhibit much less internal structure. In consequence, the outer edges of each torus are both more circular and less sharply defined than in the eccentric binary cases, where well defined edge features form as structures propagate through the tori to their outer limits. In spite of the less pronounced spiral structure, the circumbinary tori in both simulations have produced large fragments, some 10-20 AU in diameter. In each case, the fragments have grown to such an extent that they have begun to generate large amplitude spiral wakes in the torus, independently of the influence of the binary's stirring action. We will discuss the physical significance of these fragments in section 5.2.

### 3.3. Angular Momentum in the System

The observed, two-component torus/disk configuration of the GG Tau A circumbinary material provides a challenge for simple models of star formation to reproduce. While one can easily imagine mechanisms by which the actions of the binary conspire to keep a sharply bounded inner 'gap' region clear, similar arguments are more difficult to make at the outer edge of the torus. How did a sharply bounded torus form with a surrounding low density disk, and how is the structure maintained in the system over time?

An important result of the sections above was to show that the stirring action of the binary on the surrounding material is very strong, with large scale spiral structures being continually generated. Such stirring serves as a foundation for the model described in Pringle (e.g. 1991) for example, and one consequence he describes is the formation of an 'excretion' disk as a portion of the circumbinary material gains angular momentum from the binary and moves outwards in response. Is this mechanism the origin of the low density disk in the GG Tau A system? In this section, we explore this question first by simulating the evolution of a family of systems in which the initial circumbinary configuration includes *only* a torus with the same mass as the combined torus/disk configuration as above. Then, we study behavior of the torques generated by the the stars and torus on each other.

#### 3.3.1. Torus-only Initial Configurations

Figure 5 shows the counterparts of each of the four torus/disk configurations described above, each after evolving for  $\sim 6500$  yr. As in the torus/disk models discussed above, torus material migrates inwards, partially filling the gap region between the circumstellar environment and the initial inner boundary of the torus. The gap region in the close binaries is visibly smaller in size than in the wide, and more in the  $e = 0$  cases than in the eccentric orbit cases. In every case, and similarly to the torus/disk models above, well defined spiral structures form in the tori and, in several

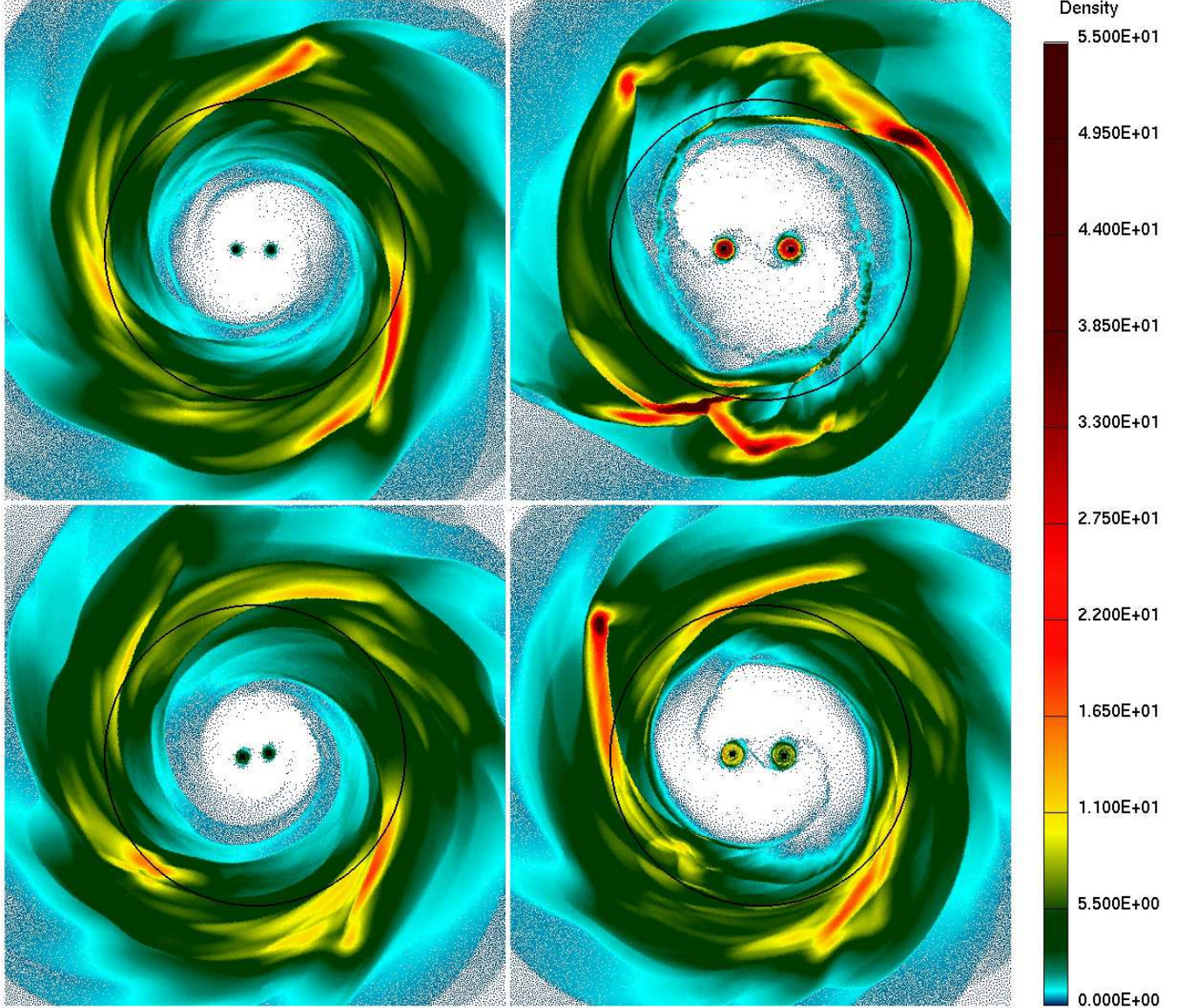


Fig. 5.— System configuration of four simulations which assume all material in the circumbinary environment is initially located in a torus. Each panel shows the configuration at the binary’s apoapse for the time closest to  $\sim 6500$  yr of evolution, corresponding to  $t \sim 3.09$  torus orbit periods, such that the systems have evolved for a similar amount of time. The top panels show the two simulations with the assumed binary eccentricity set to  $e = 0.3$  (*ClosT3ehi* and *WideT3ehi*), while the lower panels show the two configurations with assumed binary eccentricity set to  $e = 0.0$  (*ClosT0ehi* and *WideT0ehi*). The right and left panels show the  $a = 32$  AU and  $a = 62$  AU semi-major axes, respectively.

examples, they fragment into clumps. In all cases, the spiral structures are driven by the stirring action of the stars and propagate outwards, carrying material as they do so. Also as in the torus/disk models, the edges of the spiral arms are sharply defined, particularly in the two wide binary examples where the stars interact more strongly with the torus. Although sharply defined during their passage through the torus, they become less and less distinct at greater distances from the system center, eventually reaching a lower and smoother background density at distances beyond the original outer edge of the torus.

The presence of material at large separations is evidence for some level of outwards mass transport in the system. Figure 6 shows the amount of mass found there as a function of time for each of the simulations. As defined in the figure, the ‘outer disk mass’ is defined as the amount of mass found at radii larger than an arbitrarily defined critical distance from the system barycenter. Guided by the results we will describe in section 3.5 below, we set a value of 350 AU for this radius, which we choose as a compromise between capturing the true mass of the disk component over time, and masking out transient changes to it that are due to portions of the torus flexing such that parts of it extend beyond our critical radius.

In every case, the mass increases over time, showing that the process itself is robust across a wide variety of configurations. The magnitude and overall pattern of the mass transport varies however, both from simulation to simulation and from time to time within the same simulation. After  $\sim 3$  torus orbits, corresponding to 6500 yr run time of the simulations, the total mass transport corresponds to about 5% of the total initial mass of the circumbinary material in the torus+disk systems, and is 2 – 3 times higher, at  $\sim 15\%$ , in the torus only systems. In the torus+disk runs, the outer disk mass increases at a near constant rate, with small oscillations visible, superimposed on the long term trend. In contrast, in the torus only runs, the mass transport is almost entirely limited to the first  $\sim 3000$  yr of the evolution, with the outer disk mass becoming essentially constant thereafter or even decreasing slightly. Only in the last  $\sim 500$  yr of the runs, does the outer disk mass begin to increase again.

The duration of our simulations are long in the context of the circumstellar environments and the number of binary orbit periods we simulate. Unfortunately, they are short in comparison to the orbital timescales of circumbinary material, where a time of 6500 yr corresponds to only 2 – 3 orbits. Therefore, due to the high cost of running the simulations, we have not followed the evolution for the long times required to determine whether or not the outer disk masses return to their high rate of growth, or if the decrease is simply a signature of the overall flexing action of the circumbinary structures as they respond to the binary’s stirring action. We are therefore unable to conclude that the outward material migration will continue at the same rate or decrease, or even if time variations within a given simulation continue indefinitely. Nevertheless, the fact that the outer disk mass increases in all of our models, is strong evidence that the excretion process will continue in the initially torus-only systems, such that they evolve to become robust torus+disk systems.

Given the rate of outward material movement, and the fact that the disk in the GG Tau A system is observed (GDS99) to contain a mass of  $\sim 0.04M_{\odot}$ , the entire disk could be generated from such transport activity within a few  $\times 10^4$  yr. We therefore conclude that the disk material surrounding the GG Tau A torus most likely originates as torus material which was thrown outwards by the stirring action of the binary.

### 3.3.2. *Torques on the stars and gas*

Gravitational torques between the stars and circumbinary material play an important role in their mutual evolution. Here, we turn to a study of these torques, in order to understand their importance in forming multiple star systems like GG Tau A.

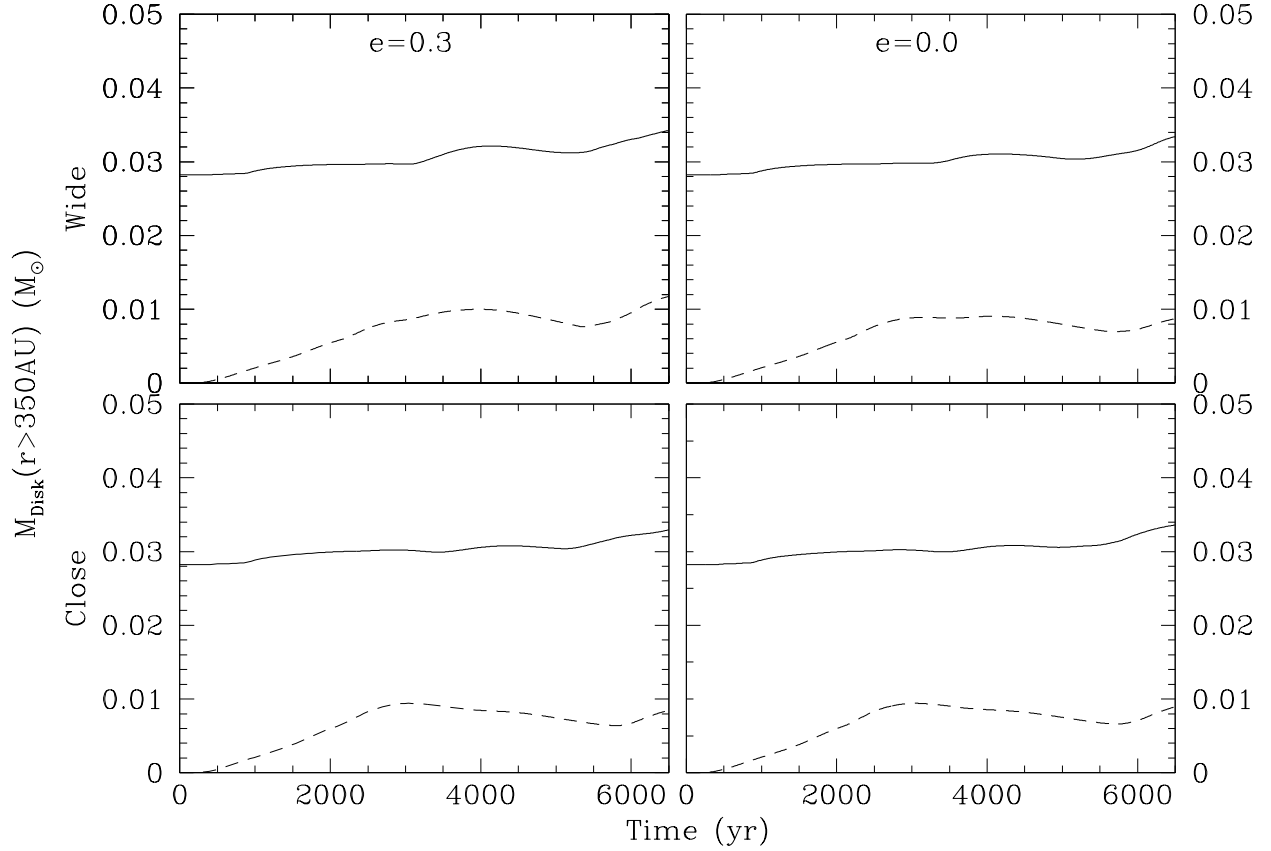


Fig. 6.— The mass further from the system barycenter than 350 AU as a function of time, for each of the torus-only and torus+disk models in our study. The top and bottom panels show the set of wide (62 AU binary orbit) and close (32 AU binary orbit) runs, respectively. The right and left panels show the circular and eccentric orbits, respectively. The dashed lines in each panel show the masses for the simulations with torus-only initial conditions. The solid lines show the masses for the simulations with torus/disk initial conditions.



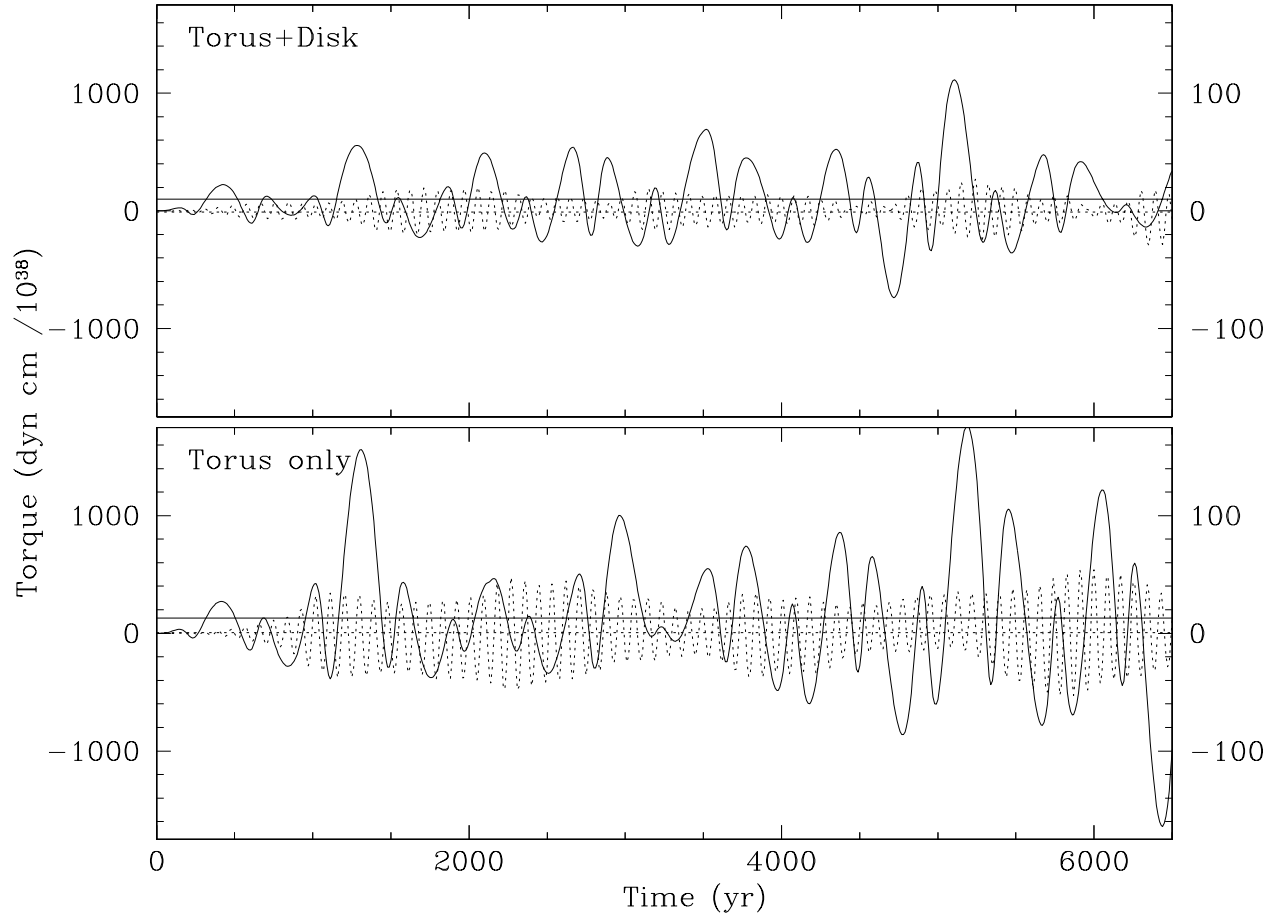


Fig. 7.— The total torque exerted on the circumbinary material as a function of time by the stars, as calculated about the system barycenter. Wide orbit simulations *Wide3ehi* and *WideT3ehi* are shown with solid curves, while close orbit runs *Clos0ehi* and *ClosT0ehi* are shown with dotted curves. The torus+disk models appear in the top panel and torus-only models in the bottom panel. The left axis labels correspond to the wide orbit models, while the right axis labels (expanded by a factor ten) correspond to the close orbit models. The horizontal lines define the time averaged torques for each of the simulations shown.

Torques between the stars and the torus will affect both and, if large enough, cause measurable changes even over the comparatively short duration of our simulations. Figure 7 shows the net torque exerted by the stars on the circumbinary material. In all cases, the torque magnitudes vary both in amplitude and sign on time scales comparable to the orbit periods of the binaries. Also, while oscillations are correlated with the binary orbit, consecutive peaks and troughs are neither evenly spaced in time nor are their amplitudes the same. The amplitude of the variations are larger in the torus-only systems than in the torus+disk systems, consistent with the increased mass concentration in the former case. With few exceptions, the magnitude of the peaks in the wide orbit examples exceed the magnitude of adjacent troughs, such that the average over many orbits is positive. As seen, e.g., in section 3.1.1 above, the torques from the binary drive strong spiral waves into the torus in wide configurations, but are much less effective in the close configurations shown later. Their absence leads to the question of what process remains to drive the excretion flow discussed above? We note that, while stellar torques are weak in such systems, torques due to self gravity remain, and we conclude that they are important contributors to the excretion flow.

With a change in sign, the total torque on the circumbinary material is the same as that on the binary. To what extent do torques of these magnitudes alter its orbit over time? Pringle (1991) makes estimates using a diffusion approximation based analysis where the torques are mediated by viscosity. Here, no such model is required, since we have a direct quantification of the torques from the simulations themselves. We therefore estimate the time scales using time averaged torques determined directly from the curves shown in figure 7. While the torques in the wide orbit runs exhibit positive maxima of  $\sim 5 - 10 \times 10^{40}$  dyn cm and negative minima of  $\sim 1 - 5 \times 10^{40}$  dyn cm, their averages over time take on values near  $\sim 1 \times 10^{40}$  dyn cm. The circumbinary material thus gains angular momentum at the expense of the binary, consistent with the analysis in Pringle (1991). The close orbit torques are each more than an order of magnitude smaller and are also more nearly symmetric over their positive and negative extrema, with time averages consistent with zero net torque.

Neglecting factors near unity, the net angular momentum of the stars around the system barycenter is given by Pringle (1991) as  $J_* = M \sqrt{GMa}/4$ , with  $M$  being the combined mass of the two stars. The time scale for changes in the semi-major axis is  $\tau = 2J_*/(dJ/dt)$ . In terms of the parameters of the wide and close orbit systems, the angular momentum translates to numerical values of  $\sim 2.5 \times 10^{53}$  or  $\sim 1.8 \times 10^{53}$  gm cm<sup>2</sup>/s, respectively. Thus, combined with the time averaged torques derived from figure 7, the timescale for significant changes to the semi-major axis becomes  $\tau \lesssim 1.4$  Myr for the wide systems and  $\tau \gtrsim 100$  Myr for the close systems. The long time scales in the close orbit models, in Pringle’s interpretation, correspond to a system in an initial phase where the torus has yet to ‘find out’ about the presence of the binary. In contrast, the shorter time scales in the wide orbit simulations correspond to the period in which the torus is gradually expelled by the torques applied by the binary. They are also comparable to the pre main sequence lifetimes of stellar systems (Haisch, Lada & Lada 2001), indicating that the final GG Tau A system configuration has yet to be established.

### 3.4. Comparison to the evolution of systems with reduced heating

Before we may conclude that the action of the orbiting stars on the circumbinary material is significant for the overall evolution of the system, we must compare the results of our simulations to systems with analogous configurations where the binary is not present. Similarly, in order to conclude that the radiative heating from the stars is important, we must compare to simulations in which that heating is omitted. To those ends, we have configured and run a simulation in which the radiative heating term has been neglected, and another in which we have replaced the two components of the binary with a single star of the same mass, located at the origin. In order to provide a similar level of heating to the system, this ‘star’ radiates with a luminosity equal to the sum of the luminosities of the binary components.

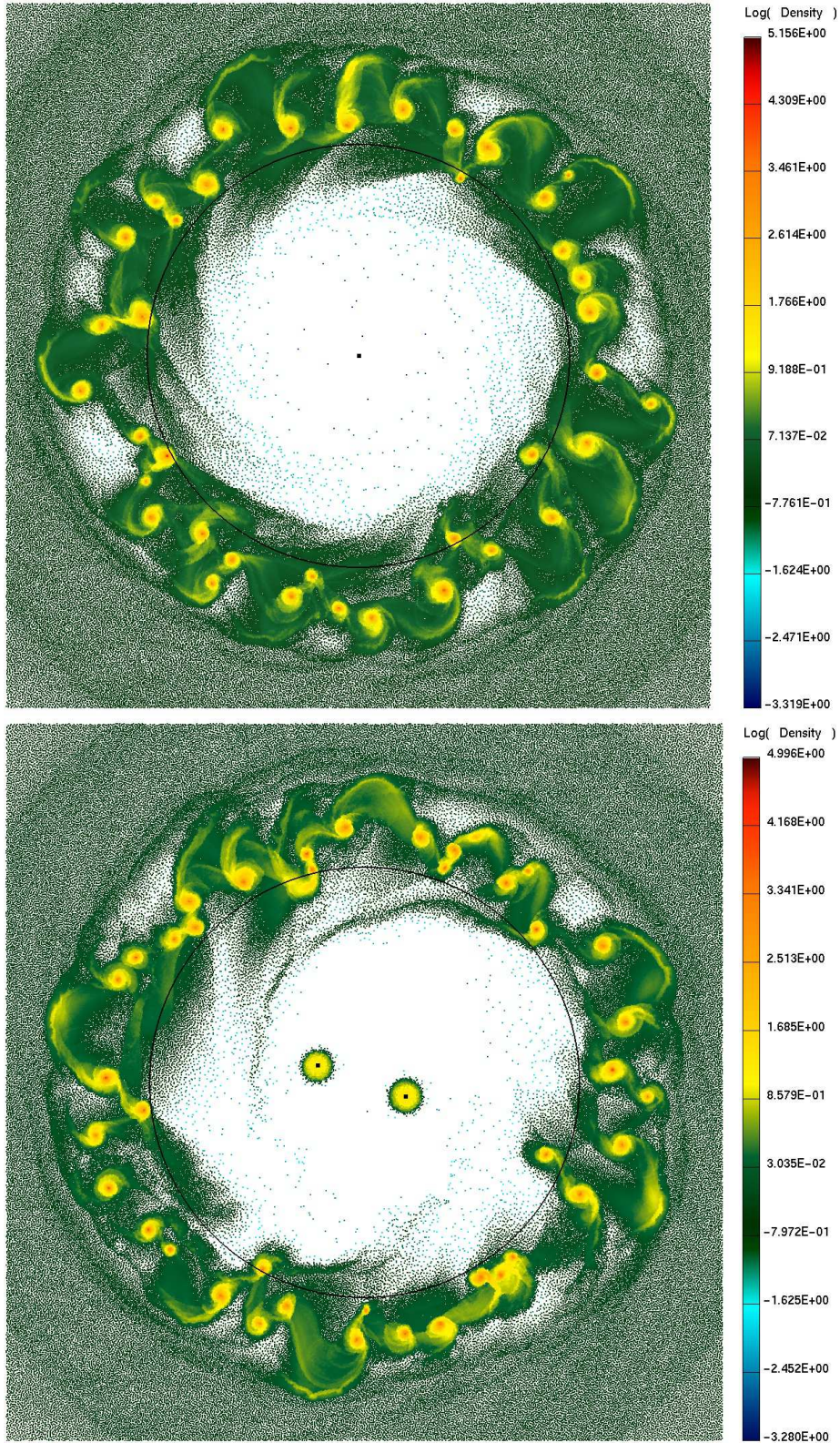


Fig. 8.— The surface density morphology of simulations *Singlehi* (top) and *Noheat3ehi* (bottom), each after  $\sim 2100$  yr (approximately one orbit of the torus) of evolution.

Figure 8 shows the results of these simulations after they have evolved for  $\sim 2100$  yr, corresponding to one orbit of the inner edge of the torus. The image shows that in each case, approximately 38-39 separate clumps have formed from the initially smooth tori during this comparatively short timescale. Although not shown in the images themselves, these clumps initially appeared after only  $\sim 1400$  yr of evolution and continued to develop further as the simulations proceeded. We monitored the status of the simulations for adherence to the numerical resolution requirements discussed in Nelson (2006) and found that these clumps are indeed sufficiently resolved according to the criteria described there.

Evidence for self gravitating instabilities is present in the torus region of all of our other simulations, including several which exhibit one or more clearly developed fragments. However, even the simulations in which fragmentation was observed do not produce fragments so quickly or in such large numbers. In this regard, the configurations that develop here are unique in our suite of simulations, and follow a clearly different evolutionary path than any of the simulations that include both the binary components and radiative heating. Since such ubiquitous fragmentation requires cold torus material, and the action of the stellar irradiation and the tidal interactions of the binary will be to increase the internal energy of the material, we conclude that both the stellar irradiation and the stirring action of the binary are critical contributors to the overall thermodynamic state of the circumbinary environment of GG Tau A.

### 3.5. Quantitative metrics of the circumbinary material

In the sections above, we have discussed the overall morphology of the circumbinary material as it evolves using qualitative metrics of its behavior. We now turn to more quantitative metrics to describe the evolution. In particular, we have noted above that the torus appears to flex both radially and azimuthally over time, with various components moving both inwards and outwards as spiral waves pass through them. Here, we quantify the changes in the shape of the torus, by fitting its shape to a set of three ellipses, chosen as approximations of its inner and outer edges and its midpoint. In the following sections, we show example fits at two snapshots in time in order to illustrate the fidelity of the fits to the underlying data, and then as functions of time, in order to show their variations as the system evolves.

For each ellipse, we fit for three important quantities: its semi-major axis, its eccentricity and its orientation. We discuss the fits for the two simulations *Wide3ehi* and *Clos0ehi*. We choose the first because both the binary’s wide orbit (semi-major axis) and its eccentricity carry it closer to the torus than any other. We choose the second for exactly the opposite reason: its tighter orbit and zero eccentricity mean that it stays most distant from the torus over the course of its orbit. We expect that these system configurations will therefore bracket the parameters for which the effect of the binary on the torus is the largest and smallest of all the configurations in our study.

#### 3.5.1. Generating fits from the simulation data

SPH particles do not easily lend themselves to standard procedures for generating fits to the ellipses we use to model the system shape. Therefore, in order to generate fits, we first map the surface density of the disk material onto an  $1800 \times 1800$  Cartesian grid, on which the fitting can be accomplished straightforwardly. The grid has spatial dimensions of  $900 \times 900$  AU and is centered on the origin, such that each grid cell is 0.5 AU in linear extent. The mapping implements the same interpolation procedure as is used in the SPH algorithm to determine the surface densities for each particle in the simulation itself. Unfortunately in the present context however, the resolution afforded by our simulations and the mapping retains very small scale features in the flow, including accretion streams and other spiral structures only peripherally associated with the torus. This level of detail frequently causes the fitting procedure outlined below to produce poorer fits of the large scale torus morphology in favor of matching these peripheral struc-

tures. In order to more accurately capture only the large scale features of the torus, we therefore convolve the density mapping with a Gaussian PSF with a characteristic length scale (i.e., its half-width, half maximum) of 10 AU.

With this modification of the density mapping, we compute an azimuth averaged surface density and extract a maximum over all radii. This maximum is used, in turn, as a critical value to extract the set of all grid points lying on three distinct isodensity contours. We define one such contour by the condition that the local surface density matches the maximum azimuth averaged value, and two others by the condition that the local density is 20% of that maximum value, and falls either radially inside of, or outside of, a circle centered on the origin and 220 AU in radius. These contours correspond roughly to the torus’ inner and outer boundaries and to its high density core. Finally, given the points defining the three contours, we use the Numerical Recipes routine ‘`mrqmin`’ (Press *et al.* 1992) to extract the semi-major axis, the eccentricity and the axis of pericenter for the best fit ellipses to each isosurface. In addition to the three fit parameters, we also permit the origin of each ellipse to be offset from the system barycenter in the  $x$  and  $y$  coordinates, taking the final ellipse parameters from the offset for which the  $\chi^2$  value for the fit is minimized.

In order to avoid contamination of our fits by circumstellar material, we mask out a circular region of the grid, centered on the origin. Its radius is defined to be slightly larger than the largest extent to which the circumstellar material extends at any time during its orbit, which will occur when the binary is at apoapse and also includes the combined radii of the two circumstellar disks. Specifically, we define radius of the circumstellar mask region as:

$$r_{mask} = \frac{a(1+e)}{2} + f(r_1 + r_2). \quad (12)$$

With the identification of the semi-major axis and eccentricity of the binary using their usual identifiers,  $a$  and  $e$ , the first term defines half the apoapse separation of the binary components. In the second term, the quantities  $r_1$  and  $r_2$  are each defined using the expression derived in Holman & Wiegert (1999), to approximate the largest radius for which an orbit around the star is stable over a suitably long duration. We multiply the combined radii by a scale factor,  $f = 1.5$ , to account for the fact that material may be present intermittently at larger distances from each star for shorter durations than are accommodated by the Holman & Wiegert (1999) formalism.

Figure 9 shows isodensity contours and fits for simulation *Wide3ehi*, at each of the three locations defined above, both as raw contours and as convolved with a 10 AU PSF. The times at which the fits were obtained correspond to the same apoapse and periapse passages shown in figure 13, below. In each panel, the fitted ellipses are shown along with the contours but are frequently obscured by the data, visually demonstrating the fit quality. Although the differences between the raw and the convolved contours are not large, they are nevertheless significant. For example, in the case of the maximum isodensity contours (center panels), the accretion streams are eliminated in the convolution. Little change occurs in the fitted ellipses in these cases, but both the inner and outer contours exhibit much larger differences, particularly so in the case of the orientation. For example, the difference is  $\sim 15 - 20$  degrees in each of the two snapshots of the outer contour, a value comparable to the precession angle over the timespan of the two fit times. The largest differences are seen in the fits for inner contour at apoapse (upper left panel), where the difference is nearly 90 degrees. The inner contours are also those for which both the difference between the two times is most significant and the fidelity of the fit to the underlying data is least accurate. While the apoapse snapshot (top) requires significant eccentricity for a good fit to both the raw and convolved data, the periapse snapshot (bottom) is best fit to a much more circular shape. In this case, although the contour is indeed intrinsically more circular, the fit remains compromised by the incompletely obscured presence of the accretion streams in the contours which contribute non-negligibly to the fit. We conclude that while our fits to the middle and outer contours are minimally affected by such features, fits to the inner contour will be of lesser quality due to such contributions.

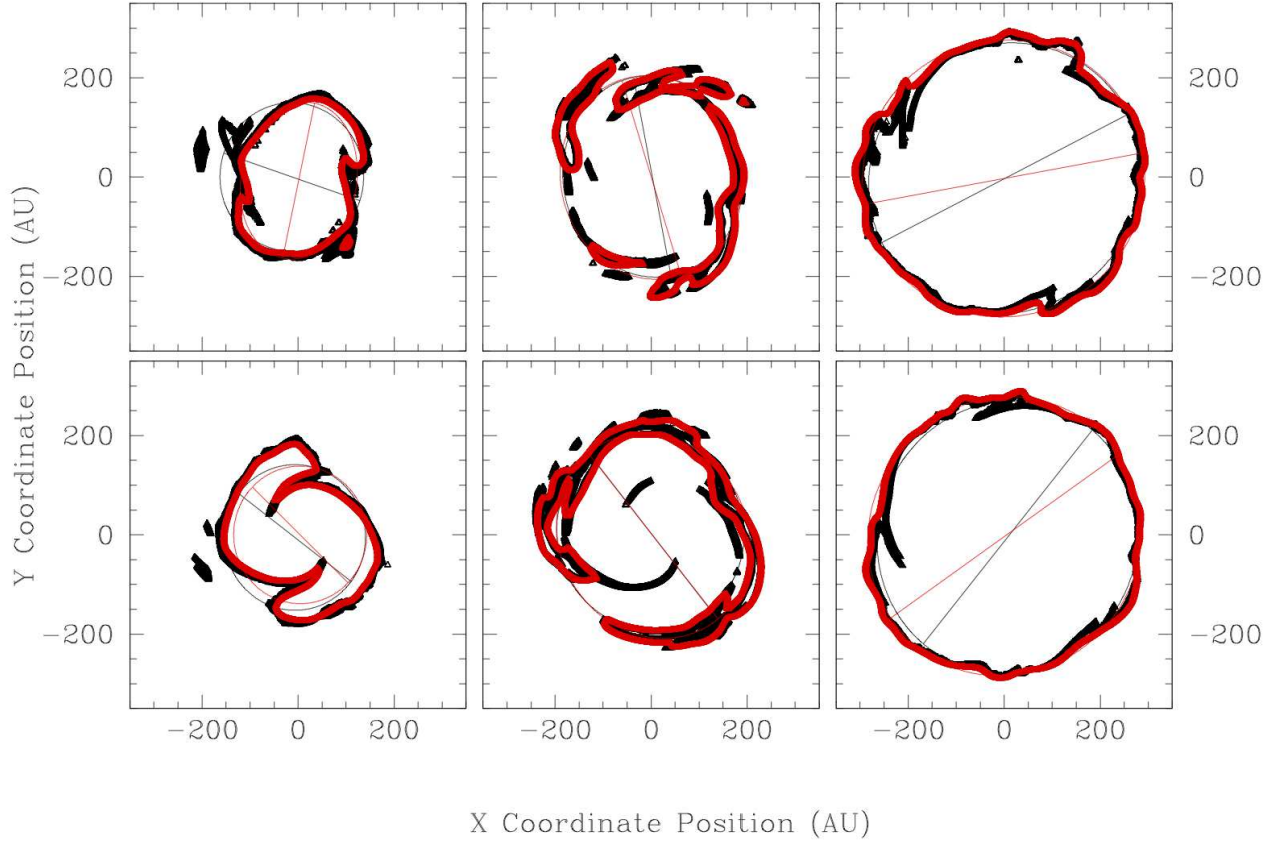


Fig. 9.— Iso-density curves and fits for the inner (left), maximum (middle) and outer (right) contours as defined in the text. The top panels show a snapshot of simulation at the binary’s orbital apoapse, the bottom panels show the immediately following periapse. Each panel shows contours and fits in black, denoting the densities derived directly from the simulation, and in red, denoting densities initially convolved with a 10 AU Gaussian PSF. The lines bisecting each fit ellipse defines the semi-major axis orientation.

### 3.5.2. *The size of the torus*

Figure 10 shows fits for each of the three semi-major axes defined above, as functions of time, along with the offset of each ellipse from the actual system barycenter. In each case the semi-major axis varies over time, with the inner ellipse featuring the most rapid changes and the outer ellipse the slowest. The amplitudes of the oscillations extend some  $\sim 20$  AU in either direction from its long term averaged value. The inner and outer ellipses also exhibit slow secular trends to smaller and larger extents, respectively, as the torus itself becomes distorted by the passage of spiral structures through it. Although the trends are visible over the entire duration of the simulation, it is unlikely that they will continue over much longer time spans. For the inner ellipse, the trend will be constrained by the fact that the action of the binary will tidally truncate the torus edge. The outer edge trend will be limited by the fact that the spiral structures decrease in amplitude as they move outwards, merging with the smooth background disk.

In each case, the offset of the best fit ellipse’s origins from the system barycenter fluctuates most rapidly of all, but with comparatively small amplitudes of  $\sim 5$  AU, and often with evident correlations between the set of offsets for the three ellipses at a given time. At late times in the simulation ( $\geq 5000$  yr), the offsets each increase to between 10 and 20 AU, in response to the larger inhomogeneities in the tori from which they are derived, as seen in section 3. Even these late time offsets remain substantially smaller than the  $\geq 30$  AU offsets derived from the GG Tau A system by GDS99 and McCabe, Duchêne & Ghez (2002) however. In part, we attribute this difference to the fact that the fits to the observations assume a circular torus, while our ellipse fits include additional degrees of freedom, which permit the ellipse origin to relax toward the system’s barycenter, while retaining a good fit to the shape. More importantly however, the discrepancy serves to highlight an important difference between the characteristics of the observations and our simulations. Namely, that the fitted parameters for our simulations do not trace exactly the same physical features as fits of various torus parameters derived from observed systems do. Here, they account only for density features in our 2D representation of the flow, while in observed systems such as GG Tau A, the various system characteristics include features that trace both the system’s 3D geometry, such as the disk scale height, and its radiated output, both from scattered and internal sources. Such characteristics may be correlated with the density, but do not trace it directly. Therefore, although the specific radii will be similar to those observed for corresponding features in the GG Tau A torus, it is important to make the distinction clear, in order to avoid confusion.

### 3.5.3. *The elliptical shape of the torus*

Figure 11 shows the eccentricities as functions of time, for the same fits shown in figure 10. In both simulations, and for all three fits, the tori quickly become significantly eccentric. The eccentricities for simulation *Clos0ehi* however, typically near  $e = 0.2 - 0.4$ , fall well below those for *Wide3ehi*, where they are found near  $e = 0.3 - 0.6$ . The difference is consistent with the fact that the torus is more strongly perturbed in the wide binary configuration. For all three fits, the eccentricities also rise to values typical of their longer term evolution within only 1-2 orbits of the binary, but continue to vary widely over the full duration of the simulation. This rise time is far shorter than a single orbit of the torus’ material defining the edge itself, and demonstrates the importance of the stars on the torus morphology. Consistent with its proximity to the perturbing effects of the stars, the torus’ inner edge suffers the largest variations from its initial circular form. In the case of the wide orbit configuration, the eccentricity undergoes repeated excursions to values greater than  $e = 0.6$  and less than  $e = 0.1$ , corresponding to a nearly circular shape. Also, the variations appear to be nearly periodic, perhaps arising as consequences of the binary’s influence on the inner torus. To the extent that they are quantifiable however, the oscillations do not correspond to the binary orbit period through any simple relationship, arguing against any direct connection.

Similar variability is present in the fits derived from central torus region, but the maxima do not extend to values

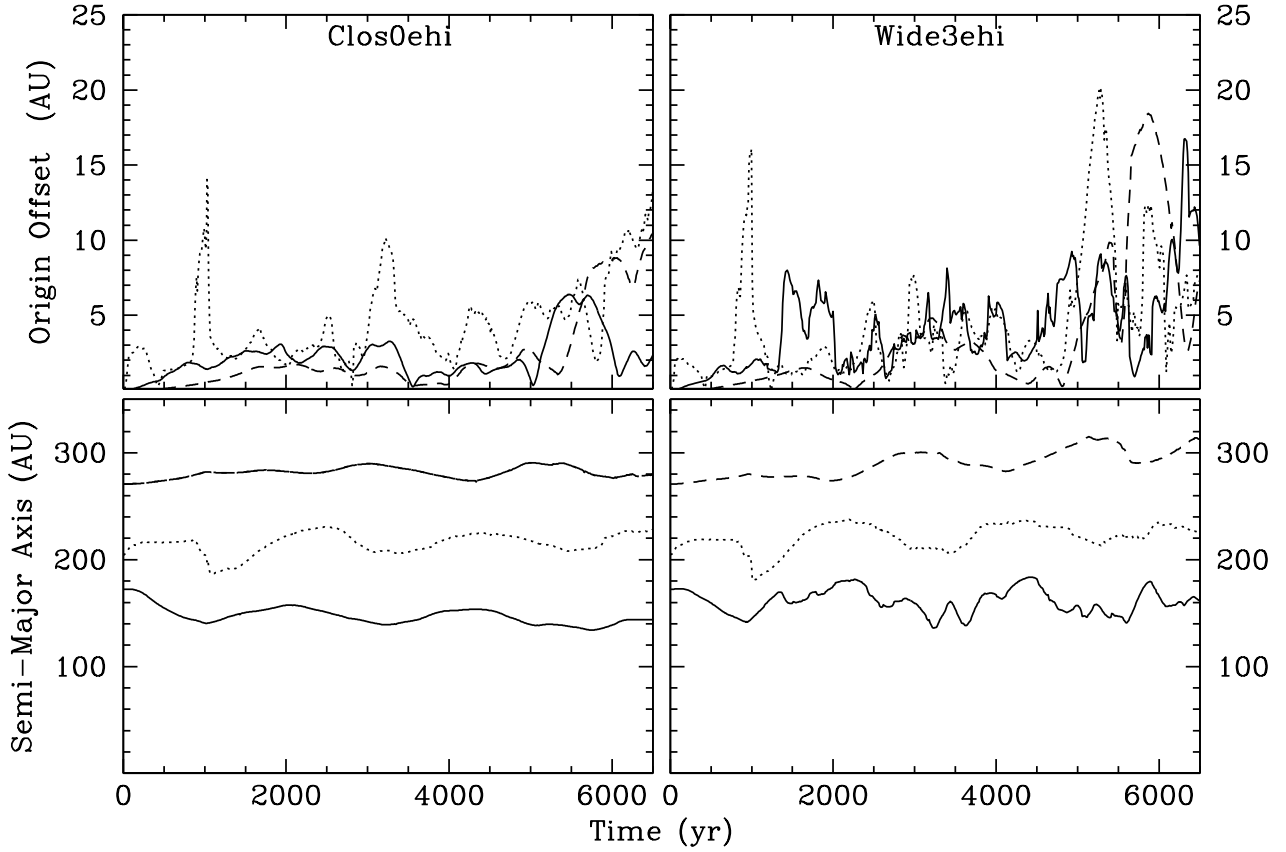


Fig. 10.— (bottom) The semi-major axes of the three ellipses described in the text, defining the inner (solid), center (dotted) and outer (dashed) limits of the torus, each as a function of time, for simulations *Clos0ehi* and *Wide3ehi*, as labeled. (top) The offset of the origin of each ellipse from the system barycenter.



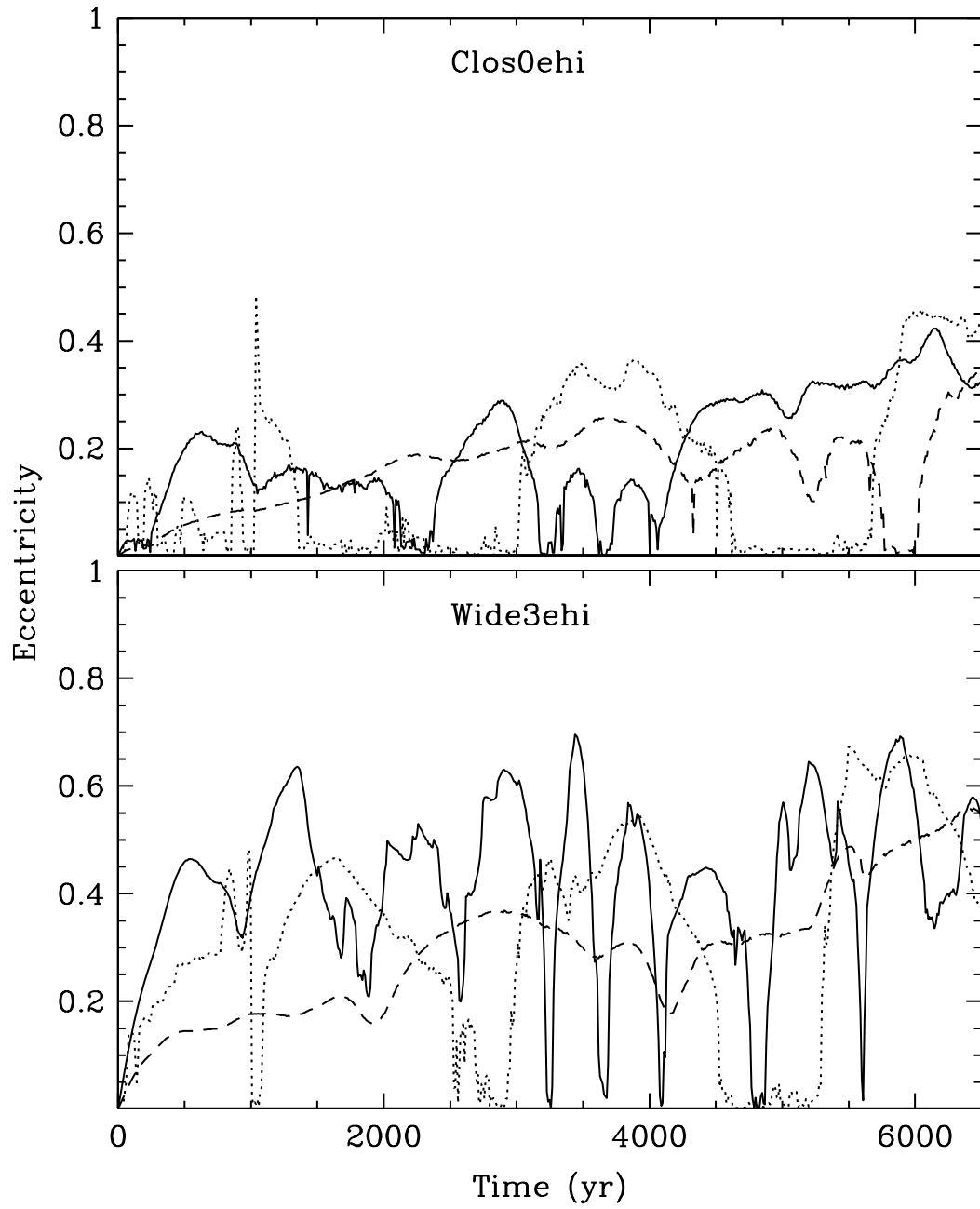


Fig. 11.— The eccentricity of the three ellipses described in the text, defining the inner (solid), center (dotted) and outer (dashed) limits of the torus, each as a function of time, for simulations *Clos0ehi* and *Wide3ehi*, as labeled.

as large as at the inner edge. Also, in both simulations, the eccentricities of the central ellipses remain near zero for long time spans, alternating with periods in which their values are much higher. In contrast, both the inner and outer ellipses typically retain their large eccentricities during these periods. Direct examination of the simulation morphology reveals that the systems have developed several, more or less equally spaced, spiral structures at these times. In consequence, though the non-axisymmetric character of the torus remains, the best fit ellipse derived from it becomes more circular, as the various features driving the fit to higher eccentricity cancel each other out. Later, as the spiral structures evolve into more asymmetric shapes, the eccentricity increases again.

The trend towards slower and smaller amplitude variations continues in the eccentricity for the outer edge. For both configurations, the outer ellipses require more time to increase to similar values as are seen for the other two. In contrast to the inner and central ellipses, the outer ellipses exhibit only comparatively small excursions away from their long term averages and the variations occur most slowly with time. They also exhibit none of the periods of near circular shapes (low eccentricities) seen for the other two. Even at the end of the simulations, the long term trend values continue to increase, meaning that the outer edge has yet to evolve to a configuration for which all artifacts in the results due to the initial conditions have been fully erased.

#### 3.5.4. *The orientation of the torus*

Figure 12 shows the axis of pericenter angles fitted for the tori over time. By definition, this parameter specifies the angle along which the long axis of the ellipse points, with a zero angle being defined here as the long axis of the stellar orbit ellipse, for the eccentric binary case, with the same zero point used for the for the circular binary simulation as well. In the case of the eccentric binary configuration, we might expect the torus to remain aligned along that same axis, since the binary’s orbital motion implies a strong forcing function to facilitate such alignment. This expectation is clearly not met in our simulations. Instead, the tori around both the eccentric and circular orbit binary appear to precess over time, as indicated by their continuing increases in angle and their periodic returns to zero as the motion sweeps around the compass.

The tori precess at different rates depending on distance from the system barycenter, with both simulations producing similar rates for the fits at the middle and outer edge of the torus, as measured by the similar slopes of the curves and the time required to return to a given orientation. In contrast, the precession behaviors for the inner ellipses in the two simulations are not similar to each other. Instead, the precession in the eccentric binary run corresponds approximately to a periodicity of twice the binary orbit period (i.e.  $\sim 860$  yr), over the course of many binary orbits, while for the circular binary run, it is much longer. We speculate that the precession in the first case is being driven by the forcing action of the binary. In the circular binary case, and for the center and outer tori, the influence of the stars on the tori is much weaker. In these regions, the precession periods correspond loosely to the orbital periods of the tori at each location, with the exception discussed below for the center torus.

Although the correspondence itself is apparent, we do not believe a direct, causal connection between the precession rates and the orbital motion of the torus material can be established however because, in general, the precession is clearly only approximately periodic. The axis of pericenter angle neither changes at a uniform rate, nor does it increase monotonically with time. Instead, occasional reversals occur, as the fit adapts to details of the local flow, and sudden discontinuities in the angle are also common, as the fit adjusts to the growth or decay of some structure in the torus. Such events are visible at  $t \approx 5800$  yr in fit for the outer torus edge in the *Clos0ehi* simulation, for example, and much more frequently in the center and inner torus fits. Jumps are particularly common in the central torus, and occur at the same times for which we noted above that the fitted eccentricity hovers near zero. Given this correspondence, we attribute the jumps there to the same cause: i.e. that the torus has evolved into a set of spiral structures of near

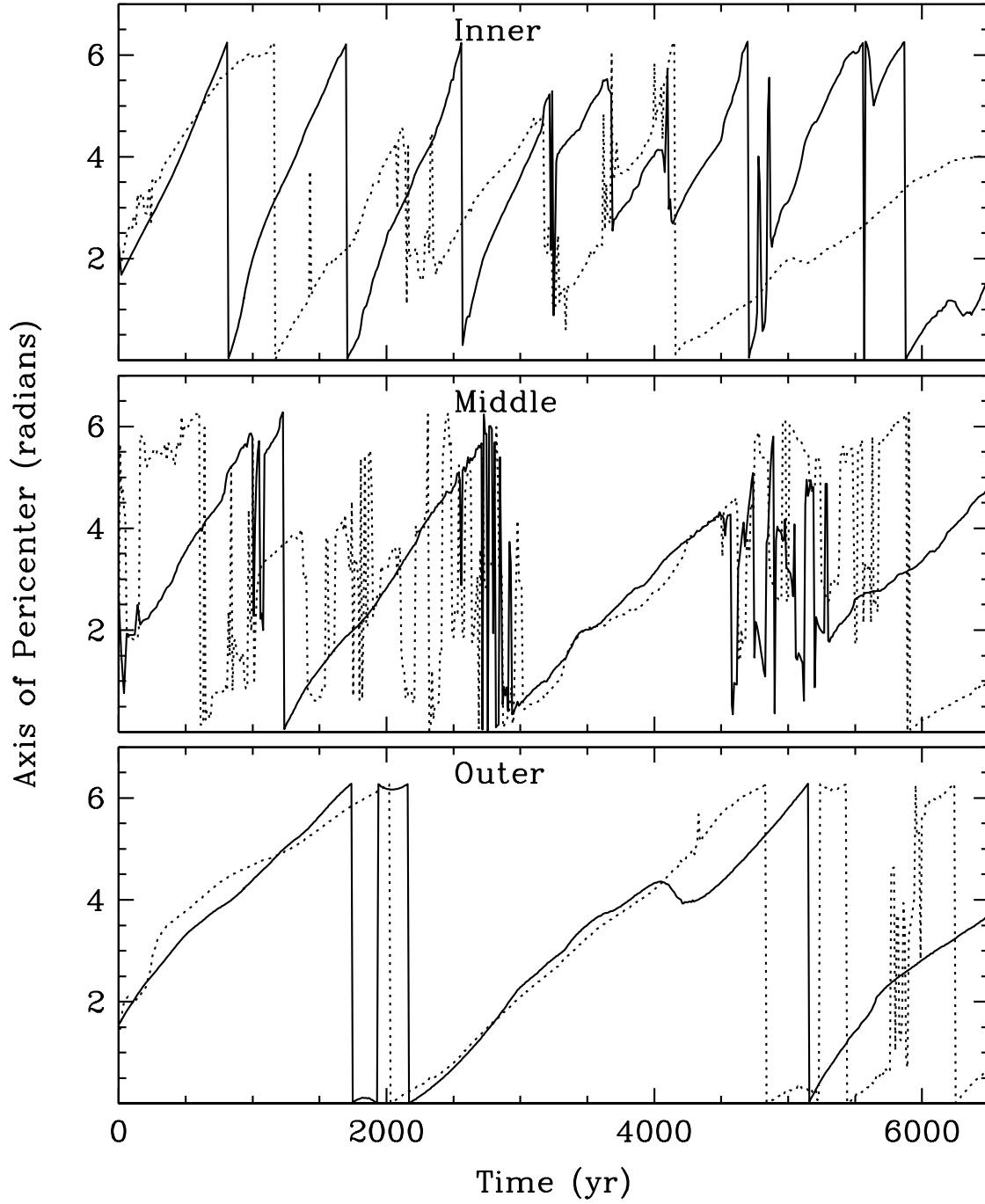


Fig. 12.— The axis of pericenter of the three ellipses described in the text, defining the inner, middle, and outer limits of the torus as labeled. Simulation *Wide3ehi* is shown with the solid curves, while simulation *Clos0ehi* is shown with the dotted curves.

equal spacing and appearance, causing the fitted axis of pericenter to become highly sensitive to small scale features of the torus as a result.

Of some interest is that the phase of the precession in one simulation is frequently similar to that in the other—the pericenter angles are nearly the same at the same times for the outer and middle tori. We believe that the similarity is not driven by any physical condition common to the two configurations, but is rather a consequence of the identical initial condition specified for the torus, which has not yet been erased by its subsequent evolution. The inner torus edge follows the same pattern as well, both for the correlation in angle and in periodicity, but the correlation remains close for less than a single orbit period there, before being lost.

#### 4. Evolution of the Circumstellar Environment

Observations of GG Tau A have conclusively demonstrated that a significant quantity of material is present in very close proximity to the stars themselves. Recent observations have even detected material in locations where its dynamical lifetime cannot be exceeded a few hundred years (Beck *et al.* 2012) before being accreted into the circumstellar disks or otherwise cleared from the system. In this work, we have assumed that all circumstellar material is initially contained in circumstellar disks orbiting each star, and in this section, we discuss the evolution of that material as it evolves. We will investigate the processes by which material is transferred into the circumstellar environment from the circumbinary environment, and what configurations the circumstellar disks evolve towards over time as material moves through them into and out of them.

##### 4.1. The configuration of the gap and the circumstellar disks

The morphology of a system with a wide, eccentric orbit (simulation *Wide3ehi*) is shown in figure 13 for various phases of its evolution through one binary orbit period. Details of the orbital evolution vary between orbits, and we have chosen to show the eighth orbit after the simulation’s beginning (i.e. beginning at  $t \approx 3400$  yr) because it exhibits the largest magnitude episode of mass accretion of any single orbit during the simulation (see section 4.2.1 below). It therefore provides the most easily visible illustrations of similar events that occur at other times, but which are of smaller magnitude. In addition, rather than show frames equi-distant from each other in time, we have chosen frames selected to highlight various aspects of the flow as the binary travels through a complete orbit, referencing the time since last apoapse for various time intervals in the orbit in the text.

In the first frame of the mosaic, where the components are at apoapse, the disks show little evidence of internal structure such as spiral density waves. Consistent with its higher mass (see section 4.2.1 below), the mass densities in the secondary disk (to the left in the image), are higher than in the primary. The shape of the cavity between the stellar components and the circumbinary material is significantly non-‘round’ and includes fragmentary spiral structures that are remnants of previous interactions between the components. These fragments are traveling outwards towards the circumbinary torus, which they will soon rejoin.

As the binary components begin another orbit, falling towards each other, large streams of material are pulled away from the torus and follow the stars on similar inward trajectories. Due to its orbital motion, the inbound material forms large scale spiral structures as it travels through the gap region and does not directly impact either circumstellar disk. By the time the stars have reached their 1/4 phase (frames 2-4, some 80-140 yr after apoapse), the leading edges of the spiral structures have overtaken the stellar components and wrapped around them, with the close tidal interactions causing them to begin to spread out again as they move away from the star. A portion of this material

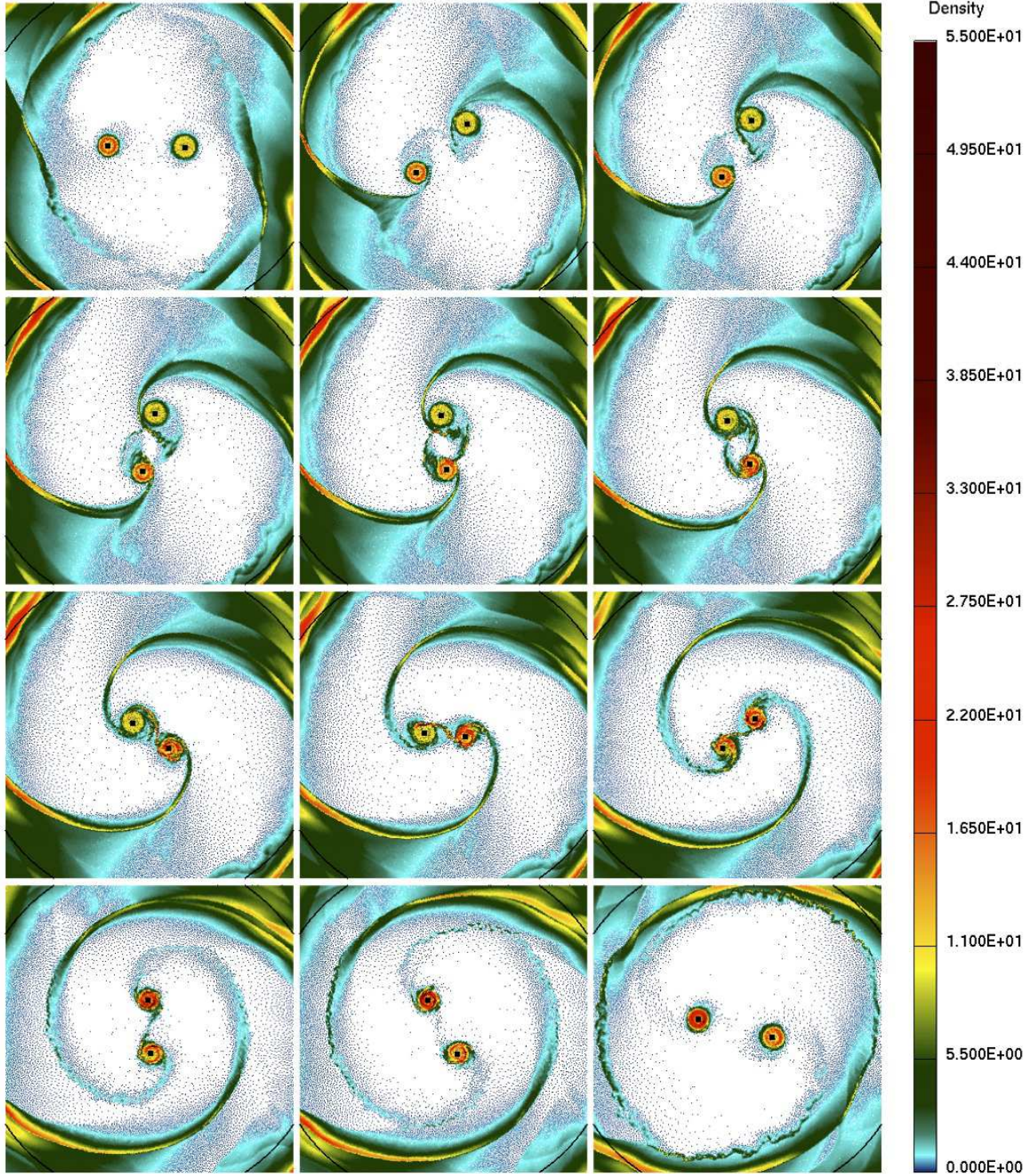


Fig. 13.— The morphology of the circumstellar disks and the inner torus/gap region at successive points along the eighth orbit of the binary from the start of simulation *Wide3ehi*, corresponding to a time  $\sim 3500$  yr after the beginning of the run. Each frame defines a  $300 \times 300$  AU region centered on the system center of mass. Time increases in successive panels from the top left, to the lower right, with the first frame chosen to be near apoapse of the orbit. The primary and secondary are initially located on the right and left sides of first frame, respectively, and their orbital motion is in a counter-clockwise sense.

may impact the other component of the binary, while the remainder forms a temporary ‘bar’ extending between the two binary components. Material arriving slightly later (frames 4-7, 140-220 yr after apoapse), does directly impact portions of the outer circumstellar disks and the flow pattern becomes quite complex.

The time interval shortly before and during periapse is, unsurprisingly, the interval over which the most complex interactions take place. The various interactions between the infalling streams, the ‘bar’ and disks cause substantial disruption in each. As a consequence, the spatial extent of the circumstellar material increases, with mass from all three sources contributing to the extended disks for each star. The amount and distribution of material in the accretion streams is near its maximum at this time as well. It is noteworthy however, that only a small fraction of the material in the streams actually accretes into the circumstellar environment, with the remainder returning to the torus. Illustrating this fact, figure 14 shows the velocity magnitude at the same periapse passage shown in the sixth panel of the mosaic in figure 13, along with velocity vectors on a small set of representative particles as well. The latter show the motion of the streams extending well around and away from both the stars and the surrounding circumstellar material. Near the circumstellar disks, velocity magnitudes in the streams increase to as much as 5-8 km/s, comparable to the Keplerian motion of the material within the circumstellar disks themselves, and well in excess of the 2-3 km/s orbital velocities of the components themselves.

The high velocities generated as the streams move through the gap are also important for conditions well within the circumstellar environment itself. Figure 15 shows the midplane temperatures of the material, again at periapse. While the accretion streams themselves contain the coldest of all material in the circumstellar environment, at temperatures below  $\sim 50$  K, temperatures in small regions near the impact points of the streams increase to 3-500 K as the kinetic energy of the infall is converted to heat. These temperatures are well in excess of the  $\sim 150$  K temperatures found in immediately adjacent regions of the disks, not affected by the streams’ impact. These  $\sim 150$  K temperatures at the outer disk edges are the lowest found within the disks. At other locations, temperatures increase to as high as 1000 K (extending to values beyond the color bar range shown in the figure) within 1 AU of each star. Non-azimuth symmetric structure is also visible, particularly in the disk around the secondary in which temperatures increase to as high as 300 K inside the spiral structures that develop. We will discuss implications of these temperatures in section 5.5, below.

As the stars pass through periapse and begin to recede from each other again (frames 7-9 of figure 13, 200-240 yr after apoapse), the extended disk begins to shrink as the material it contains begins to reintegrate into the main volume of the circumstellar disks. At the same time, the disk structures closer to the stars become more inhomogeneous, due to their interactions with the highly eccentric flows of the infalling material that disrupt their Keplerian motion. The disk structures generated by the interactions near periapse decay to near axisymmetry over the next 1-200 yr, as the stars recede from each other and again approach apoapse (frames 8-12, 250-420 yr after apoapse).

During these later phases of the orbit, and at larger distances from the stars, material in the tidal streams which was able to pass by both circumstellar regions without impacting either, continues on trajectories which returns it to the circumbinary torus from which it came. As they travel through the gap, the spiral structures into which material is organized begin to lose the sharp definition that characterizes their appearance in the earlier phases of the binary orbit. Such loss of coherence is most noticeable in the innermost portions of the streams, for which tidal interactions with the binary were largest. Nevertheless, such structures remain coherent well after their return to the main volume of the torus and, as discussed in section 3 above, their existence in and influence on the torus are of major importance for the overall density and temperature structure well beyond its inner edge.

A markedly different pattern of behavior occurs in the case of a  $a = 32$  AU orbit for the binary. Figure 16 shows the evolution of the *Clos3ehi* simulation over the course of one binary orbit. In comparison to the wide orbit case, a much larger fraction of torus material has moved inwards into what was originally the outer gap region. Despite

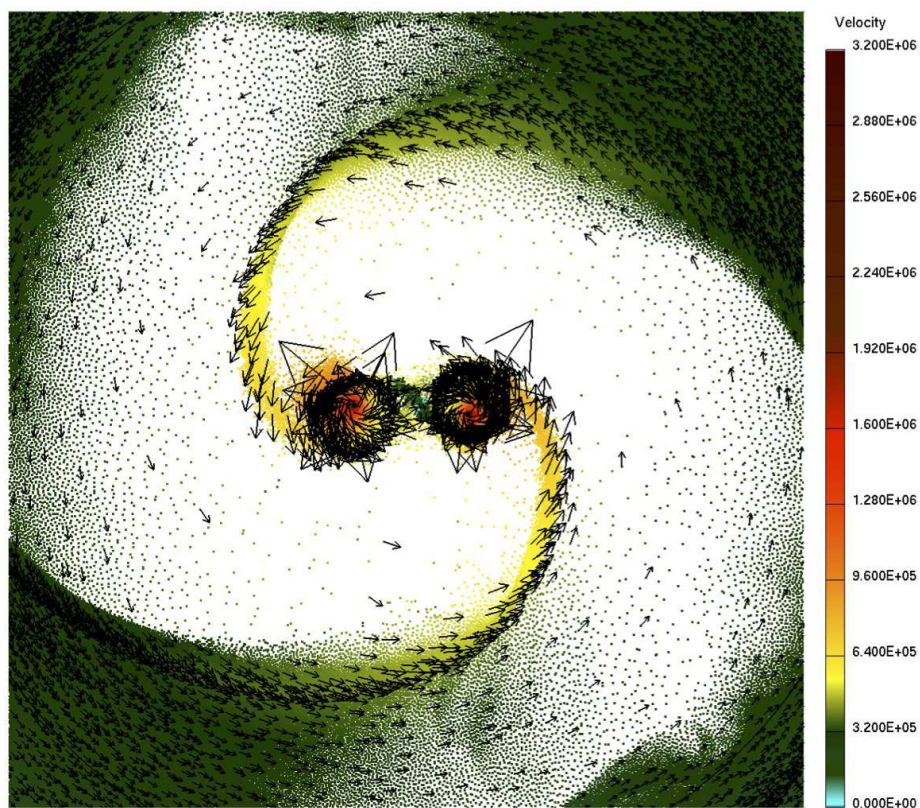


Fig. 14.— The velocity magnitude (in cm/s) relative to the system barycenter, at the same time as the sixth panel show in figure 13, for the same  $300 \times 300$  AU region centered on the system center of mass. Vectors indicating direction and relative magnitude scaled by an arbitrary constant factor is attached to one out of every 64 particles.

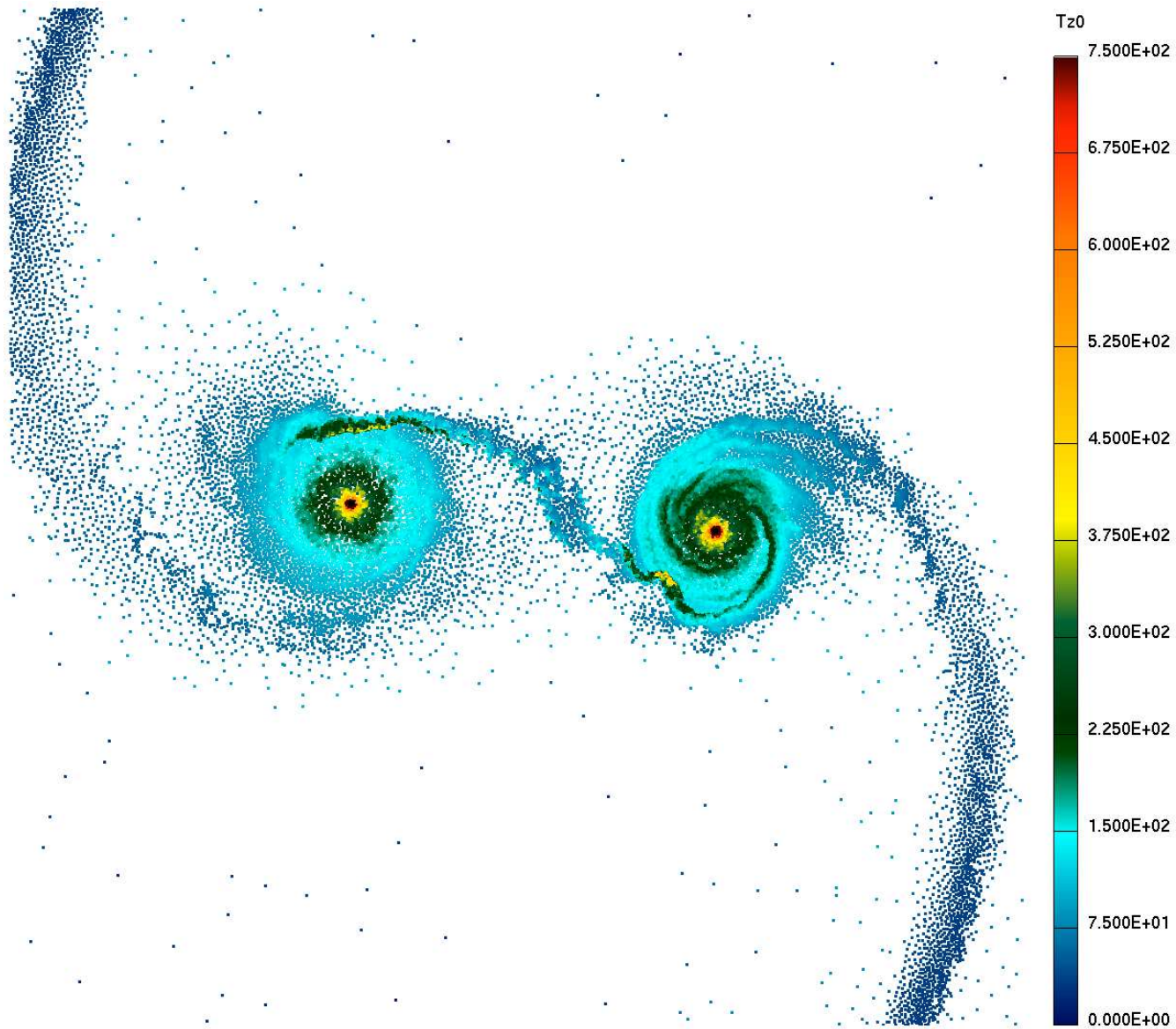


Fig. 15.— The midplane temperature distribution in the  $120 \times 120$  AU region around the system barycenter at the time of the eighth periape after simulation *Wide3ehi* begins. The secondary is on the right. Midplane temperature is determined for each SPH particle and at each time using the procedure described in section 2.3.2.



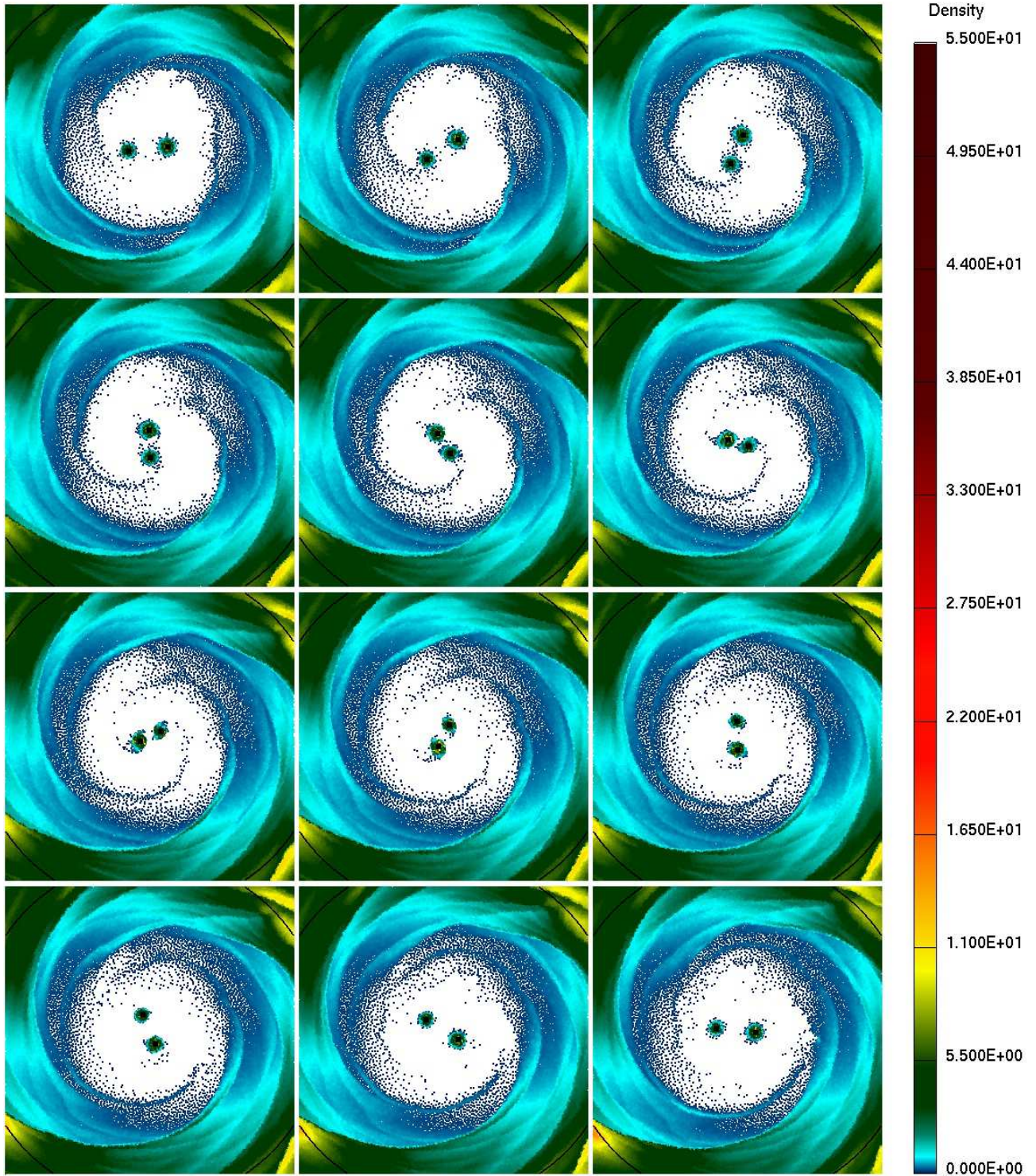


Fig. 16.— The morphology of the circumstellar disks and the inner torus/gap region at successive points along the 35th orbit of the binary from the start of simulation *Clos3ehi*, corresponding to  $\sim 5500$  yr after the beginning of the run. Each frame defines a  $300 \times 300$  AU region centered on the system center of mass. Time increases in successive panels from the top left, to the lower right. The primary and secondary are initially located on the right and left sides of first frame, respectively, and their orbital motion is in a counter-clockwise sense.

this, and in contrast to the behavior seen with the wide orbit model, the remaining gap region continues to be clear of material over the entire binary orbit. Accretion streams do develop, but are quite weak and remain distinct for only a fraction of the distance inward to the stars. No bar develops between the stars at periaapse because the weaker accretion streams are unable to feed the circumstellar region with enough material to produce one. Also, due to the closer orbital separation, the circumstellar disks are spatially more compact than in the wide orbit case and asymmetries that develop within them are also correspondingly less distinct.

With small variations, the same behaviors appear during each binary orbit in both the wide and close cases. We have not shown the  $e = 0$  models corresponding to the eccentric orbit models described here, however we note that their behaviors largely mimic those of their eccentric cousins. An important exception to this trend is the fact that only the wide, eccentric model in figure 13 shows the strong accretion streams and episodic accretion.

## 4.2. Mass transfer into and out of the circumstellar disks

We have seen that as the system evolves through time, the action of the binary generates large amplitude density structures throughout the circumbinary torus, extending outwards into the low density disk that surrounds it. Likewise, similar structures propagate inwards from the torus and, at various orbital phases, contact the circumstellar disks. Some of the mass in these streams becomes a permanent part of the circumstellar environment, while the remainder propagates outwards to rejoin the torus again. In addition to mass accretion from the circumbinary environment, mass contained in the circumstellar disks is subject to the action of the same strong gravitational torques that perturb the circumbinary material. It may therefore migrate radially inward towards the star and, when it gets close enough, be accreted by the star.

In this section, we quantify the rates and timing of the accretion into and out of the circumstellar environment, and the masses of the disks that result. As one aspect of our discussion, we will describe simulations of the same physical configuration at two different resolutions, differing by a factor of four in particle count. Through the relationship in eq. 9, this difference will be sufficient to change the numerical viscosity by a factor of  $\sim 2$ . A difference of this magnitude will in turn be sufficient to change the accretion by a similar factor, if indeed resolution plays a significant role in the accretion processes we model. We will discuss such issues in section 5.4.

### 4.2.1. Accretion onto the circumstellar disks

Figures 17 and 18 show the mass accreted by each of the circumstellar disks as a function of time for the various simulations in our study. For purposes of defining the “circumstellar disks” for the primary and secondary stars, we define an outer boundary to that environment to be 50% larger than the radius defined as the last stable orbit by Holman & Wiegert (1999). For each of the wide binary simulations, the total mass transferred into each of the circumstellar disks over the 6500 yr duration of the runs is comparable in magnitude to the assumed initial disk masses themselves. Accretion occurs preferentially onto the disk around the secondary star for both the wide and close systems, and for both eccentric and circular orbits. The torus-only models generate higher accretion rates than do the torus/disk models, presumably because the higher mass concentration in the inner circumbinary region is more readily available for transfer inward.

For the close binaries, mass transfer occurs at rates some  $\sim 20$  times lower than occurs for corresponding simulations with wide orbits, so that only a small fraction of the initial disk masses are replaced over the lifetimes of the simulations. At early times in these simulations, mass actually appears to be transferred out of the circumstellar disks.

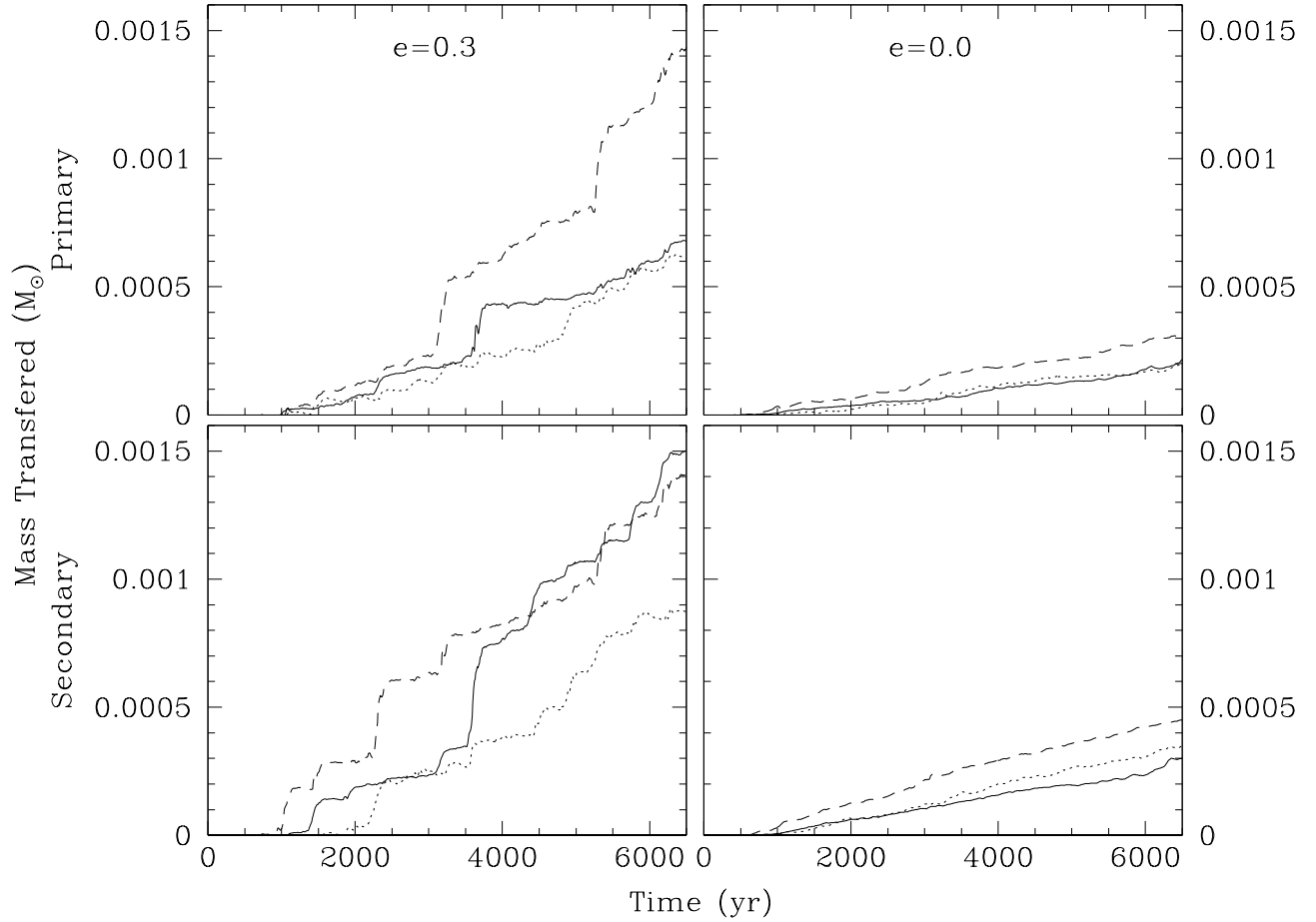


Fig. 17.— The mass transferred into the circumstellar environment of the primary (upper panels) and secondary (lower panels) stars in the binary system with orbital separation  $a = 62$  AU. The left panels show the simulations with assumed orbital eccentricity of  $e = 0.3$ , and the right panels show simulations with  $e = 0$ . The solid, dotted and dashed curves define the mass transferred for the high resolution torus/disk system, its low resolution counterpart and the high resolution torus only simulations, respectively.

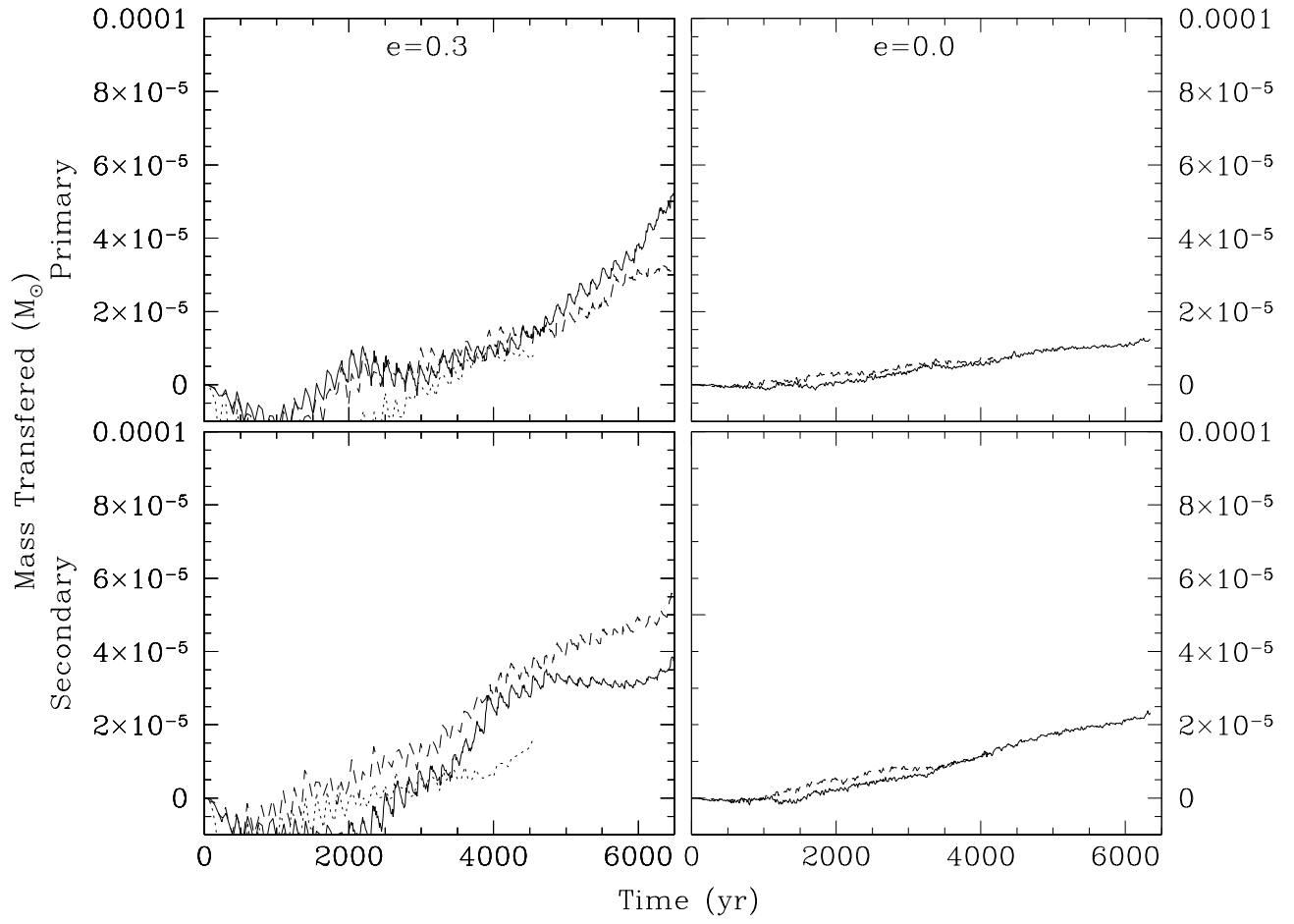


Fig. 18.— Same as figure 18, but for the simulations with orbital separation  $a = 32$  AU.

This is, however, merely a consequence of the initial spreading of the disks away from their initial condition and the artificial limit we imposed to define the disk edge. The accretion rates in these configurations are low enough to show small, apparent oscillations in the calculated disk masses for the eccentric orbit case (fig 18). In fact, these oscillations are more likely due to the changes in the disk’s spatial dimensions at different phases of its orbit. Such ‘flexing’ also causes a small fraction of the disk mass to migrate outwards temporarily, beyond the limiting radius we have defined for the disk edge, before moving again into closer proximity to its host star.

Eccentric orbital motion enhances the time averaged accretion rates over those observed for circular orbit systems, with rates a factor of  $\sim 2 - 3$  higher in an eccentric orbit system than in an otherwise identical circular orbit system. In addition, for the eccentric wide binaries, accretion is highly episodic, with substantial mass transfer occurring in bursts some 30-40 yr in duration and relatively little transfer occurring at other times. These bursts reflect the periodic gravitational perturbations of the torus by the stars as they travel closer and further from its inner edge and excite spiral structures there. As described in sections 3.1.1 and 4.1, spiral structures generated in the circumbinary disk by the action of the binary fall through the otherwise cleared gap region outside the binary orbit. As they travel through the circumstellar environment, a portion of their length may encounter one or the other circumstellar disks and be accreted by it. While similar features form in the simulations with  $a = 32$  AU (albeit much weaker), the trajectories of the spiral structures through the gap region do not intersect with the circumstellar disks due both to the smaller spatial extent of the disks and to their greater distance from the torus itself.

Due to the evident variability in the magnitude of the accretion events from orbit to orbit, we have not attempted a detailed analysis of their exact timing relative to the binary’s orbital phase. We note however that the bursts do vary from orbit to orbit, as does the instantaneous accretion rate and total mass accreted during one event. Typically, the events begin at orbital phases prior to orbital periape and reach their maximum intensity near periape, declining again as the stars recede from each other. The timing does not appear to be strongly related to the binary motion itself, but rather to the time required for material originating outside the circumstellar environments to travel inwards far enough to be accreted into one or the other circumstellar disk.

#### 4.2.2. *Accretion onto the stars*

In addition to mass transfer into the circumstellar environment from the torus, mass leaves the circumstellar disks and accretes onto the stars. Figures 19 and 20 show the total mass accreted onto the stars from their disks as functions of time, for the wide and close series of simulations, respectively. In contrast to the episodic accretion patterns of mass entering the circumstellar disks, accretion onto the stars exhibits no periodicities or outbursts, apart from an initial transient period during which the disk material loses its memory of its initial condition and moves towards a more physically appropriate distribution.

For the wide binary simulations, accretion rates after the initial transient fall between  $6 - 9 \times 10^{-8} M_{\odot}/\text{yr}$  for the  $e = 0.3$  series, and approximately half those rates for the  $e = 0$  series. The eccentric orbit models each exhibit a slight increase in rates at late times, while the  $e = 0$  models remain steady at near constant rates. Given the larger accretion rates *into* the circumstellar disks in the eccentric orbit simulations, increases in the accretion rates *out of* those same disks is a natural consequence as the larger material volume evolves along the same evolutionary path. Exactly the opposite effect is true of the close orbit models. In those cases, the initially rapid mass accretion transient drains a substantial fraction of the mass from the disks. Because this material is not replaced as rapidly (see section 4.2.1, above), the disks become depleted of material (see section 4.2.3 below) and the accretion onto the stars continues to slow down for the entire duration of the simulations.

In all of our simulations, the resolution of the circumstellar disks is extremely coarse. Of the nearly 1.9 million

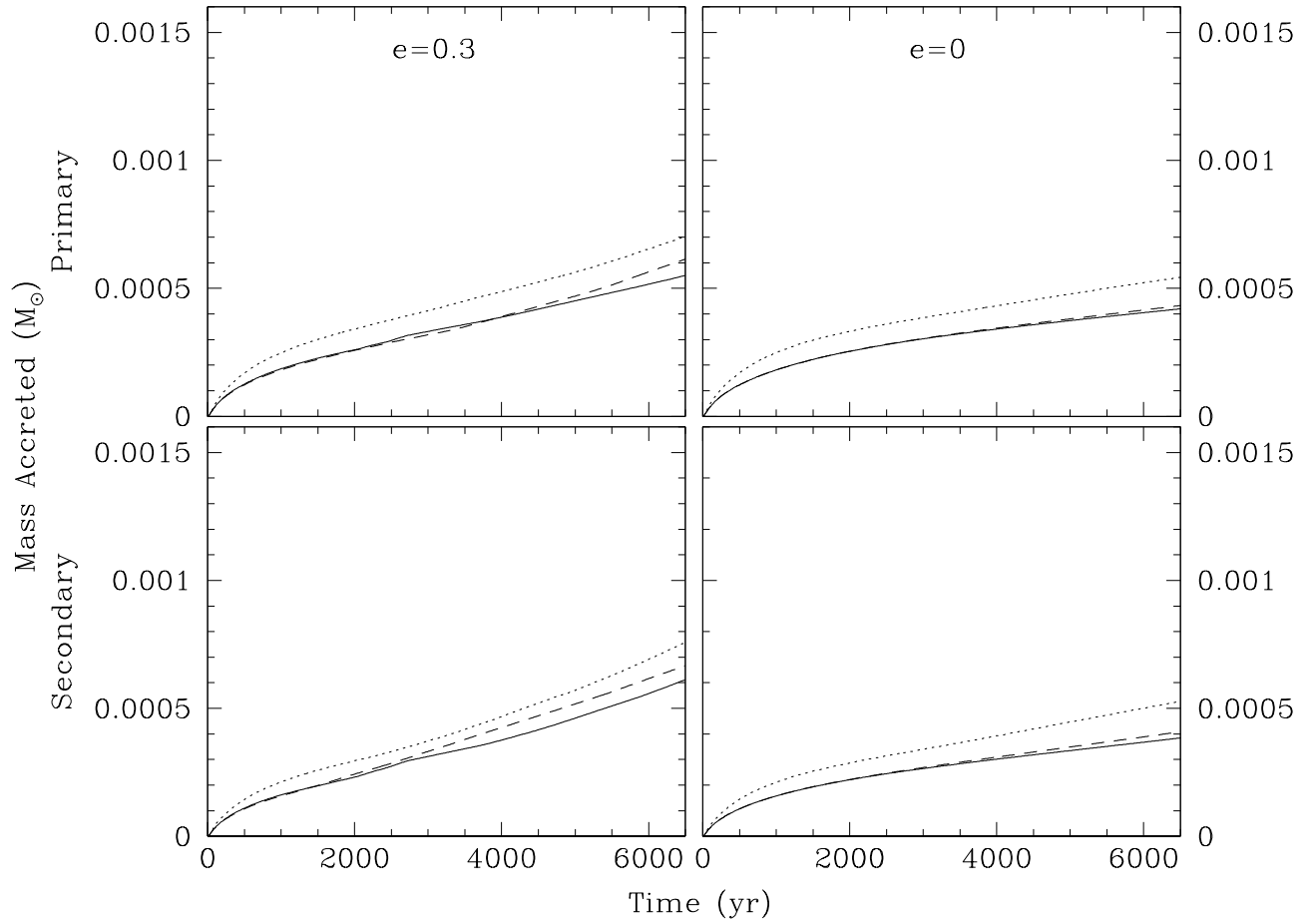


Fig. 19.— Total mass accreted by the primary (top) and secondary (bottom) stars for the series of models with binary separation  $a = 62$  AU and eccentricity  $e = 0.3$  (left) and  $e = 0$  (right). The solid, dotted and dashed curves correspond to the high and low resolution disk+torus models and to the high resolution torus-only models, respectively.

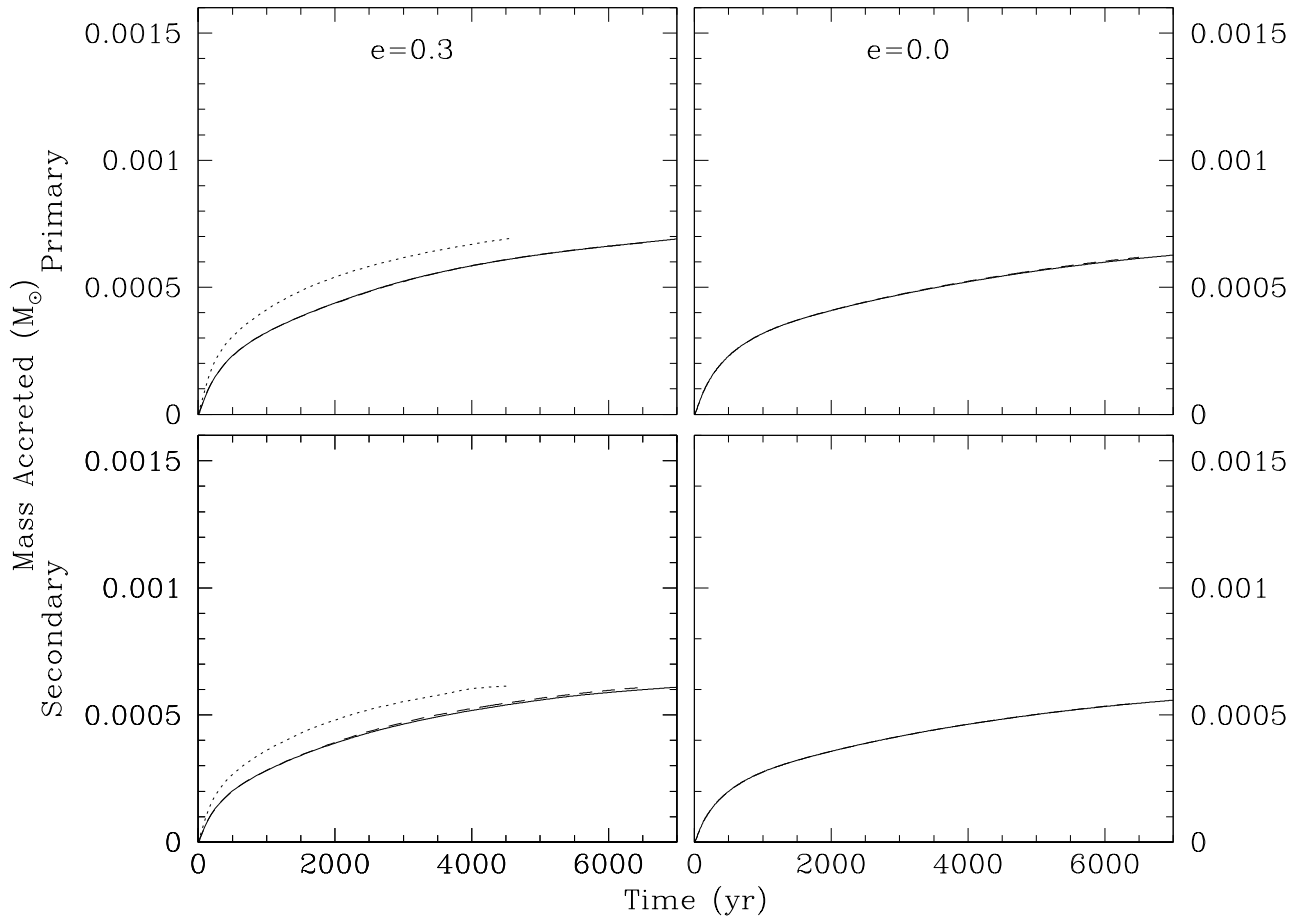


Fig. 20.— Same as figure 19, but for the  $a = 32$  AU series of simulations.

particles employed in our high resolution simulations, only about 20000 are initially allocated to the circumstellar disks and, as we shall see in section 4.2.3 below, that number does not increase substantially over the life of the runs. Because of this low resolution, the viscous dissipation originating from numerical sources is quite large. In order to ensure that our conclusions regarding the accretion rates through the disk are valid, we must therefore demonstrate that those accretion rates are not sensitive to the numerical viscosity inherent in the simulations themselves rather than to physical processes present in the actual system we are modeling.

To this end, we ran identical physical models at two different resolutions, and have included both the low and high resolution results in figures 19 and 20. In every case, apart from a larger rate of accretion during the initial transient, the cumulative mass accreted onto the stars for the low resolution variant follows a curve with an essentially identical slope to its high resolution counterpart. We conclude that our results are not sensitive to the high numerical dissipation caused by the limited resolution of the circumstellar environment. Our conclusions based on these results are therefore also insensitive to the resolution.

#### 4.2.3. *The disk masses as functions of time*

Although quantifying the mass accretion into and out of the circumstellar disks as functions of time are important measures of the system, by themselves they are incomplete because they do not specify the mass contained in the disk at any given time. Figures 21 and 22 show the mass of the disks orbiting the primary and secondary stars as a function of time, for the full set of wide and close simulations in our study. In each case, the most significant changes in the disk masses over the first  $\sim 1000 - 1500$  yr are due to the transient redistribution of disk material as it loses memory of its initial condition. Thereafter, and as the circumbinary material begins to exhibit activity, disks in the wide, eccentric orbit models exhibit periodic accretion events, which correspond to the orbital motion of the binary. In contrast, the disk masses in simulations where the orbital eccentricity is zero settle into steady states with little variation over time.

For the close orbit models, the masses of the circumstellar disks continues to decrease for both the  $e = 0.3$  and  $e = 0$  series of simulations over the entire duration of the runs. After the 6500 yr lifetime of the simulations, the masses of both circumstellar disks has fallen to values an order of magnitude or more lower than their initial masses. We anticipate that the disks would have been entirely accreted within a comparatively short time of additional evolution. Further evolution was not possible however, because the number of particles remaining in the circumstellar disks decreased to such an extent that instabilities developed in the time step controls for the simulations (due to the poor resolution of the disks). Little forward progress of the simulations was possible under such conditions, and we therefore terminated them. Because of the larger mass accretion during the initial transient, our lower resolution runs could only be run for about two orbits of the circumbinary torus, much earlier than was required for the higher resolution realizations.

### 5. Comparisons of features in our simulations with observations

So far, we have described the behavior of simulations with initial conditions specified to be very similar to GG Tau A, but we have not yet discussed in any depth, direct comparisons of our results to it. Other systems similar to GG Tau A also exist, to which the results of our simulations may be suitably generalized as well. Of these, one of the most similar is UY Aur, with the recent discussions of Tang *et al.* (2014) providing the most comprehensive description of the system to date. The similarities between it and the GG Tau A system are striking, both in the data themselves, and in the difficulties experienced in trying to reconcile them with a single self-consistent model of the system. Although the UY Aur binary has a wider separation and its disks much lower masses, both systems



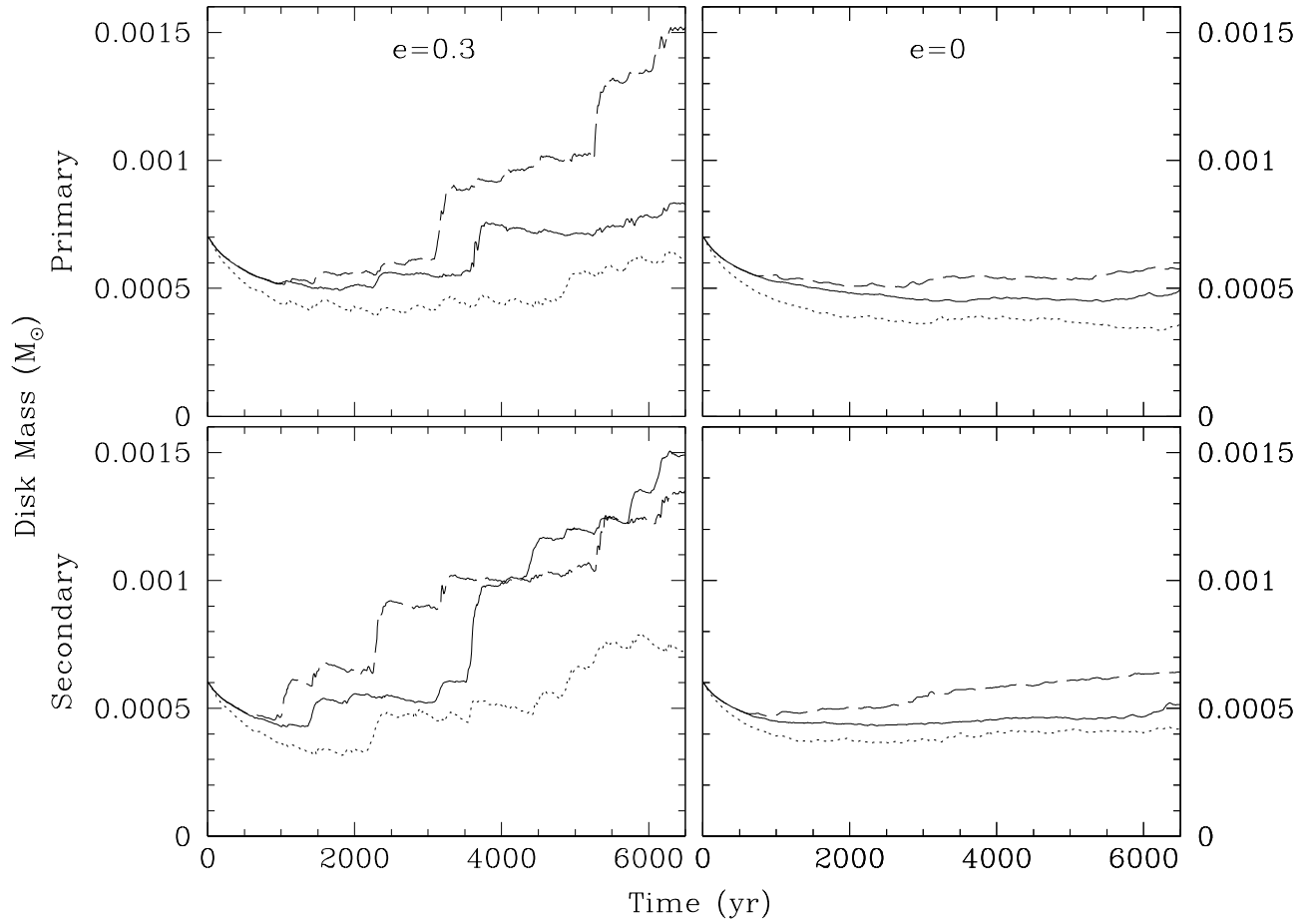


Fig. 21.— The masses of the circumprimary (top) and circumsecondary (bottom) disks for the  $e = 0.3$  (left) and  $e = 0$  series of simulations with  $a = 62$  AU. The solid, dotted and dashed curves correspond to the high low resolution disk+torus models and to the high resolution torus-only models, respectively.

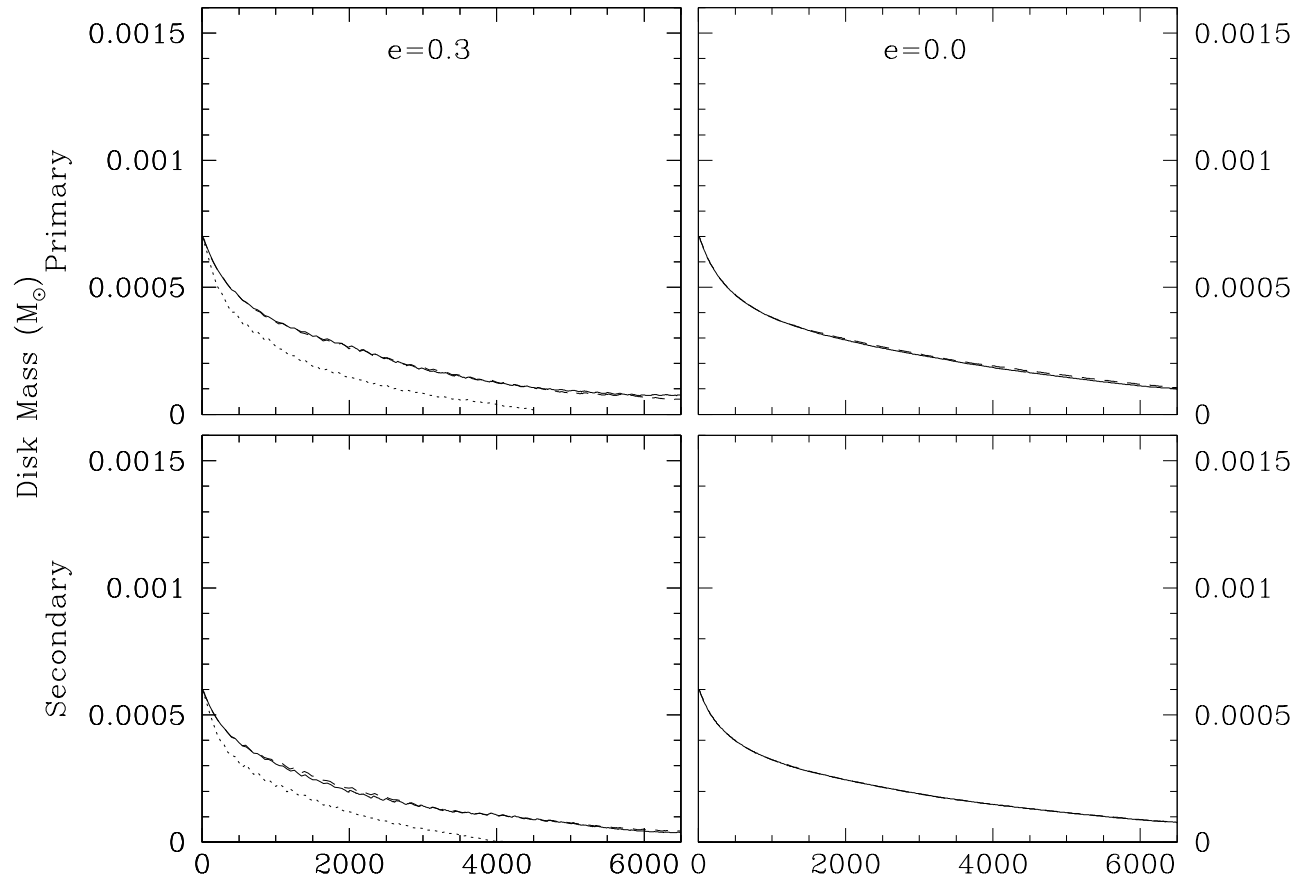


Fig. 22.— Same as figure 21, but for simulations with  $a = 32$  AU.

exhibit a remarkably similar inventory of features otherwise. Such features include structures in the circumbinary and circumstellar environments, streamers and stellar orbit planes which may be misaligned with the circumbinary disk if, as Tang *et al.* (2014) propose, the system is actually a higher order multiple rather than a binary. Here, we discuss comparisons of our results with observations of GG Tau A and make a number of conclusions about the system and its evolution, with an implicit understanding that the results will be applicable to a larger class of hierarchical multiple systems of similar character.

### 5.1. Features in the circumbinary torus

The observed circumbinary torus of GG Tau A contains a number of features (Krist, Stapelfeldt & Watson 2002; Krist *et al.* 2005), including spokes, gaps, variations in brightness and torus width at different position angles along the torus. Other work (e.g. GDS99), using high resolution interferometry, has shown that the edges of the torus are no more than  $\sim 10$  AU in radial extent. Despite these observations, detailed characterization of the structures and attribution to specific causes is difficult because the features themselves approach size scales comparable to the resolution limits of the telescopes. While similar constraints apply to our simulations, the spatial scale at which we are constrained is far smaller, thereby permitting both comparisons to be made, as well as, to some extent, predictions of types of features that may be revealed by still higher resolution observations.

Figure 23 shows a blowup of one panel of the mosaic in figure 2, along with a snapshot of the system at the preceding periapse passage of the binary. Two streamers are clearly visible in the gap region between the circumstellar material and torus, particularly in the periapse image, which extend outwards to the torus and join with it. The streamers remain distinguishable as coherent structures for well over a full revolution around the system and, as we will discuss in more detail in section 4, they do not persist as stable structures over the course of the binary’s or torus’ orbit. Instead, they travel through the gap region, with a small portion impacting the circumstellar disks, but with the largest fraction of material contained in the streamer simply traveling outwards again, where it rejoins the torus. Just such behavior has occurred in the time leading up to the apoapse snapshot, where the streamers no longer extend all the way inwards to the stars, but instead appear effectively as the torus’ inner boundary. At this time, portions of each streamer also exhibit small scale structure, particularly at the lower left and upper right portion of the gap, due to the fact that as they traveled these components have been stretched to the largest extent.

Even after reentering the torus, the structures themselves do not lose coherence. Instead, they continue to propagate as distinct entities, interacting with other streamers already present, which were generated during previous orbits of the binary. As is clear from these images, as well as similar panels in figure 2, the resulting torus is far from a smooth, azimuth invariant entity. The combined density structures continue to stretch and deform as they evolve further. In some portions of the torus, the remnants of multiple streamers converge to form closely connected filaments. In others, few such filaments are found. Each of these features is defined by very distinct edges, which appear both as its inner and outer boundaries and also as fine structure entirely within the main body of the torus. Eventually, the features reach the outer edges of the torus, where they effectively define its outer edge.

The torus’ internal structure as seen in our simulations invites comparison with the various structure observed in the GG Tau A system. Most easily compared are the streamers which appear in the gap region itself. Although many observations are at the limits of what can be observed, so that their interpretations are not without ambiguities, some, more recent observations, such as those of Beck *et al.* (2012) and Piétu *et al.* (2011) have begun to remove those uncertainties. For example, Beck *et al.* (2012) interpret their observations of emissions from hot gas as evidence for streamers of material infalling onto circumstellar material, which has been shock heated as it impacted the circumstellar disks. Long wavelength observations of Piétu *et al.* (2011) reinforce this interpretation, showing dust emission

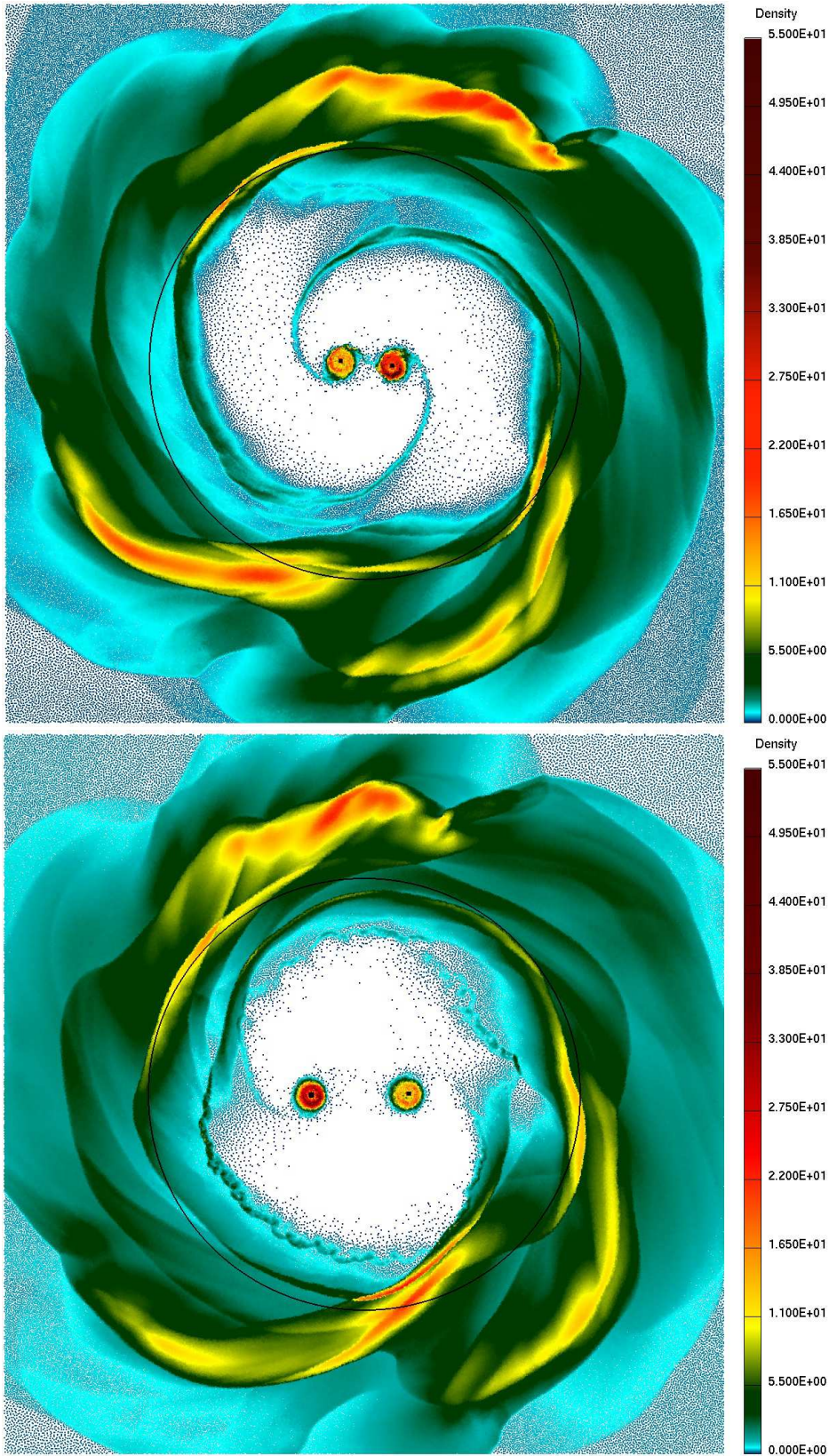


Fig. 23.— (bottom) A blowup image of the system at the start of the 12th binary orbit (at apoapse, identical to the 9th frame of figure 2) and at the immediately preceding periaapse passage (top).

extending inwards from the torus to the circumstellar environments where the hot gas resides. Correspondence between the streamers in our simulations and these features in the observed system are easily made, particularly for the images shown near periaapse, for which the streamers extend inwards all the way to the circumstellar disks. Some portions are also visible as a small ‘bar’ in the region extending between the binary components themselves. The short time scales over which the features in our simulations exist before dissipating back into the torus, also correspond well with the locations where the hot material is observed, in locations where its presence cannot be explained except as a dynamically transient phenomenon. Finally, the presence of high temperature material in the outer portions of the disks (see figure 15, above), shows that the accretion streams do, indeed, generate exactly the observed behavior pattern.

Within the torus, the distribution of spiral structure as a function of azimuth is highly inhomogeneous. For example, in the periaapse image, while some comparatively low density structures are visible in the image both to the left and right of the stars, far higher density structures (yellow and red in the images) are visible above and below them. As discussed in sections 3.1.1 and 3.1.2, such structures are visible over the entire duration of the simulations, and change their appearance as system evolves. Although the orbital timescales in the torus are thousands of years, the time scales for changes are far shorter, as evidenced by the marked differences between the two images in figure 23, which are separated in time by  $\sim 200$  yr. From the earlier image to the later, the large amplitude spiral arms have both traveled forwards in their orbits, and changed in shape. For example, the large spiral arm near the top of each image is longer and more dense in the top image than in the bottom. Similarly, the spiral arm appearing in the bottom left quadrant of each image is of higher density and angular extent in the top image than in the bottom.

The features in our simulations are qualitatively similar to the descriptions of depressions, filaments and gaps in the HST images discussed in Krist, Stapelfeldt & Watson (2002) and Krist *et al.* (2005). Unfortunately, although the features are quite clear in our simulations, the interpretation of the features in the observations themselves less so, due simply to the fact that they are near the detection limits of the telescope, where they are difficult to distinguish from various sources of noise. The features in our simulations are natural consequences of the dynamical activity generated by the motion of binary and here, we make tentative identifications of these features with those reported in the GG Tau A system. Further observations would substantially bolster the case for such identifications, but would require substantially more finely resolved images that are presently available. We anticipate that any such improved observations, repeated over the course of multi-decade timescales, may also begin to resolve variability of the systems’ appearance in time, though such an observing program would be an extremely challenging endeavor.

Finally, the streamers, and their coherence over long periods of time, provide a natural explanation for the observed sharply defined edges of the GG Tau A torus. In figure 24, we show the radial profiles of the surface density in the torus along three rays extending outwards from the system barycenter, each derived from the surface density mappings described in section 3.5, below. The high density regions in the profiles correspond to slices through the various spiral structures visible in figure 23, and their sharply defined edges to their inner and outer extents along the ray. For example, the green curves, corresponding to two rays extending upwards in the two images each intersect a spiral arm whose outer edge is found just inside 250 AU in the top panel, and just inside 260 AU in the bottom. At those locations, the surface density decreases abruptly from  $12 - 15 \text{ gm/cm}^2$  to  $\sim 5 \text{ gm/cm}^2$  over a spatial scale of  $\lesssim 5$  AU. Similar features are present at various other locations in the profiles, with those in the radially inner portions corresponding to streamers located within the gap intersecting the rays, while those at larger distances corresponding to larger scale spiral disturbances within the torus itself. In some cases, the inner edge appears more sharply defined, as is the case for the feature at  $\sim 230$  AU along the  $45^\circ$  ray in the upper panel. In others, the outer edge is sharper, as discussed above for the  $90^\circ$  rays. Features with lower surface densities and lower contrasts are also present in the profiles, extending to distances as far as  $\sim 320 - 350$  AU from the system barycenter.

Each of the profiles include density contrasts of up to factors of  $\sim 3 - 4$ , over spatial scales of  $\lesssim 5$  AU in extent

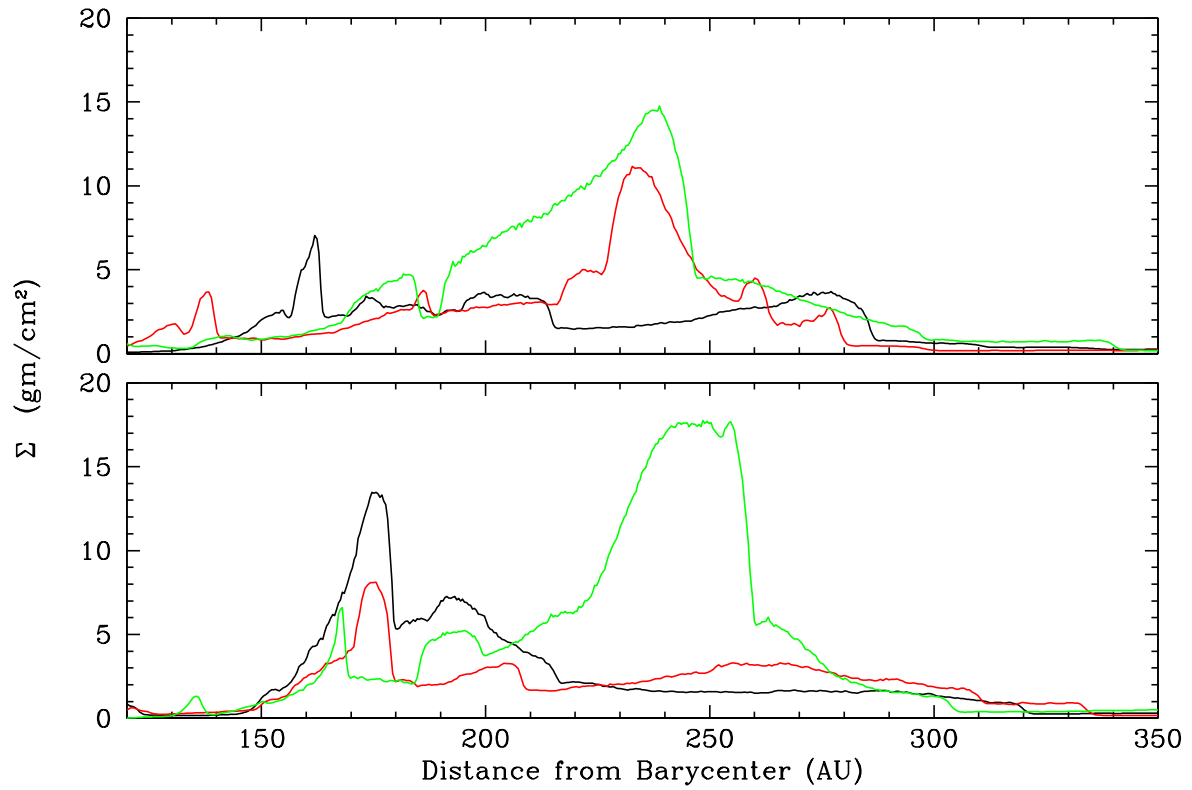


Fig. 24.— The surface densities along three rays extending from the system barycenter along azimuth angle  $0^\circ$  (black),  $45^\circ$  (red) and  $90^\circ$  (green) in figure 23, as measured with zero extending directly to the right in those images. The top and bottom panels correspond to the top and bottom panels in figure 23.

along the ray. These scales are comparable to or smaller than the  $\sim 10$  AU widths derived for the inner and outer ring edge width by Guilloteau, Dutrey & Simon (1999) and Piétu *et al.* (2011) for the GG Tau A system. Each of these edge width derivations are based on observations that approached the resolution limits of the telescopes themselves so that, in principle at least, the widths might be expected to be significantly narrower. On the other hand, the smoothing lengths of the SPH particles located in these regions is  $\lesssim 1$  AU, and we conclude that both the spiral structures and their edges are well resolved in our simulations. Therefore, given the results of our simulations, we expect that future observations will fully resolve the edge structure at size scales of a few AU.

In section 2.2.1 we described the process by which we defined initial conditions for the torus and disk and noted that determination of self consistent initial conditions (i.e. rotation velocities consistent with the implied pressure and gravitational forces) were difficult to specify self consistently at the interface between the two components. The sharp density gradients produced correspondingly large pressure gradients that generated difficulties in defining self consistent orbit velocities near the interface. To sidestep the inconsistencies, we employed the ‘workaround’ of widening the interface in our initial condition over a radial region some  $2\times$  the observed width of the interface. Given the the sharp interfaces described this section, a much more palatable physical model for interpreting the data is that the sharpness of the inner and outer edges of the torus is not a feature of a cylindrically symmetric distribution of material in rotational equilibrium, but is more likely simply to be due to the spiral structures generated by the actions of the binary on the torus and of self gravitating disturbances.

## 5.2. The meaning of fragmentation in the torus

In the discussion above, we noted that in many of our simulations the circumbinary torus fragmented into one or more massive objects. We did not however, discuss the significance of those objects, either in the context of their significance from a numerical standpoint, or in the context of what they might mean for the GG Tau A system. We now consider such questions.

### 5.2.1. Numerical criteria required for valid simulations

Of primary importance in evaluating our results is to answer the question of whether or not the fragments are simply artifacts of our numerical methods or of deficiencies in the physical assumptions used to model the system. Our first task, then, is to determine whether or not the simulations obey known requirements for resolving fragmentation, such as those described in Nelson (2006, hereafter N06). The most pertinent of these criteria is the requirement that the fragments be resolved by a sufficiently large number of particles, both as they form and afterwards. A quantification of ‘sufficiently large’ is that the locally value of the ‘Toomre mass’, as defined in N06, be resolved by no fewer than  $\sim 6\times$  the number of SPH neighbor particles, which corresponds to about 200 particles in 2D. We find that the conditions within the fragments produced in our simulations are such that the Toomre mass reaches its smallest values of  $\sim 10 M_J$  in the highest density portions of a fragment. Given the torus mass and the particle counts in our simulations, the mass of a single SPH particle is  $\sim 0.02M_\oplus$ . The ratio of these two masses is approximately  $10^5$ —far higher than the required number of SPH neighbors, and we conclude that the fragmentation is well resolved by our simulations.

Additional considerations for checking the sensitivity of our simulations to various numerical and physical parameters are found in a series of papers by Meru & Bate. In Meru & Bate (2010, 2011a), they find that, in addition to the result of Lodato & Rice (2004) that disks fragment if their cooling timescale is shorter than  $\sim 1 - 2$  orbit periods (depending on the adiabatic exponent,  $\gamma$ ), fragmentation is also sensitive to a variety of other physical parameters. In addition to the cooling timescale, they examine the sensitivity of fragmentation in disk simulations to the opacity

in models with radiative cooling, and to the mass and temperature profiles in the disk. They determine an empirical relationship between the cooling timescale required for fragmentation and the mass distribution and also note that disks heated by external radiation, from e.g. stellar irradiation (as are those in our models), tend to be less likely to fragment due to the additional heating.

Later however, in Meru & Bate (2011b), they realized that their previous results were sensitive not only to changes in the various physical models, but also to the number of SPH particles used to resolve the disks in their simulations. They concluded that in many cases, their simulations were not converged numerically, and questioned whether any numerical simulations that included radiative transport could possibly converge to a result which accurately modeled fragmentation in circumstellar disks. After a further investigation (Meru & Bate 2012), they revise their initial conclusion to note that fragmentation can be resolved, but depends strongly on the magnitude of the artificial viscosity employed. Are these conditions important for the simulations described in our work? Since our models also include an approximate radiative cooling model, they too may be affected by a similar deficiency, and we therefore explore that possibility here.

We note first, that Meru & Bate did not discuss the application of any of the N06 resolution criteria to their results. Given this fact, we begin with such a comparison in order to understand whether the N06 conditions are more or less restrictive than the convergence criteria they describe. The condition most directly available for comparison in the various Meru & Bate works is the N06 requirement that the vertical structure in 3D disks be resolved by at least  $\sim 4$  SPH smoothing lengths per disk scale height, at the disk midplane. Figure 10 of Meru & Bate (2012) shows this quantity, and we observe that the azimuth averaged values of the ratio  $h/H$  (smoothing length over scale height—the inverse of the quoted N06 criterion), are larger than the required  $1/4$  for all but the outer portions of the two million particle run shown. Based on this observation, we conclude that their simulations with two million particles are at best marginally resolved in their outer regions, while the inner regions and those runs with fewer particles are insufficiently resolved. The direct consequence, as shown in N06, is that the mass densities in the disk midplane in those runs will under-shoot their physically correct (i.e. fully resolved) values by a factor of as much as 30% when  $H/h \sim 2$ . This condition will be true for all of the simulations in (Meru & Bate 2010, 2011a) and many in their later works (Meru & Bate 2011b, 2012) as well.

The effect such errors will induce in other physics based quantities or the overall outcome of a given simulation is difficult to assess directly. It is noteworthy however that the sensitivities they describe are much less pronounced above the 2 million particle threshold (Meru & Bate 2012) at which the vertical structure criterion of N06 is marginally satisfied in the outer parts of their disks. We conclude that the trends in their simulations are likely to be manifestations of numerical inaccuracies similar to those underlying the N06 vertical structure resolution requirement. This conclusion, and the arguments on which it is based, is also shared by Lodato & Clarke (2011). In addition, those authors argue that one possible origin for the resolution sensitivity may lie in resolution dependent changes in the thermal energy input supplied by the bulk artificial viscosity, even when that contribution is small overall. They emphasize however that the case for such a mechanism is ambiguous, because some simulations, at high resolution and for which their model predicts fragmentation, actually do not fragment. That absence is then taken as evidence for physical mechanisms to suppress fragmentation. We have discussed the importance of two such mechanisms in our work (radiative heating and stirring generated by the binary interactions), and so discount the resolution criterion in Meru & Bate, in favor of satisfying the N06 Toomre mass criterion directly, as the best indicator that numerically induced fragmentation is absent in our simulations.



### 5.2.2. *Physical significance*

Given that our simulations do not contain numerical deficiencies which generate fragmentation, we now discuss the significance of the relevant physical models and their contribution to fragmentation. Fragmentation occurs when an imbalance between gravitational and pressure forces develops which favors gravitational forces in some volume so that it begins to collapse, typically on timescales of a few orbits (Durisen *et al.* 2007). The imbalance develops when either insufficient internal energy is absorbed by the disk via radiative heating, or is generated in it by dissipation of kinetic energy, or when cooling permits internal energy to escape more quickly than it can be replaced. Each of these processes decrease the gas pressure through the equation of state, and each are strongly time dependent in character, varying as the disk evolves.

All of our simulations exhibit strong spiral structures generated by the combination of self gravitating instabilities and the tidal interactions with the binary. Some also produce fragments on short timescales compared to the system lifetime. We conclude that our simulations model systems lie very near their fragmentation boundary, with some configurations being slightly more susceptible to fragmentation and others slightly less so. In contrast, and although marked structure exists, the GG Tau A system is not known to contain any well defined fragments within its torus, even though the observed torus conditions imply a strongly self gravitating structure. This means that the balance between heating and cooling must be very finely held, because the instabilities are neither fully suppressed, nor do they grow to sufficient amplitude to generate fragments. Further, this balance has been sustained over a long time, in spite of the sensitive time dependence noted in Durisen *et al.* (2007), since the system lifetime is long compared to the  $\sim$ few orbit timescale required for fragmentation to occur. Given that our simulations model configurations defined to be very similar to GG Tau A, such that similar physical behaviors are expected in both, we conclude that the balance between heating and cooling is much more finely held in reality than is possible for our models to reproduce.

Nevertheless, two important, additional conclusions about the GG Tau A system are possible based on our results. First, we recall our conclusions above that large scale structures seen in all of our simulations owe their origin not only to the tidal action of the binary but also to self gravitating instabilities in the torus. Although no clear pattern emerges from our simulations that would indicate which configurations are more likely to generate fragments in the GG Tau A system, their presence in systems with many different binary orbital parameters indicate that the conditions are generally favorable for fragmentation. We can therefore conclude that the GG Tau A system itself is very near its fragmentation boundary. Given our results however, we cannot predict whether or not such an outcome actually will occur.

Second, we conclude that the combined energy input from the radiative heating from the stars and the stirring action of the binary are responsible for a large fraction of the thermal energy input into the torus, and thereby play an important role in its long term stability. This is demonstrated by comparing the simulations described in section 3.4. In the first, we model a single star of the same mass and luminosity as the combined masses and luminosities of the binary stars in our other simulations, but with the same torus. In the second, we model a binary while omitting the stellar radiative heating source. The torus is marginally stable with an embedded binary that includes heating, producing none or at most one or two fragments within the several orbit time frame of the simulations. In contrast, removing either the radiative heating or the tidal stirring causes the torus to become violently unstable, producing nearly 40 fragments in less than a single torus orbit. Such an outcome clearly demonstrates both the unphysical nature of the evolution where those processes are absent and, at the same time, their importance where they are present.

### 5.3. The orbital parameters of the GG Tau A binary

GDS99 report an inclination of  $37 \pm 1$  degrees for the GG Tau A torus relative to the line of sight. This value is derived from the observations by deprojecting the observed eccentric appearance of the circumbinary torus into a circular shape. Given this inclination, attempts to fit the available astrometric data for the binary’s orbit presently remain somewhat ambiguous. If an orbit coplanar with a circular torus is assumed, then the best fit orbital parameters are  $a \sim 35$  AU and  $e \sim 0.3$  (McCabe, Duchêne & Ghez 2002; Beust & Dutrey 2005; Köhler 2011). Unfortunately, these parameters prove to be somewhat unsatisfactory from the point of view that the semi-major axis is smaller than is expected based on dynamical arguments and the position of the inner edge of the torus.

Recognizing this shortcoming, the same authors and others fit for the orbital parameters under the relaxed assumption that the planes of the stellar orbit and the torus may be misaligned. In this case, Beust & Dutrey (2006) determined best fit orbit parameters of  $a \sim 62$  AU,  $e \sim 0.35$  and a mutual inclination of  $i \sim 21 - 24$  degrees. They also report a second family of fits with mutual inclinations of nearly 90 degrees, but find that the disk in such systems is either disrupted entirely or becomes very thick. Following similar arguments regarding alignment, the later analysis of Köhler (2011) found the ‘most plausible’ orbit parameters to be  $a \sim 60$  AU and  $e \sim 0.44$ , with a relative inclination between the two planes of  $\sim 25$  degrees.

Under both sets of assumptions however, the fitted orbital parameters still remain unsatisfactory based on the dynamical argument that a substantial misalignment between the stars and torus would quickly generate a warp in the torus, while no such feature is observed. Given the analysis of section 3.5, we believe that the data and the analyses of them may be fully reconciled if we relax the assumption that the GG Tau A torus is circular, rather than the assumption that the torus and binary orbit planes are inclined with respect to each other. Under this alternate assumption, deprojection of the torus’ actual eccentric shape into a circular shape results in an erroneous determination of its inclination. Then, the perceived misalignment is simply a consequence of the incorrect determination of the torus inclination, rather than a property of the system itself.

This alternate assumption will be plausible if the mutual inclination determined from the fit is comparable to the inclination derived from misinterpreting an elliptical torus as a circular torus inclined at an angle,  $i$ , with respect to the line of sight. For a given ellipse which is interpreted as a circle, the inferred inclination is related to the true eccentricity,  $e$ , via the equation

$$\cos(i) = \sqrt{1 - e^2}. \quad (13)$$

Therefore, given a torus with eccentricity  $e = 0.3$ , its inclination would be perceived to be  $i \approx 17$  degrees. Similarly, a torus with  $e = 0.1$  or  $e = 0.6$  would be perceived to have an inclination of  $\approx 6$  or  $\approx 39$  degrees, respectively. The same error is made if some other plane defines the torus’ absolute orientation, rather than the plane of the sky. In the case of the GG Tau A system, this plane can be specified as the plane defining the orbit of the two stars in the binary.

The mutual inclinations derived in each of the analyses above fall well within the range of ‘false’ inclinations which could be attributed to misinterpreting the eccentric shape of the torus itself. On this basis, we conclude that the ambiguity in orbit parameters can be resolved in favor of the larger semi-major axis. This conclusion restores consistency between the observations of the torus’ dimensions—specifically the location of its inner edge—and the dynamical results of Artymowicz & Lubow (1994), which predict a wide binary orbit based on the location of Lindblad resonances that drive tidal truncation.

It is further reinforced by the fact that only the circumstellar disks in our  $a = 62$  AU simulations remain massive enough to remain consistent with the masses derived from observations. The disk masses in all of our simulations with  $a = 32$  AU decrease quickly to much smaller values due to the combination of losses through accretion onto the stars and the lack of replenishing material accreting onto them from the circumbinary environment. Observations

indicating the presence of accretion streams reinforces our conclusion further, for two reasons. First, such streams are essentially non-existent in our  $a = 32$  AU simulations, but ubiquitous in our  $a = 62$  simulations, particularly in the  $e = 0.3$  run. Second, assuming an  $a = 62$  AU semi-major axis, the GG Tau A system must be relatively close to its periape passage, given its apparent separation. This is important because our simulations indicate that accretion streams extending inward to the circumstellar disks occur only around this time, becoming weaker or entirely absent at other orbital phases. Thus, the simulations and observations suggest the same consistent model for the system itself.

We note that an important consequence of adapting this assumption is that deprojection of the apparent shape of the GG Tau A torus becomes a much less accurate method of determining the system’s actual inclination. The difficulty is compounded by the fact that the eccentricity of the torus varies widely and its orientation is not correlated with the orientation of that of the binary’s orbit plane. Other constraints will be required in order to disambiguate the torus’ actual inclination and its actual eccentricity.

#### 5.4. Implications for the Circumstellar Environment

Observations of the GG Tau A system show conclusive evidence both for circumstellar material and for accretion into the circumstellar environment. Both hot and cold material are observed (Dutrey *et al.* 2014; Beck *et al.* 2012; Piétu *et al.* 2011) in a region extending some tens of AU from the stars, in both circumstellar disks and in accretion streams. Unfortunately, the observations extend over only a very short time window in comparison to a full orbit of the binary, or even a full periape passage. They therefore define only a snapshot of the system rather than a full evolutionary picture of its behavior over time. Given the similarities we have already noted between our wide orbit simulations and those observed in GG Tau A, it will be useful to apply the comparisons first to make interpretations of the current state of the system in the context of an evolutionary model, and then to make predictions of its behavior as it evolves in the future.

Above, we concluded that the degeneracy in the orbital motion data for the stars in the GG Tau A system can be resolved in favor of an orbit with  $a \sim 62$  AU. This conclusion is further reinforced by the presence of significant amounts of material in the circumstellar environment of GG Tau A because mass accretes into the circumstellar environments at rates sufficient to sustain and even grow the disks *only* in our wide orbit simulations. Little accretion occurs in the close orbit runs. Instead, mass transfer into the circumstellar disks is very limited in those models and the disks initially assumed to be present quickly accrete onto the stars, almost entirely emptying them of material. These conditions are inconsistent with the observations of features extending tens of AU from the stars in the GG Tau A system. The presence and sizes of the circumstellar disks are also consistent with the interactions by each component of the system on the other, which lead to tidal truncation of the circumstellar disks at sizes comparable to the dynamical stability limit described by Holman & Wiegert (1999) and shown numerically by Artymowicz & Lubow (1994). The episodic accretion seen in our eccentric binary simulations is quite reminiscent of the same feature in the work of Artymowicz & Lubow (1996). As in their work, we find that accretion occurs preferentially onto the secondary component and that, due to this preference, the mass ratio between the components will tend towards equality over long periods. The same conclusion was drawn in Young & Clarke (2015), for the long term, time averaged accretion rates from massless, circumbinary disks with isothermal evolution assuming temperatures both warmer and colder than in our study.

Given that the GG Tau A system is in a wide orbit, the fits provided in Köhler (2011) show that the stars are approaching their periape passage, rather than receding from it. Examination of our simulations (e.g. panels 6-8 of figure 13) show that at this time the circumstellar environment should include a significant amount of material originating in the accretion streams and wrapping around the disks and extending outwards to the torus. A similarly

important feature of the system is that the circumstellar accretion disks should exhibit spiral structures and other asymmetries, driven by the tidal interactions of the binary components. Both classes of features are consistent with the observations. To these interpretations of the system’s short term state, we add the longer term prediction that, over the duration of the periaapse passage, as much as a few tenths of a Jupiter mass will accrete onto the circumstellar disks of the GG Tau A system, preferentially onto the secondary component, as shown in figure 17.

An important feature of the GG Tau A system that our simulations do not reproduce is that the mass determined for the disk around the secondary component is substantially less than that around the primary component (as discussed, e.g., by Piétu *et al.* 2011). In our simulations, the reverse is true—mass accretes preferentially onto the disk around the secondary, and its mass increases to  $\sim 2$  times that of the disk around the primary (figure 21). Should we interpret this inconsistency as an indication that our models should be ruled out as inconsistent with the observations? Fortunately for our models, GG Tau A itself provides the means to reconcile simulation and observation: it simply is not the binary we have modeled. Instead, recent interferometric observations of di Folco *et al.* (2014) have shown that the GG Tau Ab component is itself a binary consisting of two M stars separated by  $\sim 4.5$  AU. Unlike the system we modeled, the circumstellar disks in this system will be tidally truncated to radii no larger than about 1–1.5 AU each. The shorter dynamical times inherent such small disks will lead to correspondingly reduced disk lifetimes and masses, consistent with the observations, even in the presence of rapid replenishment from the accretion streams. Given this confounding factor, the inconsistency between our simulations and the data is to be expected, rather than being evidence for their invalidity.

After its accretion into one or the other circumstellar disk, mass continues to migrate through the disk, ultimately accreting onto the star around which it orbited. Accretion rates onto the stars in GG Tau A have been determined by Gullbring *et al.* (1998) (who derive a rate of  $\sim 1.8 \times 10^{-8} M_{\odot}/\text{yr}$ ) and Hartigan, Edwards & Ghandour (1995) (who derive a rate of  $\sim 2 \times 10^{-7} M_{\odot}/\text{yr}$ ) and are in very good agreement with the rates inferred from our simulations, of a few  $\times 10^{-8} M_{\odot}/\text{yr}$ . Each of these works consider only the accretion onto both stars as a sum, rather than onto the individual components. Our results, summed over both stars, fall roughly half way between the two observational determinations, supporting the conclusion that our simulations accurately model the GG Tau A system. Our rates, in turn, are about an order of magnitude higher than those computed by Günter & Kley (2002). While we have not investigated the origin of the differences between our results and theirs, we note that our initial setup was significantly different from theirs, as was our numerical method.

The accretion rates correspond, in numerical terms, to rates of 1-2 particles per year, or several hundred per binary orbit. Given this level of discreteness, such values suggest that we should consider the accretion in our simulations to be, at least in part, a phenomenon governed by numerical processes rather than physics. Perhaps surprisingly however, the rates do not appear to be strongly correlated to resolution. Accretion driven primarily by numerical viscosity for example, should be proportional to the particle smoothing length, through equation 9, and in turn to the square root (in 2D) of the number of particles. Instead, both the high and low resolution variants of the same physical configuration return similar patterns of accretion over time. We conclude, due to this relative insensitivity, that the accretion is not driven primarily by viscous processes derived from numerical effects, but rather by other physical processes, such as gravitational torques.

Mass transfer into the circumstellar disks occurs at rates similar to those for stellar accretion for wide systems but at much lower rates in the close systems. Thus, concerns similar to those noted for the stellar accretion must be addressed for these cases as well. Young, Baird & Clarke (2015) studied the sensitivity of the mass transfer rates into circumstellar environments to the resolution employed in 2D SPH simulations. They found that rates were numerically converged in simulations where the ratio of particle smoothing length to disk scale height fell in the range  $h/H \sim 0.05-0.5$  near Roche radii of the stars. This occurred at accretion rates of a few hundred particles per binary orbit. In our high resolution runs, we find that  $h/H \sim 0.1-0.2$  in this region. Given the similarity in these parameters between their

work and ours, we conclude that the mass transfer rates in our simulations are also converged. In contrast, the streams in the close orbit systems are far less massive and are correspondingly more poorly resolved. The comparatively poorer resolution of the mass transfer will not be fatal to our conclusion that the rates are much lower than the wide orbit runs, because the simulations are based on identical initial configurations of the circumbinary material. Thus, the weaker streams are simply a consequence of the intrinsic differences between the physical configuration of the stellar and circumstellar material rather than any shortcoming in the numerical realization.

### 5.5. The likelihood for planet formation

The results we present may be extended to considerations regarding the likelihood for planet formation in GG Tau A or other multiple systems. From an observational perspective for example, Dutrey *et al.* (2014) detect the presence of both cold and hot material in the circumstellar environment of GG Tau A and interpret the presence of the cold material as evidence for possible planet formation in the system. From a theoretical perspective however, such a conclusion requires not only the presence of substantial amounts of material in circumstellar disks, but also a mechanism for accumulating that matter into massive, condensed objects on short timescales. Theory suggests that the most likely candidates responsible for forming Jovian mass planets and low mass brown dwarfs are either gravitational fragmentation of large scale spiral structure (Durisen *et al.* 2007) or coagulation of small solid grains followed by later accretion of additional gas (i.e. ‘core accretion’—see Lissauer & Stevenson 2007) in the disks of forming stellar systems.

In N00, one of us concluded that planet formation in the circumstellar disks of equal mass binary systems with a separation similar to that in the GG Tau A system was unlikely. The conclusion was based on the fact that temperatures in the disks were too high either to support gravitational instabilities or to permit solid grain growth since grains would be vaporized in large portions of the disks. It was based on models of a system similar to L1551 IRS 5, a system much younger than GG Tau A and for which the disks are still relatively massive. To what extent does a similar conclusion hold for systems like GG Tau A, which has evolved to a much later evolutionary epoch, and for which the circumstellar disks are far less massive?

In answer to this question, we note that the temperatures seen in figure 15 (section 4.1, above) are similar to those reported in N00, while the disk masses are more than an order of magnitude lower. The effect of similar temperatures and smaller disk masses will make the disks even more stable against the growth of self gravitating structures, as defined by the value of the Toomre  $Q$  parameter, than reported in N00. Planet formation by way of gravitational fragmentation is therefore suppressed to a correspondingly greater degree. Similarly, high disk temperatures are significant for the core accretion model, because the budget of solids entrained in the gas decreases where temperatures rise above the vaporization temperatures of those solids. In the present instance, the ‘ice line’, at which planet formation via the core accretion model is enhanced by the presence of additional solid material, will lie near to or outside the actual boundaries of the disks. Water ices will therefore not be present within the circumstellar disks of GG Tau A, except perhaps at high altitudes above the midplanes, and planet formation via core accretion will be inhibited. In addition, while the accretion of new material into the circumstellar environment might be expected to enhance the growth of dust and small solid bodies, the fact that the overall accretion rate through the disk is high will negate this benefit. Any accumulations of dust grains and small planetesimals will quickly be swept along with the overall mass flow through the disk and be lost onto the star. Therefore, based on the same arguments presented in N00, we can extend the conclusion in N00 to the later stages of evolution typical of GG Tau A.

In extending the N00 conclusion, we are mindful of apparently contradictory data embodied in the detections of planets in mature binary systems (see e.g. Desidera & Barbieri 2007; Piskorz *et al.* 2015; Ngo *et al.* 2015). In many

cases, these systems are characterized by semi-major axes similar to that found in GG Tau A making the contradiction more acute. It can be resolved however, by noting that the companion masses derived for these objects (or implied for them through their effective temperatures) are substantially lower than those reported for the primaries and that few planets in binaries with near equal mass ratios were found. Such systems are therefore distinct from the cases considered here and our conclusion does not apply. Further contradictions emerge however, when observations of young systems are accounted for, such as is seen in Cheetham *et al.* (2015), who show that  $\sim 2/3$  of young, close binary systems have lost their circumstellar disks by the time they are 1-2Myr in age, without regard to stellar mass ratios. They conclude that planet formation will be less likely in binary's compared to single stars. Such contradictions suggest that a comparative study of the two classes of systems (of equal and unequal mass components) would be of great interest, to explore the physical reasons for the dichotomy between the presence of planets in unequal mass binary systems and their paucity in equal mass systems.

Given these dynamical constraints, we conclude that the cold material observed by Dutrey *et al.* (2014) has yet to interact substantially with the circumstellar environment or, for some portion, will soon return to the circumbinary torus as parts of the accretion stream moves out of the circumstellar environment. We cannot therefore confirm their conclusion that its presence in the circumstellar environment is evidence for planet formation. Nevertheless, the presence of both cold and hot material will remain of considerable interest for evolutionary models because together they define a reservoir of nearly pristine material which has either recently undergone, or will soon undergo, its first significant heating event. It may therefore retain signatures of the processes important during that event.

In a comparison study of single and moderate separation binary systems, Pascucci *et al.* (2008) conclude that the first stages of planet formation—grain growth—will not be affected by the presence or absence of a binary companion. They base their conclusions on the lack of observed differences between the  $10\mu\text{m}$  silicate features seen in the spectra of disks around stars in single and multiple systems. While the presence of silicates and other solids in disks is certainly a requirement for the formation of planets, in and of itself, simple presence is insufficient to differentiate between a system where planet formation is more likely and a similar system where planet formation is less likely. These features may instead trace material which is unlikely to become important for planet formation because of its short lifetime in the disks. We believe that such is the case in the GG Tau A system.

## 6. Summary and Discussion

Having completed our study of systems configured to be similar to GG Tau A and discussed their physical significance in relation it, we now summarize our results and suggest future studies that may profitably build on ours.

### 6.1. Summary of Our Main Results

We have modeled the evolution of a forming binary star system, configured to resemble the GG Tau A system, using the SPH code VINE. The system consists of two stars, each surrounded by a circumstellar disk and in orbit around each other, with a circumbinary torus+disk structure in orbit around the combined system. Our simulations include the self-gravity of the disk material, external heating of the gas due to radiation from two stars and radiative cooling from the disks.

We follow the evolution of a suite of systems for  $\sim 6500$ - $7500$  yr, corresponding to about three orbits of the torus around the center of mass. We find that strong spiral structures develop in the torus due to the stirring action of

the binary and to its own self gravity. The spiral structures are well defined in space, are characterized by edges of  $\lesssim 5 - 10$  AU in width and frequently extend more than  $360^\circ$  around the center of mass. We interpret the observations of sharply defined structures in the GG Tau A torus as evidence for such spiral structures. The spiral structures propagate outwards over time, generating a net outward mass flux extending into the low density circumbinary disk surrounding the torus. At large distances, they lose coherence, and we interpret the presence of the disk component of the circumbinary material as an excretion feature produced as the spiral structures transport mass to that region. In our torus-only configurations, about 15% of the mass of the torus moves outwards over the  $\sim 6000$  yr duration of our simulations—about half of the observed mass of the present disk (30% of the torus mass). The rates are much lower in the torus+disk initial configuration, and we expect that on a longer timescales, as the disk component gains mass, a nearly stationary state is reached between the outwards mass transport into the disk, and the mass escaping from it, through its outer edge or other mechanisms.

Structures created at different times frequently interact with one another and, late in the evolution of several simulations, fragment into one or two clumps with initial masses comparable to brown dwarfs. In a model where we replaced the binary with a single star of the same mass, some 38 clumps formed in less than a single orbit of the torus. We interpret this result as an indication of the importance of the binary’s stirring action as a contributor to the thermal energy input of the torus, and as a strong indication of the importance of self gravity in the GG Tau A torus. The torus changes shape and orientation as the spiral structures propagate through it. We fit its shape to an ellipse whose eccentricity varies between  $0 \lesssim e \lesssim 0.6$  and an orientation which precesses on timescales comparable to the torus orbit period. We point out a degeneracy in the interpretation of the data in the calculation of the torus’ inclination and its eccentricity, if the torus is actually eccentric rather than circular in shape. Given this degeneracy, we resolve the question of the supposed misalignment between the GG Tau A torus and the binary’s orbit, by interpreting the data as a coplanar system in which the torus is eccentric, rather than circular.

We simulate systems configured with semi-major axes of either  $a = 62$  AU (‘wide’) or  $a = 32$  AU (‘close’), and with assumed orbital eccentricity of either  $e = 0$  or  $e = 0.3$ . Although torus structure appears in all configurations, only wide configurations generate substantial streams of material extending inward to the circumstellar disks. A small fraction of the material in these streams accretes into the circumstellar environment, with the remainder returning to the torus. In wide binary configurations, and over the time span of our simulations, mass comparable to the disks themselves is accreted onto both primary and secondary components. Mass accretes preferentially onto the secondary at steady rates in  $e = 0$  configurations, but is episodic in  $e = 0.3$  configurations with highest rates occurring near binary periape. In contrast to the wide configurations, the streams in close binary configurations contain much less material and the rate of accretion into the circumstellar environment is two orders of magnitude smaller. Accretion onto the stars is steady in all cases, at rates sufficient to drain the disks almost entirely of material within the time span of our simulations, if they are not otherwise replenished.

The net mass transport into and out of the disks in the wide binary configurations, produces disk masses which remain steady near their initial values in  $e = 0$  cases, but double over the same time span in  $e = 0.3$  cases. In close binary configurations however, the net mass inflow and outflow is insufficient to replenish the disks before they accrete onto the stars. Replenishment of disk material from the torus in wide orbit configurations can therefore significantly extend the lifetime of the circumstellar disks. Mass replenishment is a necessary, but not sufficient, condition for planet formation in the circumstellar disks. We find that other conditions, such as material temperatures, are not compatible with planet formation in the circumstellar disks, and conclude that planet formation there is unlikely.

Given the results of our simulations, we interpret the observations of the GG Tau A system in favor of the wide, eccentric binary orbit solutions of Beust & Dutrey (2006) and Köhler (2011), for which parameters of  $a \sim 62$  AU and  $e \sim 0.3$  are derived. In each case, the fits require that the torus and binary orbit be inclined with respect to each other. As noted above, we resolve this inconsistency by interpreting the supposed mutual inclination as an eccentricity in the

torus. We also favor these parameters over the fits otherwise preferred by each of the previous works, namely those with  $a \sim 32$  AU and  $e \sim 0.3$ , because the circumstellar disks in such systems would be accreted onto their respective stars within a few thousand years, and because material streams in such systems would be far weaker than are observed.

## 6.2. Questions for the Future

The results presented in this work answer a number of questions regarding the character of the GG Tau A system, while raising others, and leaving others untouched. First among the questions raised by our results are the questions of whether the detailed morphology of features in the circumbinary torus as seen in our simulations are actually present in the GG Tau A system. The current best resolution observations of the torus provide tantalizing hints that such features do exist, but a definitive statement that such features are present must await higher resolution observations of quality similar to those described by ALMA Partnership (2015), for the HL Tau circumstellar disk. Another important question concerns planet formation in multiple systems. Whether or not any theoretical mechanism presently exists to explain the formation of giant planets in binary systems, the fact remains that at least a few binary systems, such as  $\gamma$  Cephei (Neuhauser *et al.* 2007), GI86 (Queloz *et al.* 2000) and HD 41004 (Zucker *et al.* 2004), do harbor planets. Therefore some formation mechanism does in fact exist. While we find that accretion into the circumstellar disks occurs rapidly enough so that they can survive for the comparatively long time scales needed to form planets, other conditions, such as temperatures, remain quite unfavorable. What are the mechanisms still missing from our models that permit such objects to form? Finally, our simulations model the evolution of the ‘A’ component of the full GG Tau system over a time span extending over only a tiny fraction of its formation time scale and in only two spatial dimensions. We neglected the full dynamical effects expected to be present in the system, insofar as our results include neither the distant binary ‘B’ component of the GG Tau system, nor the newly discovered tight binary nature of the GG Tau A b component. Even so, we find large scale morphological changes even over this short time span and restricted dimensionality and physical system. Given the vigor of the activity over such a short time scale, we would expect activity of similar scale over to occur over longer time spans as well, with correspondingly large consequences on the system morphology. To what extent will 3D effects also play a role in the evolution? What will be the end state configuration of the GG Tau system as a whole? Will the components eventually break apart? Merge? Future investigations extending the work presented here will be required in order to answer these questions.

We wish to thank the anonymous referee for comments which improved our manuscript. Portions of this work were carried out under the auspices of the National Nuclear Security Administration of the U.S. Department of Energy at Los Alamos National Laboratory under Contract No. DE-AC52-06NA25396, for which this is publication LA-UR-16-23283.

## REFERENCES

Alexander, D. R., Ferguson, J. W., 1994, ApJ, 437, 879

ALMA Partnership, 2015, astro-ph:1503.02649

Artymowicz, P., Lubow, S. H., 1994, ApJ, 421, 651

Artymowicz, P., Lubow, S. H., 1996, ApJ, 467, L77

Balsara, D., 1995, J. Comp. Phys, 121, 357



- Beck, T., Bary, J. S., Dutrey, A., Piétu, V., Guilloteau, S. Lubow, S. H. Simon, M., 2012, ApJ, 754, 72
- Beust, H., & Dutrey, A., 2006, A&A, 439, 585.
- Beust, H., & Dutrey, A., 2006, A&A, 446, 137.
- Bodenheimer, P., Burkert, A., Klein, R. I., Boss, A. P., 2000, in Protostars and Planets IV, ed. Mannings, V., Boss, A. P., & Russell, S. S., University of Arizona Press: Tucson, p. 675
- Cheetham, A. C., Kraus, A. L., Ireland, M. J., Cieza, L., Rizzuto, A. C., Tuthill, P. G., 2015, ApJ, 813, 83
- Chiang, E. I., Goldreich, P., 1997, ApJ, 490, 368
- Close, L. M., Dutrey, A., Roddier, F., Guilloteau, S., Roddier, C., Northcott, M., Menard, F., Duvert, G., Graves, J. E., Potter, D., 1998, ApJ, 499, 833
- Cohen, M., Kuhl, L. V., 1979, ApJS, 41, 743
- Desidera, S., Barbieri, M., 2007, A&A, 462, 345
- di Folco, E., Dutrey, A., L Bouquin, J.-B., Lacour, S., Berger, J.-P., Köhler, R., Guilloteau, S., Piétu, V., Bary, J., Beck, T., Beust, H., Pantin, E., 2014, A&A, 565, L2
- Duchêne, G., McCabe, C., Ghez, A. M., Macintosh, B. A., 2004, ApJ, 606, 969
- Durisen, R. H., Boss, A. P., Mayer, L., Nelson, A. F., Quinn, T., Rice, W. K. M., 2007 in Protostars and Planets V, ed. Reipurth, B., Jewitt, D., Keil, K., University of Arizona Press: Tucson, p. 607
- Dutrey, A., Guilloteau, S., Simon, M., 1994 A&A, 286, 149
- Dutrey, A., di Folco, E., Guilloteau, S. Boehler, Y., Bary, J., Beck, T., Beust, H., Chapillion, E., Gueth, F., Hurè, J.-M., Pierens, A., Piétu, V., Simon, M., Tang, Y.-W., 2014, Nature, 514, 600
- Günther, R. & Kley, W. 2002, A&A, 387, 550
- Guilloteau, S., Dutrey, A., & Simon, M., 1999, A&A, 348, 570 (GDS99)
- Gullbring, E., Hartmann, L., Briceno, C., Calvet, N., 1998, ApJ, 492, 323
- Haisch, K. E., Lada. E. A., Lada, C., J., 2001, ApJ, 553, 153
- Holman, M. J., Wiegert, P. A., AJ, 117, 621
- Hartigan, P., Edwards, S., Ghandour, L. 1995, ApJ, 452, 736
- Itoh, Y., *et al.*, 2002, PASJ, 54, 963
- Köhler, R., 2011, A&A, 530, 126
- Krist, J. E., Stapelfeldt, K. R., Watson, A. M., 2002, ApJ, 570, 785
- Krist, J. E., Stapelfeldt, K. R., Golimowski, D. A., Ardila, D. R., Clampin, M., Martel, A. R., Ford, H. C., Illingworth, G. D. & Hartig, G. F., 2005, AJ, 130, 2778
- Leinert, Ch., Haas, M., Mundt, R., Richichi, A., Zinnecker, H., 1991, A&A, 250, 407

- Lissauer, J. J., Stevenson, D. J., 2007, in *Protostars and Planets V*, ed. Reipurth, B., Jewitt, D., Keil, K., University of Arizona Press: Tucson, p. 591
- Lodato, G., Rice, W. K. M., 2004, *MNRAS*, 351, 630
- Lodato, G., Clarke, C. J., 2011, *MNRAS*, 413, 2735
- Mathieu, R. D., Ghez, A. M., Jensen, E. L. N., Simon, M., 2000, in *Protostars and Planets IV*, ed. Mannings, V., Boss, A. P., & Russell, S. S., University of Arizona Press: Tucson. p. 703
- McCabe, C., Duchêne, G., Ghez, A. M., 2002, *ApJ*, 575, 974
- Meru, F., Bate, M. R., 2010, *MNRAS*, 406, 2279
- Meru, F., Bate, M. R., 2010a, *MNRAS*, 410, 559
- Meru, F., Bate, M. R., 2011b, *MNRAS*, 411, L1
- Meru, F., Bate, M. R., 2012, *MNRAS*, 427, 2022
- Monin, J. L., Clarke, C. J., Prato, L., McCabe, C., 2007, in *Protostar and Planets V*, ed. Reipurth, B., Jewitt, D., Keil, K., University of Arizona Press: Tucson
- Murray, J., 1996, *MNRAS*, 279, 402
- Nelson, A.F., Benz, W., Adams, F.C., Arnett, W.D., 1998, *ApJ*, 502, 342
- Nelson, A. F., Benz, W., Ruzmaikina, T. V., 2000, *ApJ*, 529, 357 (DynII)
- Nelson, A. F., 2000, *ApJ*, 537, L65-68 (N00)
- Nelson, A. F., 2006, *MNRAS*, 373, 1039 (N06)
- Nelson, A. F., Wetzstein, M., Naab, T., 2009, *ApJS*, 184, 326
- Neuhauser, R., Mugrauer, M., Fukagawa, M., Torres, G., Schmidt, T., 2007, *A&A* 462, 777
- Ngo, H., *et al.*, ESS meeting #3, #403.04, November 2015, *BAAS*, 47, #6
- Pascucci, I., Apai, D., Hardegree-Ullman, E. E., Kim, J. S., Meyer, M. R., 2008, *ApJ*, 673, 477
- Piétu, V., Gueth, F., Hily-Blant, P., Schuster, K-F, Pety, J., 2011, *A&A*, 528, A81
- Piscorz, D., Knutson, H. A., Ngo, H., Muirhead, P. S., Batygin, K., Crepp, J. R., Hinkley, S., Morton, T. D., 2015, *ApJ*, 814, 148
- Pollack, J. B., McKay, C. P., Christofferson, B. M., 1985, *Icarus*, 64, 471
- Prato, L., and Simon, M., 1997, *ApJ* 474, 455
- Press, W. H., Teukolsky, S. A., Vetterling, W. T., Flannery, B. P., 1992 *Numerical Recipes*, Cambridge University Press, Cambridge
- Pringle, J. E., 1991, *MNRAS*, 248, 754
- Queloz D., Mayor M., Weber L., Blecha A., Burnet M., Confino B., Naef D., Pepe F., Santos N., Udry S., 2000, *A&A*, 354, 99

- Roddier, C., Roddier, F., Northcott, M. J., Graves, J. E. and Jim, K., 1996, *ApJ*, 463, 326
- Rodriguez, L. F., D’Alessio, P., Willner, D. J., Ho, P. T. P., Torrelles, J. M., Curiel, S., Gómez, Y., Lizano, S., Pedlar, A., Cantó J., Raga, A. C., 1998, *Nature*, 395, 355
- Semonov, D., Henning, Th., Helling, Ch., Ilgner, M., Sedlmayr, E., 2003, *A&A*, 410, 611
- Shakura, N. J. & Sunyaev, R. A., 1973, *A&A*, 24, 337
- Shu, F. H., Adams, F. C. & Lizano, S., 1987, *ARA&A*, 25, 23
- Silber, J., Gledhill, T., Duchêne, G., Ménard, F., 2000, *ApJ*, 536, 89
- Simon, M., Guilloteau, S., 1992, *ApJ*, 397, L47
- Stapelfeldt, K. R., Krist, J. E., Ménard, F., Bouvier, J., Padgett, D. L., Burrows. C. J., 1998, *ApJ*, 502, L65
- Tamazian, V. S., Docobo, J. A., White, R. J., Woitas, J., 2002, *ApJ*, 578, 925
- Tang, Y.-W., Dutrey, A., Guilloteau, S., Pietu, V., Di Folco, E., Beck, T., Ho, P. T. P., Boehler, Y., Gueth, F., Bary, J., Simon, S., 2014, *ApJ*, 793, 10
- Wetzstein, M., Nelson, A. F., Naab, T., Burkert, A., 2009, *ApJS*, 184, 298
- White, R. J., Ghez, A. M., Reid, I. N., Schultz, G., 1999, *ApJ*, 520, 811
- Young, M. D., Baird, J. T., Clarke, C. J., 2015, *MNRAS*, 447, 2907
- Young, M. D., Clarke, C. J., 2015, *MNRAS*, 452, 3085
- Zucker S., Mazeh T., Santos N. C., Udry S., Mayor M., 2004, *A&A* 426, 695

Table 1. Initial Parameters For Simulations

Name	Primary Particles	Secondary Particles	Circumbinary Particles	Disk Radius (AU)	Orbital Eccentricity	Semi-Major Axis (AU)	End Time (yr)	Rotations $T_{end}/T_{180AU}$
Clos3elo	2289	1955	421384	4	0.3	32	4400	2.09
Wide0elo	2207	1892	421384	10	0.0	62	6500	3.09
Wide3elo	2207	1892	421384	10	0.3	62	6500	3.09
Clos0ehi	9995	8592	1861769	4	0.0	32	7000	3.33
Clos3ehi	9995	8592	1861769	4	0.3	32	7500	3.57
Wide0ehi	10134	8418	1861769	10	0.0	62	6500	3.09
Wide3ehi	10134	8418	1861769	10	0.3	62	6500	3.09
Singlehi	-	-	1861769	-	-	-	2100	1.00
Noheat3ehi	10134	8418	1861769	10	0.3	62	2100	1.00
ClosT3elo	2289	1955	421081	4	0.3	32	4000	1.90
ClosT0ehi	9995	8592	1867987	4	0.0	32	6500	3.09
ClosT3ehi	9995	8592	1867987	4	0.3	32	6500	3.09
WideT0ehi	10134	8418	1867987	10	0.0	62	6500	3.09
WideT3ehi	10134	8418	1867987	10	0.3	62	6500	3.09